Separation of Oil and Other Organics from Water Using Inverse Fluidization of Hydrophobic Aerogels

by

Ding Wang

A Dissertation Presented in Partial Fulfillment
of the Requirements for the Degree
Doctor of Philosophy

Approved November 2011 by the
Graduate Supervisory Committee:

Jerry Y.S. Lin, Co-Chair
Robert Pfeffer, Co-Chair
Paul Westerhoff
David Nielsen
Mary Laura Lind

ARIZONA STATE UNIVERSITY

December 2011

ABSTRACT

This dissertation presents a systematic study of the sorption mechanisms of hydrophobic silica aerogel (Cabot Nanogel®) granules for oil and volatile organic compounds (VOCs) in different phases. The performance of Nanogel for removing oil from laboratory synthetic oil-in-water emulsions and real oily wastewater, and VOCs from their aqueous solution, in both packed bed (PB) and inverse fluidized bed (IFB) modes was also investigated.

The sorption mechanisms of VOCs in the vapor, pure liquid, and aqueous solution phases, free oil, emulsified oil, and oil from real wastewater on Nanogel were systematically studied via batch kinetics and equilibrium experiments. The VOC results show that the adsorption of vapor is very slow due to the extremely low thermal conductivity of Nanogel. The faster adsorption rates in the liquid and solution phases are controlled by the mass transport, either by capillary flow or by vapor diffusion/adsorption. The oil results show that Nanogel has a very high capacity for adsorption of pure oils. However, the rate for adsorption of oil from an oil-water emulsion on the Nanogel is 5-10 times slower than that for adsorption of pure oils or organics from their aqueous solutions. For an oil-water emulsion, the oil adsorption capacity decreases with an increasing proportion of the surfactant added. An even lower sorption capacity and a slower sorption rate were observed for a real oily wastewater sample due to the high stability and very small droplet size of the wastewater.

The performance of Nanogel granules for removing emulsified oil, oil from real oily wastewater, and toluene at low concentrations in both PB and IFB

modes was systematically investigated. The hydrodynamics characteristics of the Nanogel granules in an IFB were studied by measuring the pressure drop and bed expansion with superficial water velocity. The density of the Nanogel granules was calculated from the plateau pressure drop of the IFB. The oil/toluene removal efficiency and the capacity of the Nanogel granules in the PB or IFB were also measured experimentally and predicted by two models based on equilibrium and kinetic batch measurements of the Nanogel granules.

To my parents
for their continuous support and encouragement.

ACKNOWLEDGMENTS

This dissertation is dedicated to my family in China, for their continuous encouragement and support during my pursuit of a Ph.D. degree. I am really grateful to my parents for their constant support and their endurance of my long-term absence, as I am their only child.

I would like to express great gratitude to my advisors, Dr. Robert Pfeffer and Dr. Jerry Lin, not only for introducing me to this interesting and challenging research area, but especially for their generous guidance, great kindness, and patience throughout my Ph.D. study. As a foreign student, I will always appreciate the patience that Dr. Pfeffer exhibited when he revised my papers word by word. Their dedication to research, leadership, and their commitment to fostering student independence will continue to influence me throughout my career. I am and will continue to be extremely grateful for the opportunity they gave me to work under both of them at ASU.

I would like to thank Dr. Paul Westerhoff, Dr. David Nielsen, and Dr. Mary Laura Lind for devoting their time and effort to serve on my committee and to provide valuable suggestions and comments.

I would like to acknowledge the support of the National Science Foundation through Grant CBET 0730465, the Cabot Corporation for supplying the Nanogel granules and purchasing a dedicated GC, as well as Mr. Dan Kelley of Tierra Dynamic Company for supplying the wastewater sample. I am grateful to Drs. Nirmalya Maity, Dhaval Doshi, Elmar Pothmann, and A.J. Duplessis of Cabot Corporation for providing me with an industrial perspective as well as

technical expertise and guidance. Special thanks go to Dr. Dhaval Doshi for his guidance and advice when I was an intern at Cabot in 2010.

I also want to thank Jeremy Acton, Trent Silbaugh, and Elisabeth McLaughlin, ASU Fulton Undergraduate Research Initiative (FURI) students, who worked on this project; without their assistance much of the present work could not have been possible. I am especially indebted to Elisabeth McLaughlin, a Barrett Honors college undergraduate student, who worked with me for five semesters; she assisted me in conducting the batch adsorption experiments for VOCs and oils on Nanogels in solution or emulsion phases, and the adsorption experiments for toluene and real oily wastewater in the inverse fluidized bed. She also carefully read and suggested revisions to this dissertation.

I am also grateful to current and previous members in Dr. Pfeffer's and Dr. Lin's group: Teresa Rosa, Matthew Anderson, Carrie Eggen, Zebao Rui, Chao Ji, Shriya Seshadri, Tyler Norton, Nick Linneen, Amit Yadav, Alex Kasik, Zhenxia Zhao, Bo Lu, Xiaoli Ma, Dr. Haibing Wang, Dr. Huiyuan Gao, and Dr. Jose Landeros, for their kindness, friendship, and support during the entire course of my Ph.D. study.

Many thanks go to Fred Peña for his continued technical support. Additionally, I would like to thank various staff members at ASU for their assistance in a wide variety of ways throughout my research: Dr. Kaushal Rege (use of the shaker), Dr. Lenore Dai (use of the tensiometer and rheometer), Dr. Jonathan Posner (use of the DLS), and Michael Dodson (assistance with contact angle).

TABLE OF CONTENTS

Page

CHAPTER Page

CHAPTER Page

CHAPTER Page

CHAPTER Page

CHAPTER Page

APPENDIX Page

LIST OF TABLES

Table Page

LIST OF FIGURES

Figure Page

Figure Page

Figure Page

Figure Page

Figure Page

Figure Page

Figure Page

LIST OF PUBLICATIONS

The following chapters are modified versions of papers already published or submitted for publication:

Chapter 2

Wang, D., McLaughlin, E., Pfeffer, R., Lin, Y. S. (2011). Adsorption of organic compounds in vapor, liquid and aqueous solution phase on hydrophobic aerogel. *Ind. Eng. Chem. Res.*, accepted.

Chapter 3

Wang, D., McLaughlin, E., Pfeffer, R., Lin, Y. S. (2011). Adsorption of oils from pure liquid and oil-water emulsion on hydrophobic silica aerogels. *Environ. Sci. Technol*., submitted.

Chapter 4

Wang, D., Silbaugh, T., Pfeffer, R., Lin, Y. S. (2010). Removal of emulsified oil from water by inverse fluidization of hydrophobic aerogels. *Powder Technol.*, *203*, 298-309.

Chapter 5

Wang, D., McLaughlin, E., Pfeffer, R., Lin, Y. S. (2011). Aqueous phase adsorption of toluene in a packed and fluidized bed of hydrophobic aerogels. *Chem. Eng. J.*, *168*, 1201-1208.

Permission has been given by the co-authors to use previously published work in this dissertation.

CHAPTER 1 GENERAL INTRODUCTION

1.1. Organic Pollution in the Environment

1.1.1. Oil Pollution and Treatment

Oil pollution has become one of the most serious global environmental issues today. A large amount of oil pollution exists in different forms and is generated by various sources: the major sources of oil spill pollution in the ocean include the runoff of oil and fuel from land-based sources and accidental spills [Fingas, 2000]. Major industrial sources of oil waste include petroleum refining and petrochemical plants [Johnson et al., 1973], steel manufacturing and metal working [Paterson, 1985], vehicle repair, and other manufacturing plants. Major municipal sources of oil, which contain up to 36% oily substances, are derived from vegetable and animal oils in kitchen and human wastes [Quemeneur et al., 1994]. Large amounts of oil discharged into the aquatic ecosystem can cause serious environmental problems, including clogging of sewage treatment plants, an adverse effect on the aquatic biota, and increasing biochemical oxygen demand due to the large amount of bacteria necessary to decompose the oil.

Current technologies for oil removal from wastewater include containment booms [Fingas, 2000], chemical treatment, gravity separators such as American Petroleum Institute (API) separators [America Petroleum Institute, 1969], gas floatation devices [Bennett, 1988], adsorption or absorption by a variety of sorbents such as activated carbon [Ayotamuno et al., 2006], membrane filtration [Jian et al., 1996], and biological treatment [Walker et al., 1975; Pasila 2004].

Generally, an oil and water mixture can be classified as: free oil, with oil droplets larger than 150 μm, dispersed oil, with oil droplets in the range of 20-150 μm, and emulsified oil, with oil droplets smaller than 20 μm. API separators [America Petroleum Institute, 1969] and Dissolved Air Flotation (DAF) devices [Bennett, 1988] are used to remove free oil and dispersed oil from wastewater, respectively. They can achieve an efficiency of 98% of oil removal. However, for API separators, the oil droplets need to be relatively large in order to coalesce, and DAF separators require the injection of air and addition of PH regulators and coagulants which contribute to the operating cost. More importantly, these conventional methods cannot remove small micron or submicron sized oil droplets. Removal of emulsified oils can be achieved by using activated carbon adsorption or membrane filtration. The effluent from industrial operations contains practically no oil; however, due to the limited removal capacity of the activated carbon and very high pressures and high quality feed required by membrane filtration, these methods are not commonly used.

In addition to activated carbon [Ayotamuno et al., 2006], several other sorbents have also been studied for the removal of oil from water in packed bed filters or adsorbers. They include organic sorbents, such as sawdust [Cambiella et al., 2006], peat [Mathavan et al., 1989], hydrophobic aquatic plants [Ribeiro et al., 2003] and other carbon-based products, inorganic sorbents, such as organoclay [Alther, 1995], bentonite [Viraraghavam et al., 2003] and vermiculite [Mysore at al., 2005], and synthetic sorbents, such as polyurethane, polyethylene, and nylon fibers. Sorbents work either by absorption or adsorption. Defined by the

American Society of Testing and Materials (ASTM), absorption is a process where the material taken is distributed throughout the body of the absorbing material, while adsorption is a process where the material taken is distributed over the surface of the adsorbing materials. Therefore, absorbents collect oil by capillary action or suction forces, whereas adsorbents collect oil relying on a large amount of surface area, high porosity, molecular structure, and the affinity of the sorbent for the oil. Table 1-1 shows the oil absorption capacity of some selected materials.

Table 1-1. *Oil sorption capacity of selected materials*

Type of Media	Material	Oil type	Sorbent Capacity (g/g)	Reference
Organic	Peat-based sorbents	Diesel oil	2-12	Cojocaru et al., 2011
	Vegetable fiber	Crude oil	2.7-6.4	Annunciado et al., 2005
	Butyl Rubber	Fuel oil	15.4	Ceylan et al., 2009
Inorganic	Expanded perlite	Crude oil	3.2-7.5	Bastani et al., 2006
	Organo clay	Diesel oil	1.2-7.2	Carmody et al., 2007
	CF_3 functionalized silica aerogel	Crude oil	16	Reynolds et al., 2001
	Silica aerogel (hydrophilic)	Crude oil	<0.1	Reynolds et al., 2001
Synthetic	Polypropylene	Crude oil	7	Yoshiyuki et al., 1994
	Polyvinylalcohol	Motor oil	2	Robeson et al., 1992

1.1.2. Volatile Organic Compounds Pollution and Treatment

In addition of removing oil from wastewater, the separation of volatile organic compounds (VOCs) from water or air has received a great deal of attention. VOCs are organic chemical compounds which have significant vapor pressures and which can affect the environment and human health. VOCs include both man-made and naturally occurring chemical compounds and can cause pollution in water, air and soil. Major sources of these organic contaminants are anthropogenic such as industrial waste, leakage, spills, improper disposal, and accidents during transportation in oil-related industries [Farhadian et al., 2008]. These organic contaminants discharged into the nature environment are dangerous to the ecosystem. Also, these organic contaminants, such as benzene, toluene, and xylene (BTX) are toxic and often classified as carcinogens for humans [Irwin et al., 1997].

Several types of sorbents have been studied in an effort to develop a process to selectively adsorb VOCs from water or air, including activated carbon [Chatzopoulos et al., 1995], surfactant modified zeolites [Ghiaci et al., 2004], silicalite [Ma et al., 1985], organo minerals [Koh et al., 2001], carbon nanotubes [Su et al., 2010], polymeric resin [Simpson et al., 1993] and hydrophobic silica aerogel [Hrubesh et al., 2001; Standeker et al., 2007]. Figure 1-1 shows a comparison of the adsorption isotherms of some of the sorbents referenced above for two typical VOCs: benzene and toluene from their aqueous solutions. As can be seen in the figure, granulated activated carbon (GAC) exhibits the highest adsorption capacities for benzene and toluene of these selected sorbents.

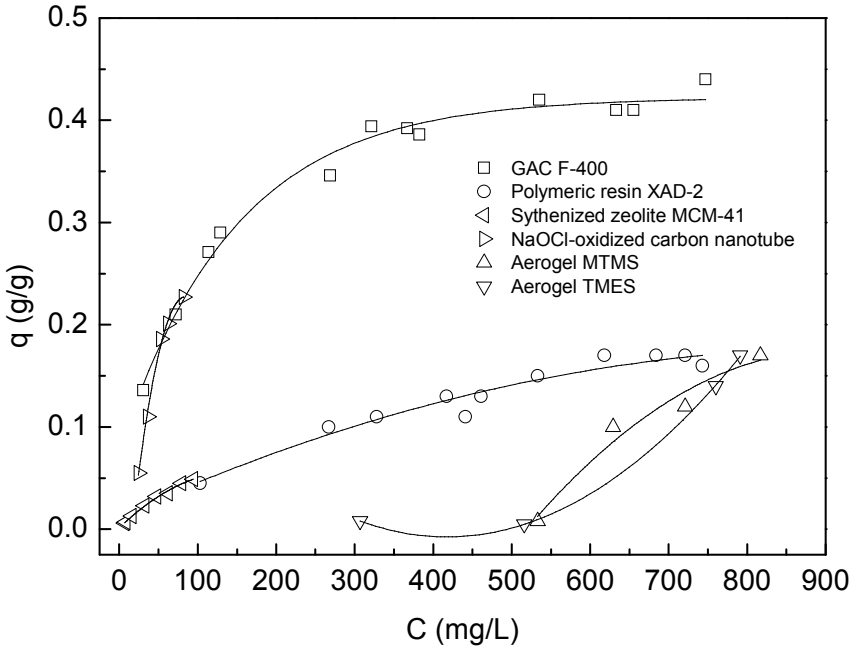

(a)

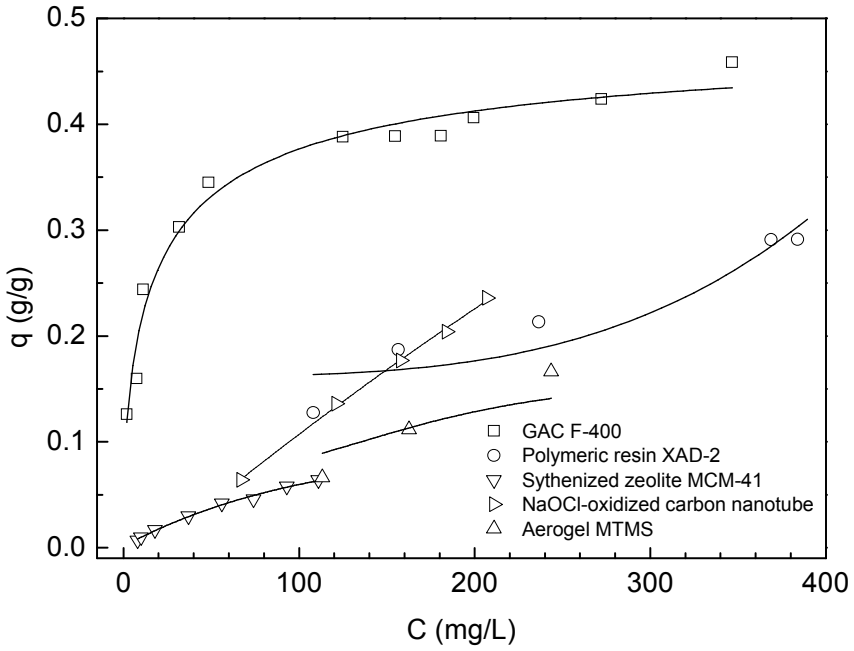

(b)

Figure 1-1. Comparison of the adsorption isotherms of (a) benzene and (b) toluene from aqueous solution on different sorbents.

Of the sorbents mentioned in this chapter, only GAC is commercially used for the removal of oil or VOCs from water and from air. However, GAC displays disadvantages such as slow kinetics and limited removal capacity. Thus, the search for better sorption materials which have a high uptake capacity and a high rate of uptake (efficiency) is ongoing.

1.2. Current Status of Hydrophobic Silica Aerogel

1.2.1. Hydrophobic Silica Aerogel

Silica aerogels are nano-porous solids which consist of silicon oxide. The structure of aerogels consists of tangled, fractal-like chains of spherical clusters of molecules each about 3-4 nm in diameter as seen in the TEM image in Figure 1-2. The chains form a solid structure surrounding air-filled pores that average about 15-20 nm in size. Typical aerogel synthesis is through the sol-gel method by supercritical drying, which uses tetramethoxysilane (TMOS) as the primary precursor. To obtain hydrophobic silica aerogels, Si-OH groups are replaced by hydrolytic stable groups such as Si-O-R groups (R = CH_3 or C_2H_5 or $CF_3(CH_2)_2$) [Reynolds et al., 2001; Standeker et al., 2007]. Hydrophobic silica aerogels are highly porous, much lighter than water and have the lowest density, highest surface area per unit volume, and lowest thermal conductivity of any solid. They are available commercially in the form of small particles in a variety of different size ranges, and because of their hydrophobicity they attract organic molecules and repel water.

Because of these desirable properties, silica aerogels (both hydrophobic and hydrophilic) are one of the most versatile materials available for a wide range of both scientific and commercial applications, including: thermal super insulation, heat storage, catalytic support, energy absorber, acoustics, target for X-ray lasers [Fricke et al., 1997; Hrubesh, 1998], architectural daylighting, insulation for oil and gas pipelines, coating formulations, outdoor gear and apparel and personal care products.

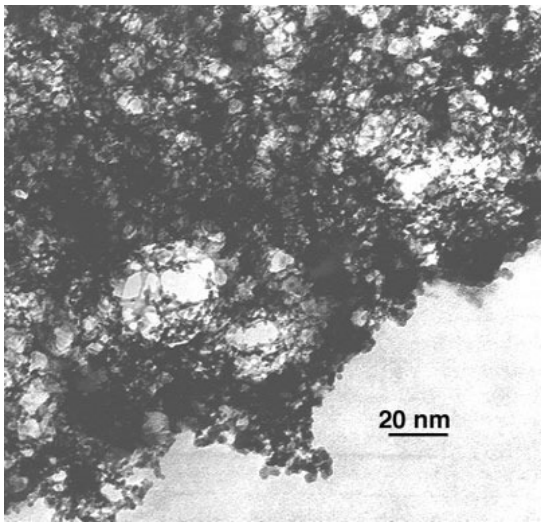

Figure 1-2. TEM image of silica aerogel [Berkeley lab].

Due to its extreme hydrophobicity and affinity for oil droplets and other organic materials, highly porous and open pore structure, and very high surface area, one relatively new application for hydrophobic silica aerogel is using it as a sorbent for the removal of organic contaminants from water or air phases. Different types of hydrophobic aerogels have been studied for the sorption of miscible organic solvents in water [Hrubesh et al., 2001; Standeker et al., 2007;

Wang et al., 2011], VOC vapors [Standeker et al., 2009], toxic organics [Liu et al., 2009], oil spills [Reynolds et al., 2001], dispersed oil (oil droplets > 20μm) [Quevedo et al., 2009], and emulsified oil (oil droplets < 20μm) using a surfactant [Wang et al., 2010].

1.2.2. Cabot Nanogel®

As the only commercially available aerogel in particulate form, Nanogel® is Cabot Corporation's trade name for its family of hydrophobic silica aerogels which have particle sizes ranging from 5 μm to 3.5 mm, densities of 40 to 100 kg/m^3, and surface areas of 600 to 800 m^2/g, in both opaque and translucent forms. The surface of Nanogels is covered with tri-methyl-silyl groups ($-Si(CH_3)_3$) and is hydrophobic. Instead of the traditional supercritical drying method in the sol-gel process, Nanogels are made via silation of organogels to control gel shrinkage during the manufacturing process. Figure 1-3 shows computer simulation of Nanogel and Table 1-2 shows some of the key characteristics of Nanogels.

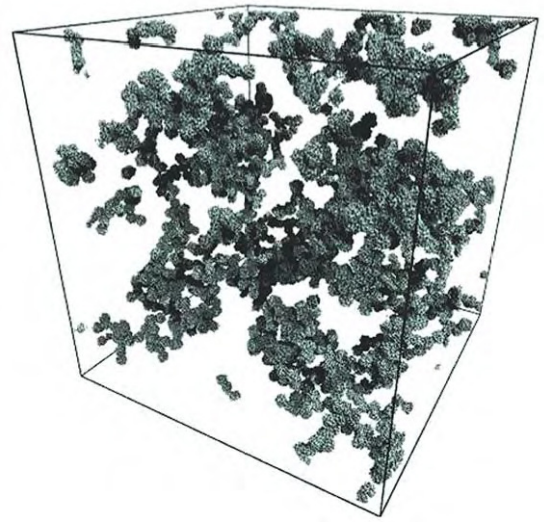

Figure 1-3. Computer simulation of a silica aerogel product called Nanogel®, which is surface-treated to be hydrophobic [Cabot Corp.].

Table 1-2. *Key characteristics of Nanogels [Cabot]*

Thermal conductivity	9-12mW/mK
Porosity	>90% air
Nano-sized pores	20-40 nanometers
surface area	~750 m^2/g
tap density	30-125 kg/m^3
Specific heat capacity	.7-1.15 kJ/(kg*K)
Variety of particle sizes	5 microns - 4mm
Surface chemistry	Completely hydrophobic
Opacity	Translucent, IR opacified and opaque

1.3. Principles of Adsorption Process

Adsorption is the accumulation of substances, i.e., atoms, ions, biomolecules or molecules at a surface or interface, and occurs in large measure

as a result of forces active within surface boundaries [Weber et al., 1980]. Various forces exist between molecules of the adsorbate and the surface of the adsorbent, all having their origin in the electromagnetic interactions of nuclei and electrons. Among these, there are four major types of binding forces: ion exchange, physical, chemical, and specific [Slejeiko, 1981]. Ion exchange adsorption is electrostatic attachment of ionic species to sites of opposite charge at the surface of an adsorbent. Physical adsorption results from the action of Van der Waals forces, comprised of London dispersion forces and classical electrostatic forces. Chemical adsorption results from chemical bond formation between an adsorbate and an adsorbent resulting in a change in the chemical form of the adsorbate. The chemisorptive bond is localized at active centers on the adsorbent and is usually stronger than the physical Van der Waals forces [Weber et al., 1980]. Many adsorption processes involving organic molecules result from specific interactions between identifiable structural elements of the adsorbate and the adsorbent: such interactions are designated as specific adsorption. Specific adsorption exhibits a large range of binding energies, from the values associated with physical adsorption on the lower end of the spectrum to the higher energies involved in chemical adsorption [Mattson et al., 1969].

Adsorption processes are generally exothermic. Therefore, with increasing temperature, the adsorption capacity in a given system usually decreases. However, the rate of the adsorption is found to increase with increasing temperature, which is because the adsorption kinetics is generally controlled by diffusive mass transfer.

The adsorptive capacity of an adsorbent for an adsorbate will depend on both the properties of the adsorbent and the adsorbate. On the adsorbent side, hydrophobicity, surface area, and the distribution of area with respect to pore size generally are primary determinants of adsorption capacity [Slejeiko, 1981]. On the adsorbate side, molecular structure, solubility, etc., all affect the adsorbability [Eckenfelder, 2000].

1.3.1. Adsorption Equilibria

When a quantity of adsorbent is contacted with a given volume of a liquid containing an adsorbable solute, adsorption occurs until equilibrium is achieved. Generally, the majority of physisorption isotherms may be grouped into the six types, as shown in Figure 1-4 [Sing et al., 1985].

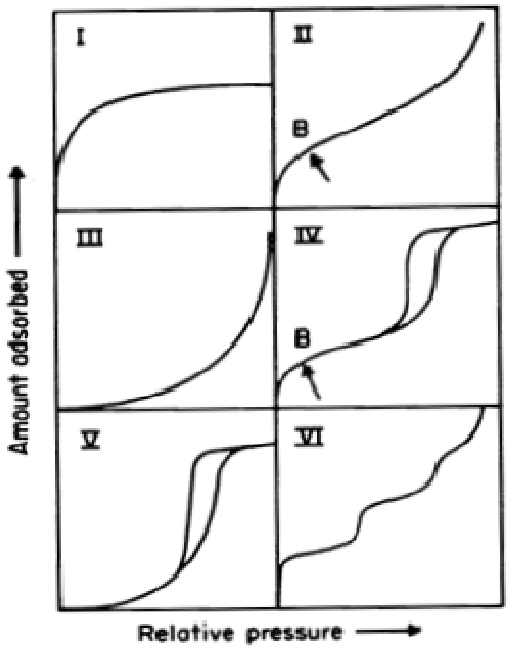

Figure 1-4. Types of physisorption isotherms [Sing et al., 1985].

In Figure 1-4, Type I isotherms characterize micropore adsorbents which have relatively small external surfaces. Type II and type III isotherms are obtained with a non-porous or macroporous adsorbent with strong or weak adsorbate-adsorbent interactions. Type IV isotherms have been observed for gas phase adsorption with some mesoporous adsorbents. Type V isotherms are uncommon and represent the adsorption isotherm by certain porous adsorbents with weak adsorbate-adsorbent interactions. Type VI isotherms represent stepwise multilayer adsorption on a uniform non-porous surface.

There have been a variety of different equilibrium isotherm equations proposed, some of which have a theoretical foundation, and others having a more empirical nature. Among these, the Langmuir equation, the Freundlich equation, and the BET equation are three of the most commonly used isotherm equations.

1.3.1.1. The Langmuir Isotherm Equation

The Langmuir equation [Langmuir, 1916] relates the coverage or adsorption of molecules on a solid surface to concentration of a medium above the solid surface at a fixed temperature. There are four important underlying assumptions for the Langmuir equation: 1. the adsorption occurs at definite localized site on the surface; 2. each site can hold only one molecule of the adsorbing species; 3. all sites are equivalent; and 4. there are no interactions between adsorbate molecules on adjacent sites. The Langmuir isotherm is defined as

$$q = \frac{abC_e}{1 + aC_e} \tag{1.1}$$

where q is the mass of adsorbate adsorbed per unit mass of adsorbent, C_e is the equilibrium concentrations of the solution, a is a constant related to energy or net enthalpy between the adsorbed solute molecule and the adsorbent, and b is the mass of adsorbed solute required to completely saturate a unit mass of adsorbent.

1.3.1.2. The Freundlich Isotherm Equation

The Freundlich adsorption model [Freundlich, 1926] is widely used to fit adsorption isotherm data since it takes into account the heterogeneity of real surfaces for adsorption. For the Freundlich isotherm, it should be noted that: 1. this model does not impose any requirement that the coverage must approach a constant value corresponding to one complete monomolecular layer as C_e gets larger; and 2. this model implies that the energy distribution for the adsorption sites is essentially an exponential type, rather than the uniform type assumed in the Langmuir model. The Freundlich isotherm is defined as

$$q = kC_e^{1/n} \tag{1.2}$$

where k and 1/n are Freundlich capacity and intensity parameters, respectively.

1.3.1.3. The BET Isotherm Equation

The BET model [Brunauer et al., 1938] is a multilayer adsorption theory as an extension of the Langmuir model. There are three assumptions in the BET model: 1. adsorbate molecules physically adsorb on a solid in layers infinitely; 2.

there is no interaction between each adsorption layer; and 3. the Langmuir theory can be applied to each layer. The BET isotherm is defined as

$$q = \frac{AC_e x_m}{(C_s - C_e)[1 + (A-1)\frac{C_e}{C_s}]} \tag{1.3}$$

where A is a constant to describe the energy of interaction between the solute and the adsorbent surface, x_m is a constant related to amount of solute adsorbed in forming complete monolayer, and C_s is the saturation concentration of solute.

1.3.2. Adsorption Kinetics

Extensive studies have been conducted on the adsorption kinetic processes of different adsorbates onto different adsorbents. Based on the different sorption mechanisms, there are generally several stages that exist in the adsorption kinetics. Figure 1-5 [Weber et al. 1987] gives one example of the four-steps of adsorption on GAC.

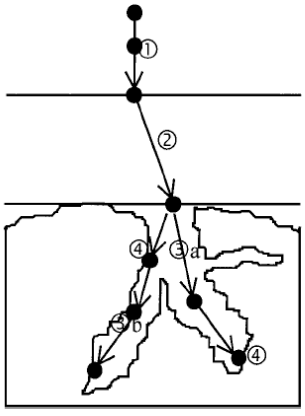

Position	Phenomenon	Coefficient
Bulk of solution	① Diffusion/Convection	Fast
Outer layer	② External Mass Transfer	k_f
GAC particle	③a Porous Diffusion	D_p
	③b Surface Diffusion	D_s
	④ Adsorption	Instantaneous

Figure 1-5. The four steps of adsorption on GAC [Weber et al. 1987].

For the adsorption of miscible VOCs from an aqueous solution using hydrophobic aerogels, Hrubesh et al. [Hrubesh et al., 2001] proposed the following physical model. The water shedding property of the hydrophobic aerogel results in a liquid-solid interface on the surface of the aerogel particles. Since the aerogel pores are open (filled with air), volatile organics from a miscible organic-water solution can transport across the liquid-solid interface to the aerogel pores, vaporize, diffuse in the pores, and be adsorbed on the pore surface. Based on these assumptions, the sorption kinetics should include the following three steps: (1) mass transfer of the organic across the liquid-vapor interface to organic vapor; (2) diffusion of organic vapor into the aerogel pores; and (3) adsorption of the organic on the surface. However, there are no studies reported in the literature about the sorption mechanisms of organic compounds onto hydrophobic aerogels in either the vapor phase or for a pure liquid phase. Also, there are no studies reported in the literature on sorption kinetics. i.e., sorption as a function of time; these data could be used to verify the possible sorption mechanisms of organic compounds onto hydrophobic aerogels in vapor, liquid and solution phases.

There are several kinetic expressions developed and used to describe the kinetics of sorption on a solid surface, such as the pseudo-first order equation [Lagergren, 1898; Ho et al., 1999], the pseudo-second-order equation [Ho et al., 1999], and the intraparticle diffusion model [McKay, 1983], etc. Most these kinetic models are empirical; therefore they do not really discriminate between the influences made by the different adsorption stages, such as a rapid or

instantaneous adsorption stage compared to a rate-limiting adsorption stage [Choi et al., 2007].

The linear driving force (LDF) model, which was originally proposed by Glueckauf and Coates [Glueckauf et al., 1947] for adsorption chromatography, is another type of model frequently used for describing the adsorption kinetics since it is analytical, simple, and physically consistent [Sircar et al., 2000]. This model assumes that the uptake rate of the adsorbate in the adsorbent is proportional to the difference between the concentration of the adsorbate at the outer surface of the sorbent and its average concentration in the interior of the sorbent, and is defined as

$$V\frac{dC}{dt} = -\frac{m}{\rho_P}K(C - C_e') \tag{1.4}$$

$$V\frac{dC}{dt} = -m\frac{dq'}{dt} \tag{1.5}$$

with initial condition

$$t = 0, \quad C(0) = C_0 \tag{1.5a}$$

where K' is the overall adsorption rate constant, ρ_P is the density of the Nanogel, C is the organic concentration in the liquid phase, C_e' is the local equilibrium concentration in the liquid phase corresponding to the adsorbate concentration at the aerogel particle boundary, q' is the mass of organics per unit mass of aerogel in the aerogel particle at time t, and C_0 is the initial organic concentration. In the LDF model, the overall adsorption rate constant, K, can be correlated to the rate

parameters of the different adsorption stages and used to determine the rate-limiting adsorption stage.

1.4. Concept of Liquid-Solid Phase Packed Bed and Inverse Fluidized Bed

1.4.1. Liquid-Solid Phase Packed Bed

In chemical engineering, a packed (or fixed) bed is a hollow pipe, tube, or other vessel filled with a solid packing material. The purpose of a packed bed is typically to improve contact between two phases during a chemical or physical separation or reaction process. Due to the low initial cost and low maintenance costs, packed bed systems are commonly used to perform separation processes in industry, such as absorption, stripping, and distillation, and to carry out chemical reactions involving sold particulates either as a reactant or a catalyst. Packed bed adsorption processes are ubiquitous throughout the chemical process and other industries.

The hydrodynamics of flow through liquid-solid and gas-solid packed beds have been thoroughly studied. Pressure drop in flow through packed beds has been investigated by Furnas [Furnas, 1929], Chilton [Chilton et al., 1931], Leva [Leva, 1949] and Ergun [Ergun, 1952]. A key work in the field was the Ergun equation presented by Ergun [Ergun, 1952] in 1952, which can used to predict the pressure drop along the length of a packed bed given the fluid velocity, the packing size, and the viscosity and density of the fluid. The dispersion phenomena in flow through a packed bed have also been extensively studied. The quantitative treatment of dispersion in a liquid-solid phase packed bed is based on

the use of an equation having the form of Fick's law with using appropriate dispersion coefficients which can be found in several papers in the literature [Lapidus et al., 1952; Chung et al., 1968].

Many studies using packed beds for the adsorption of oil and VOCs from an aqueous phase are also well documented in the literature [Hand et al., 1984; Faust et al., 1987; Noll et al., 1992; Chatzopoulos et al., 1994; Crittenden et al., 1997; Cooney, 1999; Pelech et al., 2006; Cambiella et al., 2006; Zhou et al., 2008]. As the aqueous solution passes through the packed bed column, the organic contaminant is adsorbed by the sorbent and the quality of the effluent is improved. However, packed bed operation has some disadvantages, including dead zones, channeling, and a high pressure drop across the column.

1.4.2. Inverse Liquid-Solid Phase Fluidized Bed

When a liquid is passed through a granular material at a sufficient flow rate to overcome gravity and/or buoyant forces, the granular material is converted from a static solid-like state to a dynamic fluid-like state, and is defined as liquid-solid fluidization. Liquid-solid fluidization systems have been applied extensively in industry for physical, chemical, petrochemical, and biochemical processing, including: classification of particles by size and density; backwashing of granular filters and washing of soils; crystal growth; leaching and washing; adsorption and ion exchange; electrolysis with both inert and electrically conducting fluidized particles; liquid-fluidized bed heat exchangers and thermal energy storage; and bioreactors [Epstein, 2003].

In liquid-solid phase fluidization, when the density of the particulate material is less than the density of the liquid, inverse fluidization, i.e., liquid flowing downward in the column so that drag forces can overcome buoyancy forces, can be applied to disperse the solid particles in the liquid. Inverse fluidization has been applied using a three phase (liquid-solid-gas) reactor in a number of papers for microbiological aerobic or anaerobic wastewater treatment [Garcia-Calderon et al., 1998; Nikov et al., 1999; Kyrst et al., 2001]. In these studies, inert carrier particles are coated with different bacteria strains to from a biofilm, and aerobic and anaerobic conditions are maintained by bubbling either oxygen or nitrogen upward through the inverse fluidized bed reactor.

Aerogel granules have a density much lower than water and are robust enough to be fluidized; they can be configured in an inverse fluidized bed, where the organic-contaminated water flows downward through a distributor and through the bed of particles. The benefits of using inverse fluidization as compared to a more simple packed bed of particles are a low and constant pressure drop when operating above the minimum fluidization velocity, excellent mixing between the solid particles and the liquid (approaching CSTR conditions), high heat and mass transfer rate, an adjustable voidage of the fluidized bed by changing the fluid velocity, and the ability for continuous operation.

One of the key works for the hydrodynamic characterization of liquid-phase fluidization is that of Richardson and Zaki [Richardson et al., 1954], published in 1954, and still applicable today. They found that the settling velocity of the particles or the superficial velocity of a liquid in a fluidized bed divided by

the terminal velocity of a single particle is an exponential function of the void fraction in the bed. Since then, many studies of the hydrodynamic characteristics and bed expansion of inverse liquid-solid and inverse liquid-solid-gas fluidization have been reported in the literature. For examples, Fan et al. [Fan et al., 1982] studied the hydrodynamic characteristics of inverse fluidization in both liquid-solid and liquid-solid-gas systems and proposed the correlations of the bed expansion and gas hold-up for the inverse liquid-solid-gas fluidization system. Karamanev et al. [Karamanev et al., 1992] studied bed expansion characteristics of liquid-solid fluidization using polystyrene and polyethylene spheres of varied sized and densities and verified their experimental results with the Richardson-Zaki equation. Rengannathan et al. [Rengannathan et al., 2005] measured the local void fraction using particles of wide ranging characteristics in a liquid-solid inverse fluidized bed and proposed a correlation for predicting the wall effect corrected experimental terminal velocities. Other interesting studies of hydrodynamic characterization of inverse liquid-phase fluidization can be found in the literatures [Chuang et al., 1963; Ibrahim et al., 1996; Bendict et al., 1998; Lakshmi et al., 2000; Cho et al., 2002; Nikov et al., 2003; Rengannathan et al., 2003; Rengannathan et al., 2004].

Some research has been done on the adsorption behaviors in a liquid-solid fluidized bed. Veerarghavan et al. [Veerarghavan et al., 1989] used granulated activated carbon (GAC) to adsorb phenol from an aqueous feedstock and set up a model to simulate the breakthrough curve of the fluidized bed. This model took into account the effects of axial dispersion in the solid and liquid phases, mass

transfer resistance in the laminar fluid boundary surrounding an individual adsorbent particle, and diffusional resistance within the particle. Wright et al. [Wright et al., 1998] investigated the adsorption of lysozyme by macroporous and hyper-diffusive resins in the liquid-solid fluidized bed, and simulated fluidized bed adsorption by accounting for mass transfer, hydrodynamics and adsorption. Correa et al. [Correa et al., 2006] studied the removal of phenol from wastewaters by adsorption onto polymeric resins in the liquid-solid fluidized bed and used a simple batch adsorption model based on the Freundlich isotherm to predict final phenol concentrations. However, there are no studies to my knowledge, experimental or modeling, reported in the literature to describe the adsorption behavior of silica aerogels in an inverse liquid-solid fluidized bed.

1.5. Project Objectives and Dissertation Organization

1.5.1. Project Objectives

Published literature has shown that hydrophobic silica aerogels might have a high uptake capacity and a high rate of uptake (efficiency) for the adsorption of oil and VOCs from either water or air, and fluidization technology might be used in the adsorption process. However, data on the sorption properties of hydrophobic silica aerogels for free oil, emulsified oil, and VOCs in vapor, liquid and solution phases available in the literature are scarce and there are no studies reported in the literature on using hydrophobic silica aerogel granules to remove emulsified oil and VOCs from aqueous solutions, configured either as a packed bed or fluidized bed.

Therefore, the main objective (Objective (1)) of this dissertation is to provide a systematic study to investigate the performance of hydrophobic, commercially available, silica aerogel (Cabot Nanogel®) granules for removing: a) laboratory prepared emulsified oil (oil-in-water emulsions using a surfactant to disperse the oil), b) oil from real oily wastewater, and c) various VOCs at low concentrations so that they are completely soluble in water, in both packed bed and inverse fluidized bed modes. Other objectives of this work are to study: (2) the hydrodynamic characteristics of the Nanogel granules in the inverse fluidized bed, (3) the performance of Cabot Nanogel to remove free oil or liquid VOCs, e.g, oil floating on water due to an oil spill from a tanker or VOCs spilled during transport, (4) the performance of Cabot Nanogel to remove VOCs in the gas phase and (5) the sorption mechanisms of free oil, emulsified oil and VOCs in vapor, liquid or solution phases onto Nanogel.

Objective 1

In order to investigate the performance of Nanogel granules for removing a) laboratory prepared emulsified oil, b) oil from real oily wastewater, and c) various VOCs at low concentrations, in both packed bed and inverse fluidized bed modes, two size range Nanogels were chosen for study. The breakthrough curve of the packed bed or inverse fluidized bed at different experimental conditions, e.g., flow rate, inlet concentrations, or size of Nanogel particles, will be measured to estimate the adsorption capacity and efficiency. Two models will be established to simulate packed bed and fluidized bed adsorption behavior by

taking into account hydrodynamics, mass transfer, and adsorption at equilibrium, and compared with the experimental results. A parametric sensitivity analysis will be performed to assess the contribution of the following parameters on breakthrough behavior for both the packed bed mode and the fluidized bed mode: the adsorption rate constant, the Freundlich isotherm constants, and the liquid phase axial dispersion coefficient.

Objective 2

In order to investigate the hydrodynamics characteristics of the Nanogel granules in the inverse fluidized bed, several Nanogel particles with different size ranges, shape, and density were chosen for study. The hydrodynamics parameter, pressure drop and bed height will be detected with different superficial velocity. Mathematical models, e.g. the Richardson-Zaki equation, will be used to simulate the expansion of the inverse liquid-solid fluidized bed. The pressure drop data when particles are fully fluidized will be used to calculate the granule density of particles fluidized based on the force balance in the inverse liquid-solid fluidized bed. The granule density of different Nanogel particles measured using the fluidization method will be compared with results from some commercial available method, such as the Geopyc method.

Objective 3

In order to investigate the performance of Nanogel granules to remove free oil or liquid VOCs, three types of oils (vegetable oil, motor oil, and crude oil)

and six liquid VOCs (benzene, toluene, chlorobenzene, trichloroethylene, p-xylene and o-xylene) were chose for study. The sorption process will be monitored using an electronic microbalance for each oil and VOC sample. Sorption kinetics will be investigated and analyzed using the Washburn equation. Sorption capacity will be investigated and compared based on the different properties of each oil and VOC sample.

Objective 4

In order to investigate the performance of Nanogel granules to remove VOCs in the gas phase, five VOCs (benzene, toluene, chlorobenzene, trichloroethylene, and p-xylene) were chose for study. The adsorption kinetics and capacity of these VOCs on Nanogel will be monitored using an electronic microbalance. The adsorption kinetics and capacity of Nanogel will be investigated and compared with other sorbents.

Objective 5

In order to investigate the sorption mechanisms of free oil, emulsified oil and VOCs in vapor, liquid or solution phases onto Nanogel, the properties of Nanogel, e.g., granule density, pore volume, pore size distribution, surface area and contact angle will be measured. Batch sorption equilibrium and kinetic experiments will be conducted for two types of oil-in-water emulsions (vegetable oil and motor oil) using Tween 80 as the surfactant to stabilize the emulsion, six VOC solutions (benzene, toluene, chlorobenzene, trichloroethylene, p-xylene and

o-xylene) and one real oily wastewater sample. The oil emulsion and VOC solution concentrations will be detected either by a Hach colorimeter or by gas chromatography (GC). The adsorption isotherms and kinetics for VOC solutions or oil emulsions will be fitted by the Freundlich equation, and the linear driving force mode, respectively. Four different sorption mechanisms of vapor VOCs, liquid VOCs and oil, VOC solution, and oil-in-water emulsion on Nanogels will be proposed based on the sorption equilibrium and kinetic results.

1.5.2. Structure of the Dissertation

This dissertation mainly consists of five parts, each one addressing and accomplishing the aforementioned objectives. Chapters 2 & 3 address the tasks described in objectives 3-5. Chapter 2 presents the adsorption isotherm and kinetics results for six VOCs on Nanogel in vapor, liquid, and solution phases and three different adsorption mechanisms for the vapor, liquid, and solution phases are proposed. Chapter 3 presents the adsorption isotherm and kinetics results for free oil and emulsified oil on Nanogel and two different adsorption mechanisms are proposed. Chapters 4 & 5 address the tasks described in objective 1. Chapter 4 presents the performance of Nanogel granules for removing emulsified oil in an inverse fluidized bed at different experimental conditions and a model to describe the adsorption behavior of Nanogel in the fluidized bed is proposed. Chapter 5 presents the performance of Nanogel granules for removing toluene from aqueous phases in packed bed and inverse fluidized bed modes at different experimental conditions and two models to describe the adsorption behavior of Nanogel in are

proposed for these two modes. Chapters 6 addresses objective 2, the hydrodynamics characteristics of the Nanogel granules in the inverse fluidized bed and Nanogel density measurements by using the inverse fluidized bed method. Chapter 7 summarizes the work reported in this dissertation and discusses future directions for the adsorption/absorption applications of Nanogel and fluidization technology.

Since the material in Chapters 2, 3, 4, and 5 has either already been published or has been submitted for publication in peer reviewed scientific journals, some of the introductory material in these chapters may repeat what has already been discussed in this first chapter. I have tried to keep repetition to a minimum, but some repetition is necessary for the understanding of each of these individual chapters. Regarding the Nanogel density measurements described in Chapter 6, this work was done as a summer intern at Cabot Corporation in 2010; Cabot specifically requested that this work not be submitted for publication.

CHAPTER 2 ADSORPTION OF ORGANIC COMPOUNDS IN VAPOR, LIQUID, AND AQUEOUS SOLUTION PHASE ON HYDROPHOBIC AEROGELS

2.1. Introduction

As discussed in Chapter 1, due to the desirable properties, different types of hydrophobic aerogels have been studied for the sorption applications. Hrubesh et al. [Hrubesh et al., 2001] have proposed a possible mechanism for the adsorption of miscible VOCs from an aqueous solution using hydrophobic aerogels that includes three steps: (1) mass transfer of the organic across the liquid-vapor interface to organic vapor, (2) diffusion of organic vapor into the aerogel pores, and (3) adsorption of the organic on the surface. However, there are no studies reported in the literature about the sorption mechanisms of organic compounds onto hydrophobic aerogels in either the vapor phase or a pure liquid phase. Also, there are no studies reported in the literature on sorption kinetics. i.e., sorption as a function of time; these data can be used to verify the possible sorption mechanisms of organic compounds onto hydrophobic aerogels in vapor, liquid and solution phases.

Since data on the sorption properties of hydrophobic silica aerogels for organics in vapor, liquid and solution phases available in the literature are scarce, especially for the only commercially available particulate silica aerogel, Cabot Nanogel®, the objectives of the work in this chapter are: (1) to obtain adsorption capacity and kinetic data for hydrophobic Nanogels in vapor, liquid and solution

phases for six common VOCs, (2) to compare the different sorption behaviors for these three cases, and (3) to propose different possible sorption mechanisms for these three cases. The VOCs that were studied are benzene, toluene, p-xylene, o-xylene, chlorobenzene and trichloroethylene.

2.2. Experimental

2.2.1. Adsorbents

The hydrophobic silica aerogels used were Nanogels TLD-301 (0.7-1.2 mm size range) and sieved TLD-302 (1.7-2.35 mm size range) supplied by Cabot Corporation.

2.2.2. Adsorbates

The VOCs used in this study: benzene, toluene, p-xylene, o-xylene, chlorobenzene and trichloroethylene (TCE) were all purchased from Sigma-Aldrich as anhydrous reagent grade.

2.2.3. Vapor Phase Adsorption Experiments

Adsorption and diffusion experiments were conducted on a Cahn electronic microbalance system (Cahn D-101) as shown in Figure 2-1. One arm of the microbalance had a stainless-steel pan suspended at its end to hold the aerogel sample. The pan was attached to the microbalance arm by a platinum wire (Gauge 36, Fisher Scientific). The temperature of the sample pan was

maintained at room temperature (25 ℃) with a temperature controller (Omega CN 7600) connected to a tubular furnace mounted on the outside of the 2 inch i.d. Pyrex balance tube. The furnace was mounted so that the sample pan was exactly at its center. The temperature of the sample pan was monitored by a thermocouple (K-type Omega K-72-SRTC).

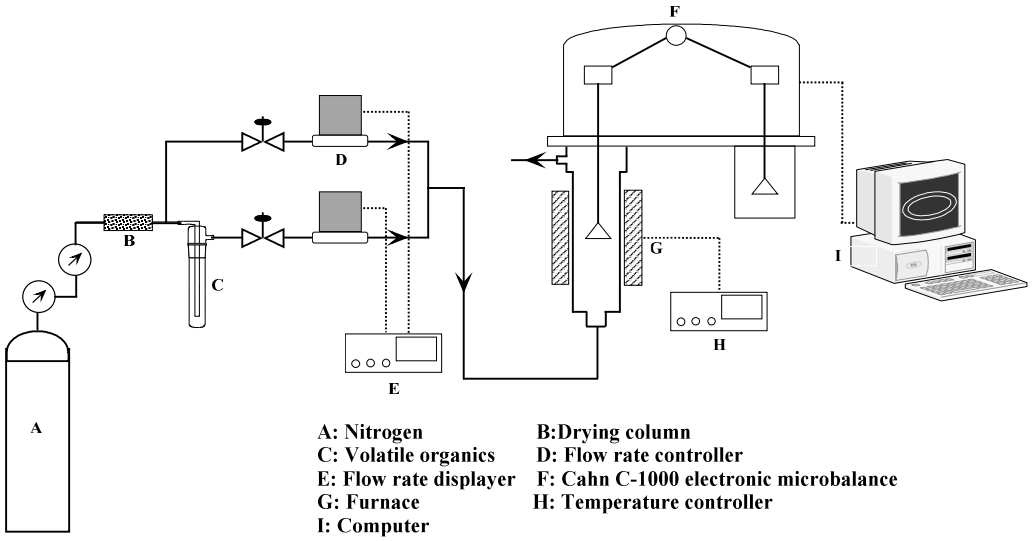

Figure 2-1. Schematic diagram of Cahn microbalance system for studying organic vapor adsorption on Nanogel.

During the experiment, about 20-30 mg of Nanogel TLD-301 sample was held in the stainless steel sample pan and degassed at 200 ℃ for 2 hours under N_2 purge flow at 100 mL/min. After the sample weight became constant, the temperature was cooled to room temperature. Then, the adsorption process started by sending the purge gas N_2 saturated with a specific VOC through the tube of the microbalance. The transient and equilibrium weight changes were recorded using a computer-aided data acquisition system. The adsorption uptake of organics on aerogel was calculated as follows:

$$q_e = \frac{m_e - m_{Nanogel}}{m_{Nanogel}} \tag{2.1}$$

$$q_t = \frac{m_t - m_{Nanogel}}{m_{Nanogel}} \tag{2.2}$$

where m_{Nanogel}, m_{t}, and m_{e} are the weight of Nanogels at the initial time, time t, and at equilibrium in the experiment, respectively, and q_{e} and q_{t} are the weight of adsorbed organic per gram at equilibrium and at time t, respectively. The change of the organic liquids in the tube (C in Figure 2-1) was also measured with time to assure that the gas flow is indeed saturated with the specific organic vapor.

2.2.4. Liquid Phase Absorption Experiments

The absorption kinetic and capacity experiments were conducted on a Cahn electronic microbalance system (Cahn D-101) by placing the Nanogel TLD-302 samples in a mesh basket hung under a weighing wire as shown in Figure 2-2. The elevating platform was then raised to allow aerogel to come in contact with the organic liquid through the air/liquid interface. The weight change data were collected by computer connected to the microbalance. In these experiments it was more convenient to use the larger TLD-302 Nanogel granules as the sorbent.

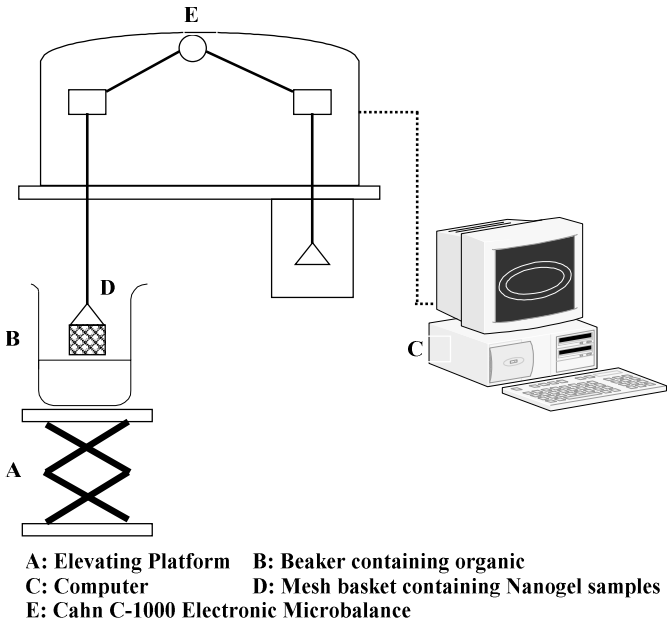

Figure 2-2. Schematic diagram of Cahn microbalance system for studying adsorption of pure liquid on Nanogel.

2.2.5. Solution Phase Adsorption Experiments

To determine the adsorption isotherm of the Nanogels, batch adsorption experiments were conducted using 120 mL glass bottles with addition of 100 mg of TLD-301 Nanogels and 100 mL of adsorbate solutions of different initial concentrations. The concentrations of these adsorbate solutions were lower than their solubility limit in water to prevent the formation of two phases. The glass bottles were sealed with 20 mm stoppers to prevent vapor from escaping and shaken in a shaker (Innova 4080 incubator shaker) at room temperature and 200 rpm. Upon reaching equilibrium (about 3 hours), all the samples were withdrawn and analyzed using a gas chromatograph (GC) equipped with a flame ionization detector (SRI 8610C). Blank experiments, without the addition of Nanogel, were also conducted to ensure that the decrease in concentration measured was actually

caused by adsorption rather than volatilization of the VOCs. In batch equilibrium experiments, the mass of adsorbate adsorbed per unit mass of adsorbent, q, is determined by

$$q = \frac{V(C_0 - C_e)}{m} \tag{2.3}$$

where V is the volume of the treated solution, m is the mass of Nanogels used in the experiments, and C_0 and C_e are the initial and equilibrium concentrations of the solution, respectively.

Batch kinetic experiments were also conducted at room temperature. A sealed glass bottle containing 100 mL adsorbate solution of a desired concentration was continuously mixed with 100 mg of TLD-301 Nanogels using a magnetic stirrer (Cimarec). The adsorbate concentration of the liquid sample was measured by the GC at different time intervals. The experiment was stopped when the concentration approached the equilibrium concentration.

2.3. Results and Discussion

2.3.1. Vapor Phase Adsorption

Figure 2-3 shows the fractional adsorption curves (q_t/q_e) of five VOCs on Nanogel TLD-301 samples. The values of the equilibrium adsorption capacity (q_e) and the "half time" when the weight of organic adsorbed is equal to half of the equilibrium adsorption capacity of Nanogel for these compounds are listed in Table 2-1. As shown in Figure 2-3, the adsorption kinetics of these five organics is relatively slow, e.g., 3 hours for benzene and as long as 26 hours for

chlorobenzene before q_t/q_e approaches unity, which is much slower than the kinetics for common gas phase adsorption. However, this slow adsorption kinetics has also been found by Standeker et al. [Standeker et al., 2009] for toluene adsorption on their laboratory synthesized hydrophobic aerogels when configured as a packed bed column (5 hours for the outlet concentration to approach the inlet concentration). Gas diffusion into the pores of the aerogel of about 15 nm is governed by Knudsen diffusion, with a diffusivity of about 0.01 cm^2/s for those organic compounds. Using a characteristic radius of about 1 mm for the aerogel particles, the characteristic time for gas diffusion should be around 1 s. Thus, the adsorption process is most likely controlled by another mechanism.

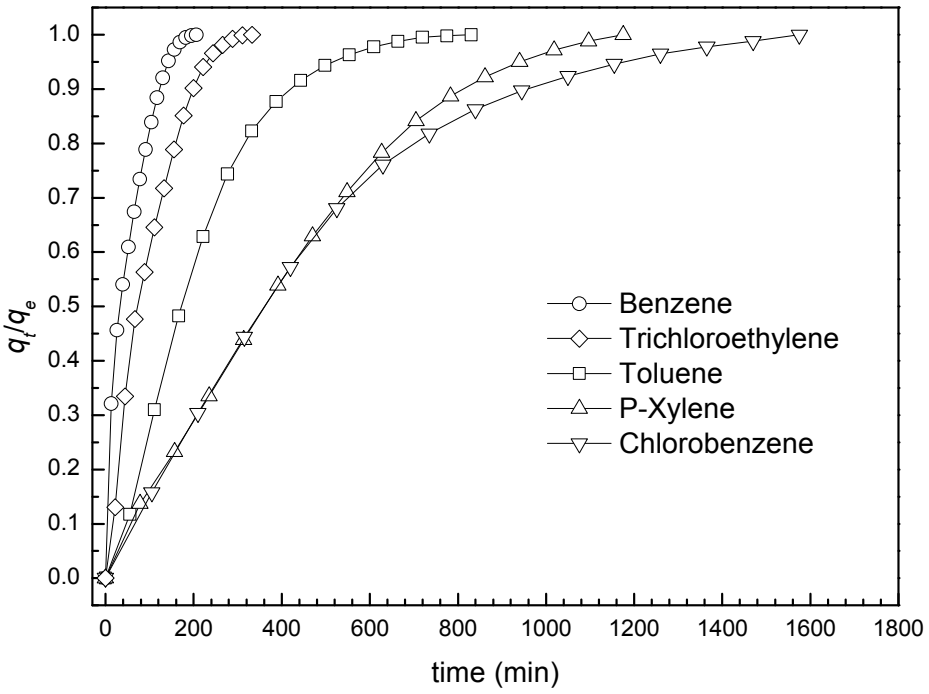

Figure 2-3. Adsorption of organic vapors on Nanogel TLD-301 by Cahn C-1000 Electronic Microbalance.

Table 2-1. *The adsorption capacities, half time and the thermal conductivity of five VOCs in the vapor phase adsorption experiments*

Organic compound	Benzene	Toluene	P-Xylene	Chlorobenzene	TCE
Adsorption capacity (g/g)	0.49	1.56	1.39	1.93	1.77
Half time (min)	32	172	360	361	72
Thermal conductivity k (W/m·K)[19]	0.147	0.135	0.132	0.130	---

Compared to other solid adsorbents, silica aerogel has a much lower thermal conductivity (about 0.009 W/m·K for Nanogel, as compared to 0.9 W/m·K for glass). The slow adsorption kinetics is most likely due to the very low thermal conductivity of aerogel during gas adsorption. The adsorption of organic compounds onto Nanogel can be described by the following mechanism: (1) the organic vapors diffuse and are adsorbed into the pores of the aerogel, (2) heat is released during the exothermal adsorption process and kept in the aerogel particle due to its poor thermal conductivity, (3) the temperature in the aerogel particle increases lowering the equilibrium amount of organics adsorbed, and (4) the temperature decreases in the aerogel particles as the heat is slowly released, increasing the equilibrium adsorption rate and adsorption continues.

Non-isothermal adsorption of vapor on solid particles has been studied in the literature [karger et al., 1992]. These models however consider simultaneous mass and heat transfer on the solid sorbent with high thermal conductivity (assuming uniform temperature in the solid, with heat transfer controlled by the particle surface external heat transfer coefficient). The modeling results show that the heat effect slows the adsorption updates. In the present case, the heat transfer

is more likely controlled by the heat conduction within the aerogel particle due to its much lower thermal conductivity. Modeling of combined mass and heat transfer during the adsorption of organics on aerogel particles is possible assuming spherical geometry for the complex aerogel particles but it is beyond the scope of the present work. However, the slow adsorption uptake rates can be explained qualitatively by comparing the thermal diffusivity with the mass diffusivity in the aerogel particles.

The thermal diffusivity of an aerogel particle is given as

$$\alpha = \frac{k}{\rho C_P} \tag{2.4}$$

where k is the thermal conductivity of Nanogel (0.009 W/m·K), ρ is the density of Nanogel (125 kg/m^3), and C_P is the specific heat capacity of Nanogel (1.15 kJ/kg·K). Therefore, the value of the thermal diffusivity of Nanogel is around order of 10^{-8} m^2/s. Since the mass diffusivity in Nanogel particles is about 10^{-6} m^2/s, the thermal diffusivity is about 100-1000 times smaller than the mass diffusivity; thus, the adsorption uptake is controlled by heat-conduction in the particles.

The actual thermal conductivity of the Nanogel particles during adsorption of vapor is influenced by the adsorbed organic phase. Assuming the thermal conductivity of the organic in the adsorbed phase is the same as that for the liquid phase; it turns out that the lower the thermal conductivity of the organic liquid, the lower the average thermal conductivity inside the Nanogel particles, and the slower the adsorption. The values of the thermal conductivity for the five VOC

liquids are listed in Table 2-1 cited from reference [Miller et al., 1976]. As seen, the thermal conductivity of four of the VOCs studied decrease in the following order: benzene > toluene > p-xylene > chlorobenzene, which agrees with the experimental observations, i.e., the adsorption rate (half time) decreases in the same order, i.e., lowest for benzene. Therefore, the hypothesis presented above seems to be reasonable.

Table 2-2. *Comparison of adsorption capacities of five different adsorbents used for adsorption of organic vapors*

Adsorbent	Adsorption capacity (g/g)		
	Benzene	Toluene	P-Xylene
Nanogel	0.49	1.56	1.39
TMOS-Aerogel*	0.96	0.91	1.03
TMES-Aerogel*	0.71	0.81	0.70
Silica gel*	0.65	0.65	0.60
Activated carbon*	0.34	0.37	0.35

* Data from Standeker et al. [Standeker et al., 2009]

The adsorption capacities of Nanogel and the comparison between Nanogel and other sorbents used as adsorbents of organic vapors are given as Table 2-2. As seen in this table, the adsorption capacities of Nanogel for these organics increase in the following order: Benzene < P-Xylene < Toluene < Trichloroethylene < Chlorobenzene with relatively large adsorption capacities in the range of 0.49 to 1.93 g adsorbate per gram of Nanogel. It should be noted that this comparison is not made under the same conditions, i.e., the partial pressure of these VOCS in N_2 are different since their vapor pressure are quite different. Also, it can be seen in Table 2-2 that the adsorption capacity of Nanogel is higher

than that of the two hydrophobic aerogels used by Standeker et al. [Standeker et al., 2009] and much higher than that of the two commercial sorbents (silica gel and activated carbon) for toluene and xylene. However, for benzene, the adsorption capacity of Nanogel is lower than that of the two Standeker et al. hydrophobic aerogels and silica gel, but higher than that of activated carbon.

2.3.2. Liquid Phase Absorption

Figure 2-4 shows the experimental results for sorption of six VOC liquids on Nanogel TLD-302. As seen in this figure, during the absorption, Nanogel reaches saturation in a very short time (< 30 s) for all six VOC liquids. It should be noted that the heat of adsorption for liquid adsorption has a much lower effect on the adsorption rate than for the vapor adsorption on Nanogel. This is because the thermal conductivity of organic liquids is about 100-1000 times larger than the thermal conductivity of the Nanogel. When the Nanogel particles are brought in conduct with the liquid, heat generated during the adsorption dissipates away quickly through the liquid phase. Therefore the temperature of the aerogel particle remains fairly constant during liquid adsorption and the adsorption rate is controlled by the mass transport process.

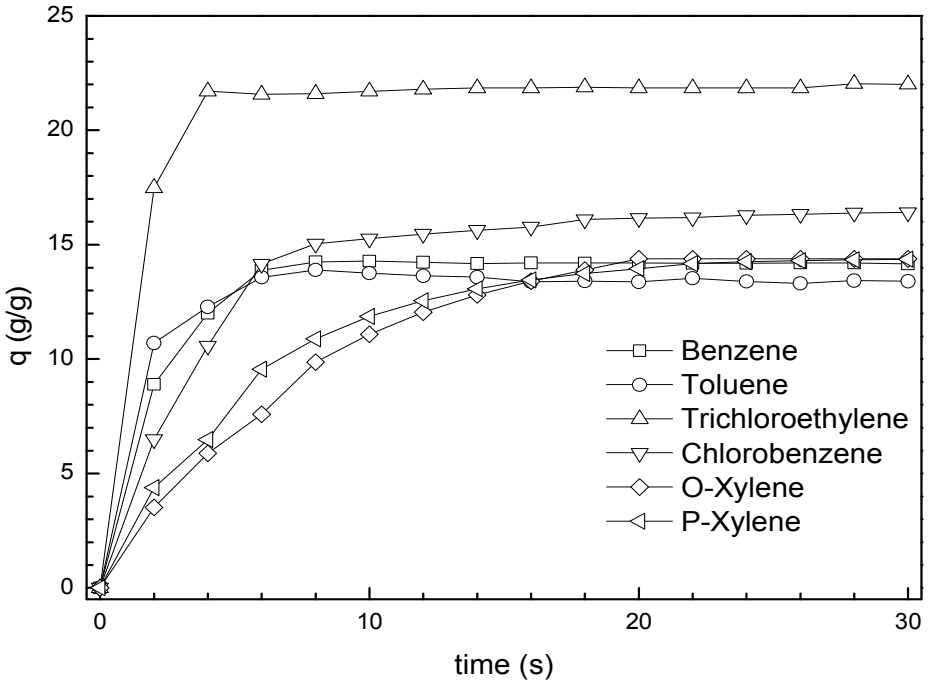

Figure 2-4. Sorption of organic liquids on Nanogel TLD-302 by Cahn C-1000 Electronic Microbalance.

The mechanism of sorption of liquid organics on aerogels is thought to be due to viscous flow of liquid sucked into the pores of the aerogel due to the capillary force, which can be described using the Washburn equation

$$L^2 = (\frac{\gamma}{\eta}\frac{\cos\theta}{2})rt = Art \tag{2.5}$$

where t is the time for a liquid of viscosity η and surface tension γ to penetrate a distance L into a wettable, porous material whose average pore radius is r. By using Equation (2.5), the theoretical absorption time for the six organics was calculated and listed in Table 2-3. In the calculation, the distance L was assumed as the average radius of aerogel particles (0.95 cm) and the average pore radius r of the Nanogels was taken as 7.5 nm based on BET experiments. As shown is

Table 2-3, the values of the theoretical absorption time are close to the experimental values for these six organic liquids.

Table 2-3. *Sorption time and sorption capacity of six VOCs in liquid phase on Nanogel TLD-302*

Organic compound	γ (N/m)	η (Pas)	t (s) Eq. (2-4)	t (s) Experiment	Sorption Capacity (g/g)
Benzene	2.85×10^{-2}	5.50×10^{-4}	3.5	6	14.3
Toluene	2.89×10^{-2}	6.08×10^{-4}	3.8	8	13.6
P-Xylene	2.78×10^{-2}	6.21×10^{-4}	4.0	20	14.4
O-Xylene	3.01×10^{-2}	7.59×10^{-4}	4.6	20	14.4
Chlorobenzene	3.30×10^{-2}	7.53×10^{-4}	4.1	12	16.7
TCE	2.87×10^{-2}	5.30×10^{-4}	3.3	4	22.3

It also can be seen in Figure 2-4 that Nanogel granules absorb organic liquids around 14 to 23 times its own mass. If the sorption capacity is expressed in units of mL/g, the volumetric sorption capacities of aerogel for the six organic liquids are all around 16 as shown in Figure 2-5. The density and porosity of Nanogel are around 0.125 g/mL and 0.95, respectively, and if the pores of Nanogel are filled up with organic liquid, the theoretical volumetric absorption capacity should be equal to 7.6, which is about half of the measured value of 16. However, during the absorption, when Nanogel granules are contacted with the organic surface, not only the pores of Nanogel, but also the inter-particle spaces between Nanogel particles become occupied by the organic liquids. Since the voidage of the Nanogel granules is roughly 50%, the measured volumetric sorption capacities of around 16 are reasonable.

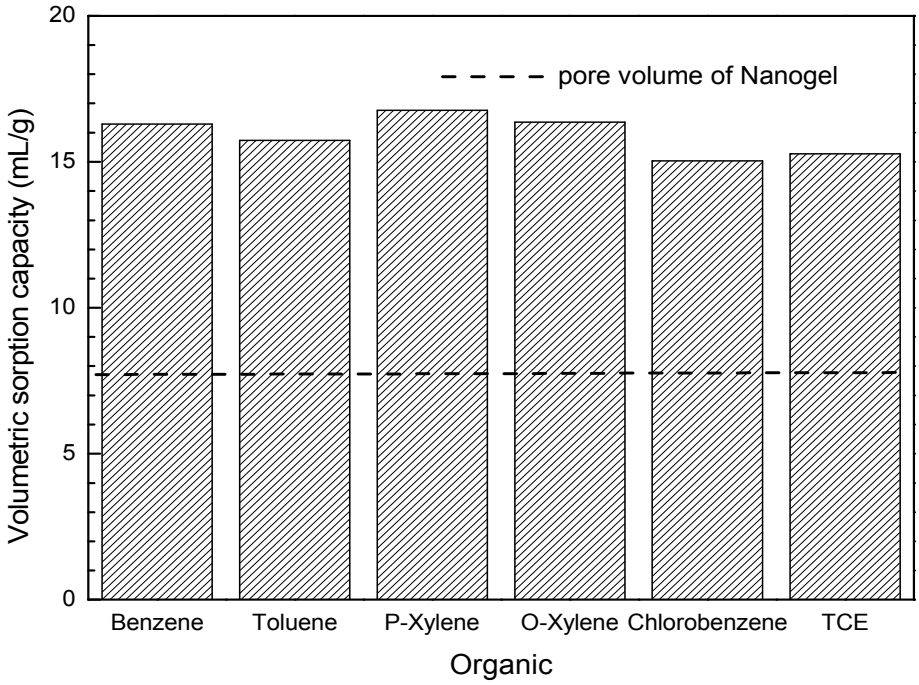

Figure 2-5. Volumetric sorption capacity of six organic liquids on Nanogel TLD-302.

2.3.3. Solution Phase Absorption

Figure 2-6 shows the comparison of the adsorption isotherms for six VOCS miscible in water on aerogels. As shown in this figure, the adsorption capacities for these organics increase in the following order: benzene < trichloroethylene < toluene < chlorobenzene < p-xylene and o-xylene.

The adsorption capacity of an adsorbent for an adsorbate is dependent on both the properties of the adsorbent and the adsorbate. On the adsorbate side, molecular structure, solubility etc., all affect the capacity. Generally, an increasing solubility of the solute in the liquid carrier decreases its adsorbability, and large molecules are more easily adsorbed than small molecules of similar chemical nature [Eckenfelder, 2000]. For the monoaromatic hydrocarbon compounds benzene, toluene, p-xylene and o-xylene (BTX), the solubility

decreases with increasing molecular weight. The adsorption isotherm data are plotted on arithmetic coordinates in Figure 2-6. As can be seen in Figure 2-6a, the adsorption capacity of aerogel for BTX increases with increasing molecular weight and decreasing solubility, which is in agreement with the general rule. Figure 2-6b also shows that the adsorption capacity of aerogels for chlorobenzene is higher than that of trichloroethylene.

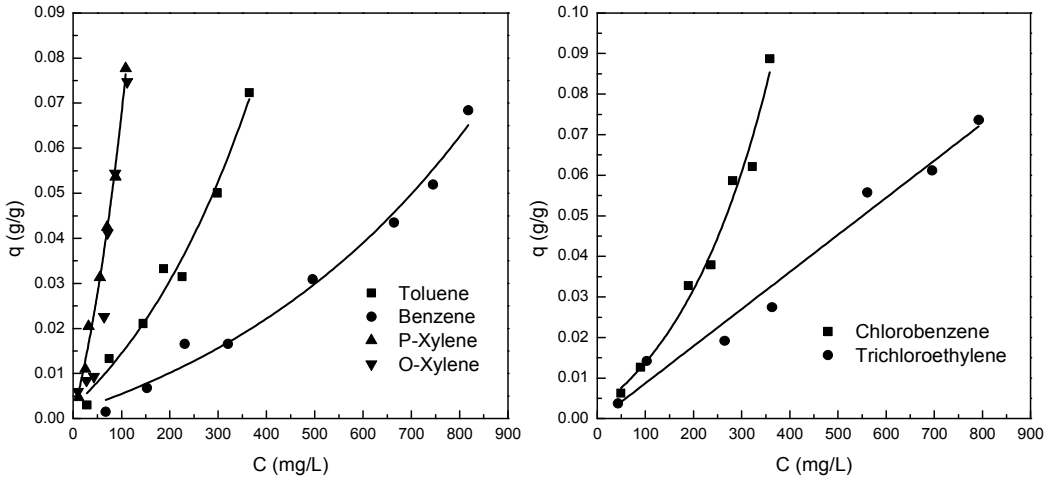

(a) (b)

Figure 2-6. Adsorption isotherms for six miscible organics from aqueous solution on Nanogel TLD-301: arithmetic scale adsorption comparison: (a) benzene, toluene, p-xylene and o-xylene, and (b) chlorobenzene and trichloroethylene.

The Freundlich adsorption model [Freundlich, 1926] was used to fit the adsorption isotherm data since it takes into account the heterogeneity of real surfaces for adsorption. The Freundlich isotherm is defined by Equation (1.2). Figures 2-7a and 2-7b show the adsorption isotherm data plotted in the form of the Freundlich adsorption model (Equation (1.2)). The Freundlich constants, k and $1/n$, are determined from the slope and intercept of the best-fit straight lines through the data points. A summary of the Freundlich parameters is presented in Table 2-4. It is widely recognized [Sontheimer et al., 1988] that a change of the

isotherm concentration ranges may require adjustment of the *k* and 1/*n* Freundlich constants, therefore it should be noted that the *k* and 1/*n* values shown in Table 2-4 are only applicable for the listed concentration ranges.

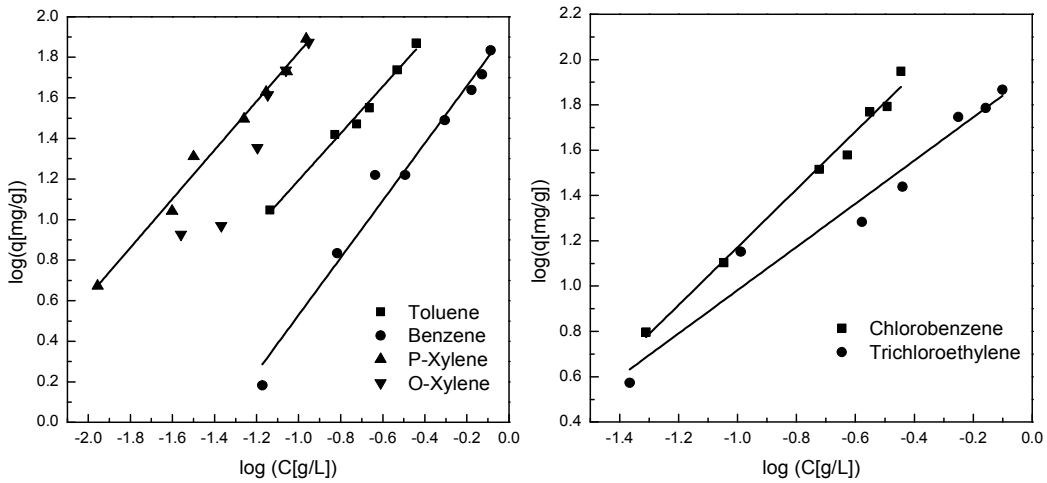

(a) (b)

Figure 2-7. Freundlich isotherms for adsorption of six miscible organics from aqueous solution on Nanogel TLD-301: (a) benzene, toluene, p-xylene and o-xylene, and (b) chlorobenzene and trichloroethylene.

Table 2-4. *Freundlich isotherm parameters for the adsorption of six VOCs on Nanogel TLD-301*

Organic compound	Freundlich isotherm parameters			
	k (mg g^{-1} $(g/L)^n$)	$1/n$	R^2	C_e range (mg/L)
Benzene	87	1.4	0.976	60-820
Toluene	223	1.15	0.987	60-370
P-xylene	1064	1.20	0.988	5-120
O-xylene	582	1.09	0.921	5-120
Chlorobenzene	281	1.28	0.989	40-360
Trichloroethylene	86	0.95	0.961	40-800

In order to compare the organic adsorption capacities of aerogel with other sorbents throughout the measurement range, the adsorption capacities of benzene and toluene at the concentrations below their aqueous solubility are compared in Figure 2-8. There are three papers in the literature [Hrubesh et al., 2001; Novak

et al., 2005; Standeker et al., 2007] from two research groups that report equilibrium adsorption isotherms for organic compounds dispersed in water using different types of hydrophobic silica aerogels. Both of these research groups synthesized their hydrophobic silica aerogels in their own laboratories using supercritical drying, Hrubesh et al. [Hrubesh et al., 2001] used silica aerogels doped with 30% by weight of a fluoro-methyl containing alkoxide while Standeker et al. [Standeker et al., 2007] and Novak et al. [Novak et al., 2005] prepared super hydrophobic silica aerogels using methyltrimethoxysilane (MTMS) or trimethyltethoxysilane (TMES) as precursors. However in reference [Hrubesh et al., 2001], the concentrations of the organic compounds used (except for ethanol) are much higher than their solubility limit in water, i.e., two phases existed instead of a single phase homogenous solution. Therefore, only the data for MTMS-aerogel and TMES-aerogel from literatures [Novak et al., 2005; Standeker et al., 2007] are used in the comparison. The data for activated carbon (AC-F400) and polymeric resin (XAD2) are from Simpson et al. [Simpson et al., 1993], since the adsorption capacity data provided in this study used concentration ranges similar to the ranges used for our own data.

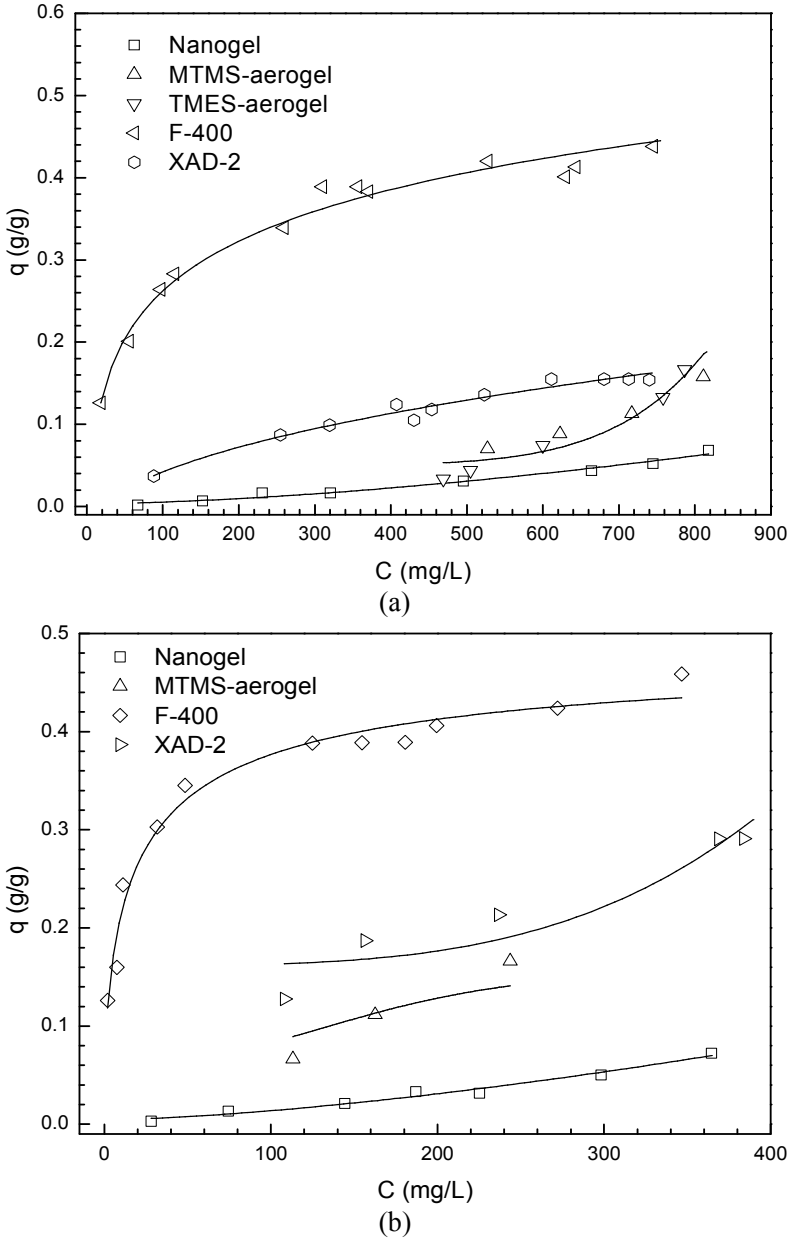

Figure 2-8. Comparison of the adsorption isotherms of (a) benzene and (b) toluene from aqueous solution on different sorbents.

As can be seen in Figure 2-8, the adsorption capacity of commercially produced aerogel is slightly lower than that of the MTMS-aerogel and TMES-aerogel used by Standeker et al. and Novak et al. [Novak et al., 2005; Standeker et al., 2007], and much lower than that of GAC and polymeric resin for benzene and

toluene. One possible reason for the lower adsorption capacity of Nanogel compared with MTMS-aerogel and TMES-aerogel might be because these three aerogels are quite different in structure. For example, the contact angle of the MTMS-aerogel and TMES-aerogel are 173 ^{o} and 180 ^{o}, respectively, which are much higher than that of Nanogel (130^{o}~140^{o}), indicating a higher hydrophobicity, and this certainly will affect the adsorption capacity. For aqueous solutions of benzene and toluene, the data show that activated carbon (AC-F400) and polymeric resin (XAD2) are much better sorbents than hydrophobic aerogels.

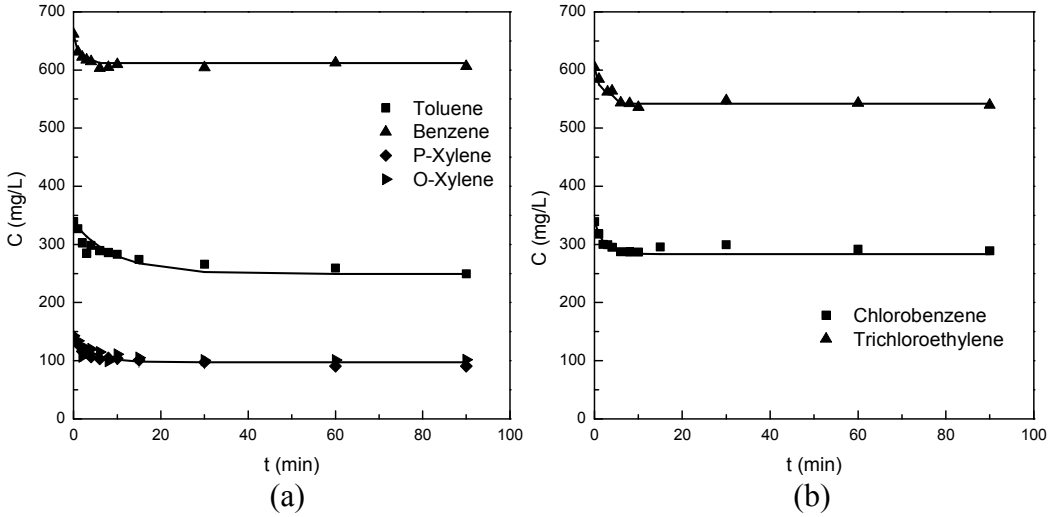

Figure 2-9. Adsorption kinetic results for six miscible organics on Nanogel TLD-301: (a) benzene, toluene, p-xylene and o-xylene, and (b) chlorobenzene and trichloroethylene.

Figure 2-9 shows the experimental results for the adsorption kinetics of the six miscible organics on Nanogel. As shown in this figure, the adsorption reaches equilibrium in a short time (~20 min) for each organic studied. Similar to adsorption of pure organic liquids, heat effects for the adsorption of organic

compounds from aqueous solution are minimal due to the large thermal conductivity of the liquid and the Nanogel particles are well dispersed in the liquid phase. The adsorption rate is also controlled by the mass transport with a mechanism different from the mass transport during adsorption of pure liquid on Nanogel.

In order to compare the adsorption kinetics of organics on aerogel with other traditional sorbents, the adsorption kinetics of different sorbents for benzene and toluene are plotted in Figure 2-10. The particle and pore properties of these sorbents are also listed in Table 2-5. Figure 2-10 shows that hydrophobic silica aerogel has the fastest adsorption kinetics for the adsorption of benzene and toluene from their aqueous solution and GAC kinetics are the slowest.

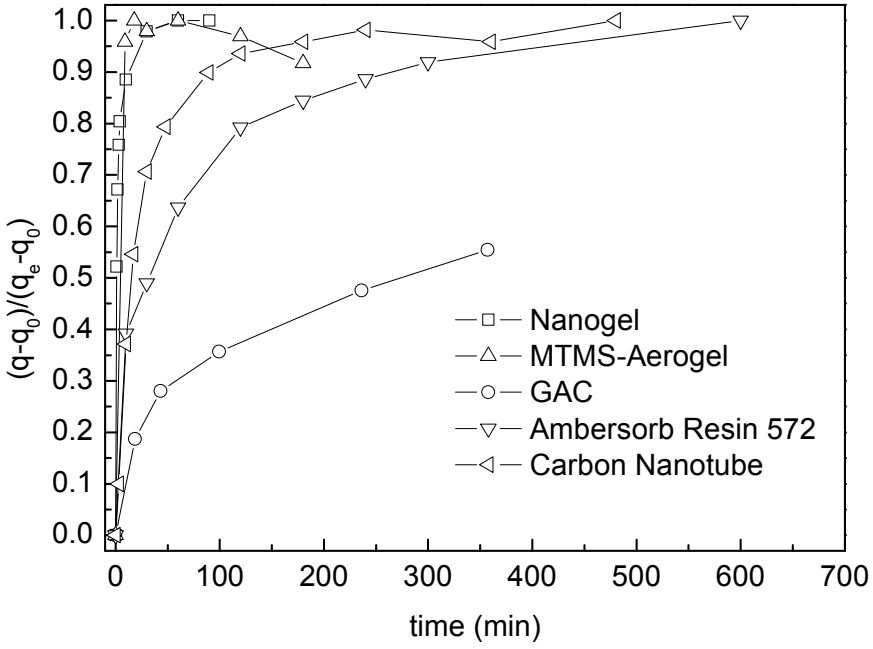

(a)

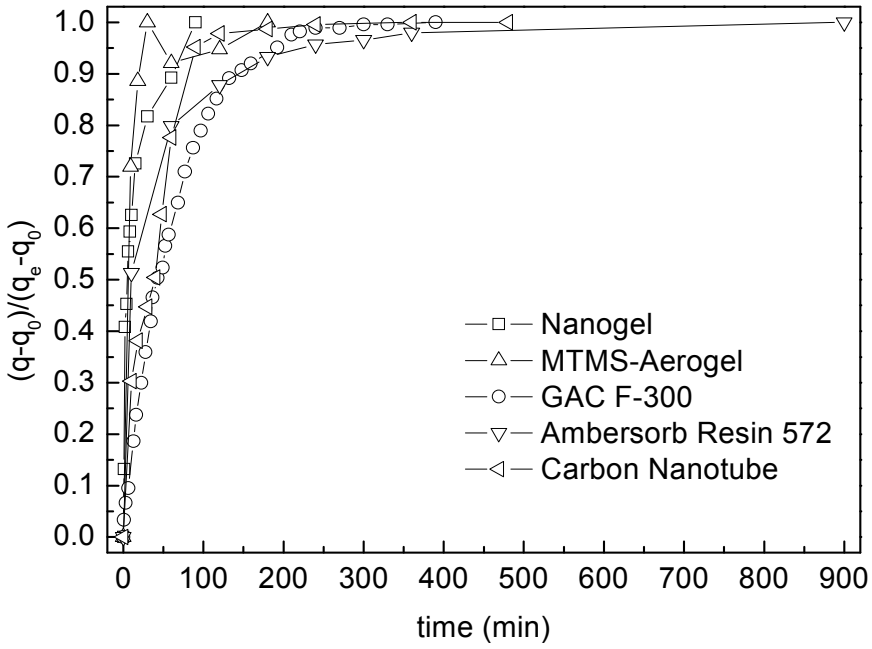

(b)

Figure 2-10. Comparison of the adsorption kinetics of (a) benzene and (b) toluene from aqueous solution on different sorbents.

Table 2-5. *Particle and pore properties of sorbents in Figures 2-8 and 2-10*

Sorbent	Reference	Particle size (mm)	Pore size (nm)	Surface area (m^2/g)	Pore volume (cm^3/g)
Nanogel	This work	0.7-1.2	15.7	686	7.05
MTMS-Aerogel	Standeker et al., 2007	<0.25	4.8	-----	-----
GAC-F300	Chatzopoulos et al., 1995	0.998	< 2 nm	970	0.890
GAC-F400	Simpson et al., 1993	0.38-1.4	-----	1075	0.62
Polymeric Resin XAD-2	Simpson et al., 1993	0.25-1.4	-----	330	0.69
GAC	Choi et al., 2007	-----	-----	-----	-----
Ambersorb Resin 572	Lin et al., 1999	0.27-0.83	Microporous	1100	-----
Carbon Nanotube	Su et al., 2010	-----	Microporous	-----	-----

As mentioned in the introduction section, Hrubesh et al. [Hrubesh et al., 2001] proposed a physical model for sorption of organics from water on hydrophobic aerogel. The water shedding property of the hydrophobic aerogel results in a liquid-solid interface on the surface of the aerogel particles. Since the aerogel pores are open (filled with air), volatile organics from a miscible organic-water solution can transport across the liquid-solid interface to the aerogel pores, vaporize, diffuse in the pores, and be adsorbed on the pore surface. Based on this assumption, the sorption kinetics should include the following three steps: (1) mass transfer of the organic across the liquid-vapor interface to organic vapor, (2) diffusion of organic vapor into the aerogel pores, and (3) adsorption of the organic on the surface. The three-step-in-series rate process can be described by the linear driving force (LDF) model [Glueckauf et al., 1947], as discussed in *1.3.2*. This model assumes that the uptake rate of the adsorbate in the adsorbent is proportional to the difference between the concentration of the adsorbate at the outer surface of the sorbent and its average concentration in the interior of the sorbent, and is defined by Equations (1.4 and 1.5).

Figure 2-11 shows the plot used to determine the overall adsorption rate constant K for chlorobenzene in a batch kinetic experiment. As seen in this figure, the solution C' and C_{en}' can be compared with experimental data to obtain the overall adsorption rate constant K by means of a least squared regression. The results are given in Table 2-6. The overall adsorption rate constant, K, can be correlated to the rate parameters for the three steps mentioned above by the following equation [Ruthven, 1984]

$$\frac{1}{K} = \frac{R_p}{3k_{lv}} + \frac{R_p^{\,2}}{15\varepsilon_P D_k} + \frac{1}{k_a} \tag{2.6}$$

where k_{lv} and k_a are the liquid-vapor phase mass transfer coefficient for the volatile organic and the sorption rate constant on the internal pore surface, respectively, R_p is the Nanogel particle radius, ε_P is the Nanogel porosity, and D_k is the Knudsen diffusion coefficient, which can be calculated from the Nanogel pore size, temperature and molecular weight of the organic [Butt, 2000]. By comparing the values of $1/K$, $R_P/3k_{lv}$, and $R_P^2/15\varepsilon_P D_k$, the potential rate controlling step during the adsorption process can be determined.

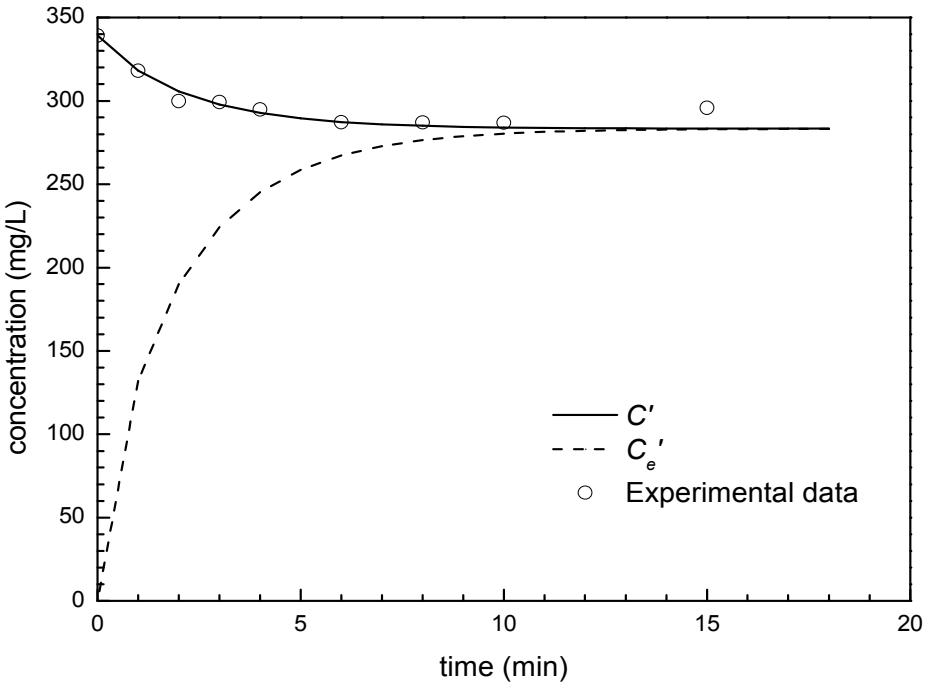

Figure 2-11. Chlorobenzene concentration as a function of time in a batch kinetic experiment: C' and C_e' are obtained from the linear driving force model when K' is 0.183 s^{-1}.

Table 2-6. *Values of parameters in Equation (2.6)*

Organic compound	K (s^{-1})	$1/K$ (s)	$R_P/3k_{lv}$ (s)	$R_P^2/15\varepsilon_P D_k$ (s)	$1/k_a$
Benzene	0.215	4.65	2.42	1.12×10^{-2}	2.2188
Toluene	0.284	3.52	2.64	1.22×10^{-2}	0.8678
P-Xylene	0.164	6.10	2.67	1.31×10^{-2}	3.4169
O-Xylene	0.158	6.33	2.39	1.31×10^{-2}	3.9269
Chlorobenzene	0.183	5.46	2.62	1.35×10^{-2}	2.8265
Trichloroethylene	0.145	6.90	2.54	1.46×10^{-2}	4.3454

In Equation (2.6), k_{lv} was calculated by using the following correlation [Cussler, 1997]

$$\frac{k_{lv}d_P}{D} = 0.31\left(\frac{d^3 g\Delta\rho/\rho}{v^2}\right)^{1/3}\left(\frac{v}{D}\right)^{1/3} \tag{2.7}$$

where d_P is the pore size of areogelparticle, $\Delta\rho$ is the density difference between gas and liquid, D is the dilute diffusion coefficient of organic in water, g is the accelaration due to gravity, and v is the kinematic viscosity.

The Knudsen diffusion coefficient, D_k, was calculated by using Equation (2.8):

$$D_k = \frac{4850 d_P T^{1/2}}{M_w^{1/2}} \tag{2.8}$$

where T is the temperature, and M_w is the molecular weight of the organic.

The values of $1/K$, $R_P/3k_{lv}$, and $R_P^2/15\varepsilon_P D_k$ in Equation (2.6) for the six organics studied were calculated and are listed in Table 2-6. As seen in the table, the value of $R_P/3k_{lv}$ and $1/k_a$ is of the same order of magnitude as the value of $1/K$, while the value of $R_P^2/15\varepsilon_P D_k$ is much less than the value of $1/K$, which indicates that step (1) and (3) of this adsorption model, mass transfer of the organic across

the liquid-vapor interface to organic vapor, and adsorption of the organic on the surface might be the rate controlling steps.

2.4. Conclusions

The rate for adsorption of organic compounds in the liquid, solution and vapor phase on aerogels is very different, with the update time in the order of about 100 min for vapor, 10 min for solution and 10 sec for liquid. The slowest rate of adsorption for vapor is due to the fact the aerogel has an extremely low thermal conductivity and therefore the adsorption process is controlled by the slow dissipation of the heat generated during adsorption. Effects of heat of adsorption are minimal for the adsorption in the liquid and solution phases due to enhanced heat conduction facilitated by the liquid phase. The adsorption in these two cases is controlled by the mass transport of the VOCs, either by capillary flow for the adsorption of liquid or vapor diffusion/adsorption for the adsorption from water solution.

Equilibrium capacity of the adsorption of vapor on aerogel increases in the order: benzene < p-xylene < toluene < trichloroethylene < chlorobenzene. The adsorption capacity of the commercial aerogel studied in the work in this chapter is higher than that of two other hydrophobic aerogels that were synthesized in the laboratory using supercritical drying, and much higher than that of two commercial sorbents (silica gel and activated carbon) for toluene and xylene, and the adsorption capacity of Nanogel is lower than that of the two other hydrophobic aerogels and silica gel but higher than that of activated carbon for

benzene. The volumetric sorption capacities of the six VOC liquids on Nanogel are all around 16 mL/g. This very high uptake capacity and high rate of uptake indicates that Nanogel or other hydrophobic silica aerogels can potentially be effectively used to clean up organic liquids in case of accidental spillage during the transportation of organic liquids on roads or in rivers and sea water, as long as the organic liquids remain floating on the surface of the water. The equilibrium adsorption capacities for the VOCs from aqueous solution increase in the following order: benzene < trichloroethylene < toluene < chlorobenzene < p-xylene and o-xylene.

CHAPTER 3 ADSORPTION OF OILS FROM PURE LIQUID AND OIL-WATER EMULSION ON HYDROPHOBIC SILICA AEROGELS

3.1. Introduction

As discussed in Chapter 1, oil pollution has become one of the most serious global environmental issues during the last 30 years. As a novel sorption material, different types of hydrophobic aerogels have been studied for the sorption applications, as proposed in Chapter 1. Reynolds et al. [Reynolds et al., 2001] synthesized a hydrophobic aerogel containing $CF_3(CH_2)_2$ surface groups to remove crude oil from a 3% salt water and Prudhoe Bay crude oil mixture. They found that the $CF_3(CH_2)_2$-aerogels separated all of the oil from the water for an oil to aerogel ratio up to 3.5. For an oil to aerogel ratio of 4.6 to 14, an emulsion was formed which was also easily separated from the water, and for an oil to aerogel ratio greater than 16, only part of the oil was absorbed, with a free oil phase clearly present. Rao et al. [Rao et al., 2007] used a superhydrophobic aerogel prepared by the sol-gel process using methyltrimethoxysilane (MTMS) as a precursor to absorb oils and organic liquids and obtained a very high uptake capacity (9.83-20.64 g/g). They proposed that the absorption of oil and organic liquids onto hydrophobic aerogels is due to capillary action.

However, there are no studies reported in the literature about the sorption mechanism of emulsified oil, which is defined as an oil-in-water emulsion with an oil droplet size smaller than 20 μm, onto hydrophobic aerogels, or from real wastewater that contains low concentrations of oil and is stable, i.e., the oil

droplets remain emulsified indefinitely and do not coalesce). Also, there are no studies in the literature which report oil sorption kinetics data; these data are necessary to verify possible sorption mechanisms of oil onto hydrophobic aerogels in the pure liquid phase, emulsion phase, and for real wastewater. Therefore, the objectives of the work in this chapter are: (1) to obtain oil adsorption/absorption capacity and kinetic data for oil as a pure liquid, oil-in-water emulsion, and real wastewater onto hydrophobic silica aerogels, (2) to compare the different sorption behaviors for these three cases, and (3) to propose different possible sorption mechanisms for these three cases. The hydrophobic silica aerogel used in this study is Cabot Nanogel®, available in particulate form in many different size ranges.

3.2. Experimental

3.2.1. Adsorbents

The hydrophobic silica aerogels used were Nanogel TLD-301 (0.7-1.2 mm size range) and sieved TLD-302 (1.7-2.35 mm size range) supplied by Cabot Corporation.

3.2.2. Adsorbates

Three oils were used in this study: supermarket vegetable oil (Food Club®), motor oil 10W30 (ACE®) and light crude oil (supplied by Venoco Inc.). The density, viscosity and surface tension of these three oils at 25 ^{o}C were measured in the lab by using the mass-volume method, AR-G2 Rheometer, and KSV

Tensiometer, respectively. The values are listed in Table 3-1. In the emulsion phase adsorption experiments, the surfactant Tween 80, $C_{64}H_{124}O_{26}$ (Aldrich), was used to stabilize the oil-in-water emulsion after forming the emulsion using a blender. The real oily wastewater sample was obtained from Williams AFB provided by Tierra Dynamic Company. Its primary components are JP-4 and JP-8 jet fuel in water, and its chemical oxygen demand (COD) concentration was around 1100 ppm.

Table 3-1. *Properties and sorption capacities of the three oils studied on Nanogel TLD-302*

Oil Type	ρ (g/mL)	γ (N/m)	η (Pas)	t (s) Eq. (2-5)	t (s) Experiment	q (g/g)	q (mL/g)
Vegetable oil	0.82	0.031	0.050	388	400	14.6	17.8
Motor oil	0.87	0.030	0.130	1043	1200	15.1	17.6
Crude oil	0.70	0.024	0.0014	14	25	11.7	16.7

3.2.3. Pure Liquid Sorption Experiments

The sorption kinetic and capacity experiments were conducted on a Cahn electronic microbalance system (Cahn D-101) by placing the Nanogel TLD-302 samples in a mesh basket hung under a weighing wire, as detailed in Chapter 2, *2.2.4*. The elevating platform was then raised to allow Nanogel to come in contact with the pure oil (vegetable oil, motor oil, or light crude oil) through the air/liquid interface. The weight change data were collected by a computer connected to the microbalance. In these experiments it was more convenient to use the larger TLD-302 Nanogel granules as the sorbent.

3.2.4. Emulsion Phase Adsorption Experiments

The concentration of oil in the emulsion phase was measured by analyzing chemical oxygen demand (COD) in the sample. Since oil was the dominating organic substance added to the water, it was reasonable to assume that any increase in COD levels was due to the addition of oil. COD was measured by using a HACH DR/890 colorimeter following the procedure indicated in the HACH manual, in particular, Method 8000: reactor digestion method USEPA approved for COD [Jirka et al., 1975; Hach, 2004].

The adsorption isotherm of Nanogel was determined for two types of oils in water: an emulsion of vegetable oil with different proportions of Tween 80, and an emulsion of motor oil with different proportions of Tween 80 (volume % of Tween 80 as compared to the amount of oil added). In the experiments, 100 mL of around 1000 ppm COD concentration oil-water mixtures stabilized with a certain proportion of Tween 80 were blended in an Oster kitchen blender for 3 minutes and then poured into 120 ml bottles. Several representative weights of TLD-301 Nanogel, in the range of 20-400 mg, were added into the different bottles. These bottles were shaken in an Innova 4080 incubator shaker (200 rpm) at room temperature. Upon reaching equilibrium (> 3 hours), all the samples were withdrawn and analyzed by the HACH DR/890 colorimeter. Blank experiments, without the addition of Nanogel, were also conducted to ensure that the decrease in concentration measured was actually caused by adsorption rather than instability of the emulsion (coalescence of oil droplets). In batch equilibrium

experiments, the mass of adsorbate adsorbed per unit mass of adsorbent, q, is determined by Equation (2.3).

Batch kinetic experiments were also conducted at room temperature. A number of glass bottles containing 100 mL of around 1000 ppm COD concentration oil-in-water emulsions were mixed with 100 mg of TLD-301 Nanogel in the Innova shaker at 200 rpm for different time periods. The concentration of each of the liquid samples was measured by the HACH DR/890 colorimeter. The experiment was stopped when the concentration approached the equilibrium concentration.

In order to understand the possible sorption mechanisms of oil onto hydrophobic aerogels in emulsion phase, several properties of the vegetable oil emulsion were also studied, including: the contact angel between the emulsion and Nanogel, the average oil droplet size of the emulsion, and the stability of the emulsion.

Contact angles of sessile droplets of emulsions with different proportion of Tween 80 on TLD-301 were measured with a goniometer (Kruss EasyDrop Contact Angle Meter DSA20B). In this measurement, TLD-301 particles were first pressed into flat surface disks by using a high pressure press (Carver-3925) operated at 20,000 psi for 3 minutes. The size of the oil droplets in the emulsions with different proportion of Tween 80 was measured by using a particle sizer (NICOMP 380 ZLS). The stability of the emulsion with different proportion of Tween 80 was characterized by two ways: the coalescence time measurement [Nielsen et al., 1958] and the concentration-time measurement. In the

coalescence time measurement, a drop of oil was released underneath the oil-water interface by a hypodermic needle through the stopper in the bottom of the glass vessel, and the coalescence time of a single drop of oil at an oil-water interface containing Tween 80 was measured and used to represent the stability of the emulsion. In the concentration-time measurement, the concentration of the emulsion was measured after 24 h of its preparation and compared with the initial concentration of the emulsion.

3.2.5. Adsorption Experiments for Oily Wastewater

In the batch adsorption equilibrium experiment, 100 mL wastewater samples were mixed with five representative weights of TLD-301 Nanogel, in the range of 20-400 mg in 120 mL bottles. These bottles were shaken in an Innova 4080 incubator shaker (200 rpm) at room temperature. Upon reaching equilibrium (> 3 hours), all the samples were withdrawn and analyzed by the HACH DR/890 colorimeter.

In the batch adsorption kinetic experiments, a number of glass bottles containing 100 mL wastewater samples were mixed with 100 mg of TLD-301 Nanogel in the Innova shaker at 200 rpm for different time periods. The concentration of each of the liquid samples was measured by the HACH DR/890 colorimeter. The experiment was stopped when the concentration approached the equilibrium concentration.

3.3. Results and Discussion

3.3.1. Liquid Phase Sorption

Figure 3-1 shows the experimental results for sorption of three pure oils on Nanogel TLD-302. As seen in this figure, during the absorption, the time when Nanogel reaches saturation varies from 25 s to 1200 s for the three different oils. The absorption rate increases in the order: absorption rate of crude oil > vegetable oil > motor oil. The viscosity of the three oils, as listed in Table 3-1, decreases in the same order: viscosity of crude oil < vegetable oil < motor oil. This suggests a sorption mechanism controlled by the viscous flow in the pores of Nanogel.

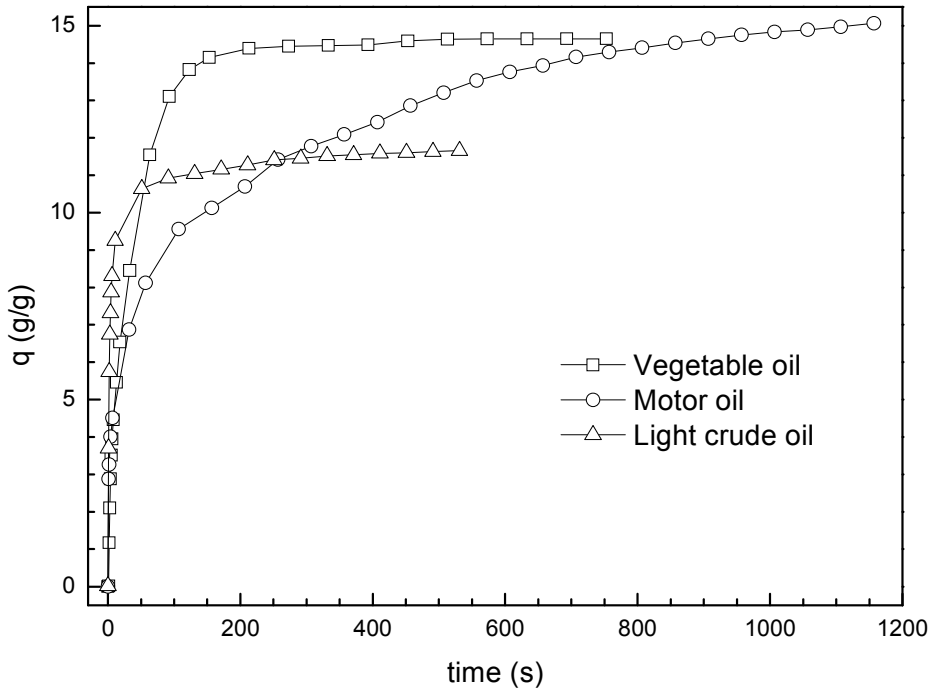

Figure 3-1. Sorption of pure oil on Nanogel TLD-302 by Cahn C-1000 Electronic Microbalance.

The penetration depth of a viscous flow of liquid sucked into the pores (replacing the air) of the Nanogel due to the capillary force can be described using the Washburn equation (Equation (2.5)) [Washburn, 1921]. By using Equation (2.5), the theoretical absorption time for the three oils was calculated and listed in Table 3-1. In the calculation, the distance L was assumed as the average radius of Nanogel particles (0.95 mm) and the average pore radius r of the Nanogels was taken as 7.5 nm based on BET experiments. As shown is Table 3-1, the values of the theoretical absorption time are close to the experimental values for these three oils. This confirms that the viscous flow driven by the capillary force is the dominating mechanism for sorption of oil in Nanogel.

It also can be seen in Table 3-1 that Nanogel granules absorb oils around 11.7 to 15.1 times their own mass. If the sorption capacity is expressed in units of mL/g, the volumetric sorption capacities of Nanogel for these three oils are all around 17 as shown in Table 3-1. The density and porosity of Nanogel are around 0.125 g/mL and 0.95, respectively, and if the pores of Nanogel are assumed to be completely filled with oil, the theoretical volumetric absorption capacity should be equal to 7.6, which is a little bit lower than half of the measured value of 17. However, during the absorption process, when Nanogel granules are contacted with the oil surface, not only the pores of Nanogel, but also the inter-particle air spaces between Nanogel particles become occupied by the oil. Since the voidage of Nanogel granules is roughly 50%, the measured volumetric sorption capacities of around 17 are reasonable. Hence Nanogel particles will serve as an excellent "sponge" for oil, and can be used for oil spill clean-up.

3.3.2. Emulsion Phase Adsorption

Figure 3-2 shows the adsorption isotherms (Type III) for vegetable oil and motor oil from oil-in-water emulsions with different proportion of surfactant, Tween 80, on Nanogel TLD-301. Unlike solution phase adsorption (for example, molecular toluene dissolved in water below its solubility limit [Wang et al., 2011], the adsorbate in the emulsion exists together with the surfactant as a colloid. Therefore, the adsorption is not only dependent on the relationship between adsorbent and adsorbate, but also dependent on the properties and amount of the surfactant. As shown in Figure 3-2, the adsorption capacities for both vegetable oil and motor oil decrease with an increasing proportion of Tween 80 in the emulsion. Obviously, the surfactant plays an important role in the emulsion phase adsorption process.

The Freundlich adsorption model [Freundlich, 1926] was used to fit the emulsion phase adsorption isotherm (Type III) data since it takes into account the heterogeneity of real surfaces for adsorption. The Freundlich isotherm is defined by Equation (1.2). Figure 3-2 shows the adsorption isotherm data fitted in the form of the Freundlich adsorption model (Equation (1.2)). The values of the Freundlich constants, k and $1/n$, were determined by regression of the experimental data, and, together with the regression coefficients, are summarized in Table 3-2. It is widely recognized [Sontheimer et al., 1988] that a change in the isotherm concentration ranges may require adjustment of the k and $1/n$ Freundlich constants; therefore, the concentration ranges of the measurements are also listed in the table.

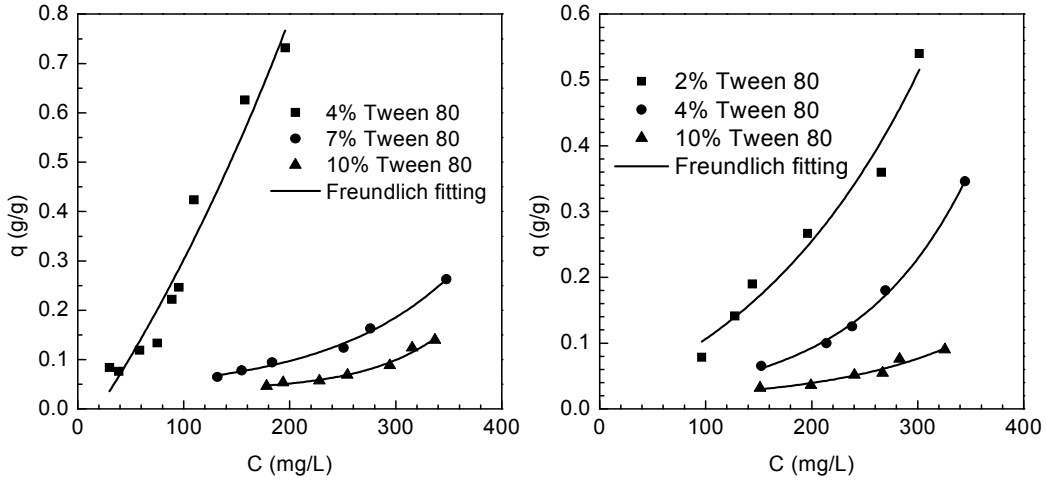

Figure 3-2. Adsorption isotherms for vegetable oil and motor oil from oil-in-water emulsions with different proportion of Tween 80 on Nanogel TLD-301: (a) vegetable oil and (b) motor oil.

Table 3-2. *Freundlich isotherm parameters for the adsorption of vegetable oil and motor oil emulsions, and real wastewater on Nanogel TLD-301*

Oil type	Volume % Tween 80 of oil	Freundlich isotherm parameters			
		k (mg g^{-1} (g/L)^n)	$1/n$	R^2	C_e range (mg/L)
Vegetable oil	4%	6133	1.33	0.945	
	7%	1495	1.47	0.987	20-350
	10%	775	1.68	0.925	
Motor oil	2%	3206	1.54	0.966	
	4%	2692	2.05	0.956	80-350
	10%	399	1.40	0.908	
Wastewater	----	79	1.47	0.960	< 400

Figure 3-3 shows the experimental results for the adsorption kinetics of vegetable oil and motor oil from an oil-in-water emulsion with 4% Tween 80 on Nanogel TLD-301. When compared to Figure 3-1, the sorption rate for vegetable oil and motor oil from an oil-in-water emulsion stabilized by Tween 80 is about 5 to 10 times slower than that from pure oil. In Chapter 2, the sorption kinetics and capacity for six volatile organic compounds (VOCs) in solution phase on Nanogel

was studied. When these results are compared to Figure 2-9, it appears that the sorption rate for vegetable oil and motor oil from an oil-in-water emulsion is about 10 times slower than that for VOCs from aqueous solutions.

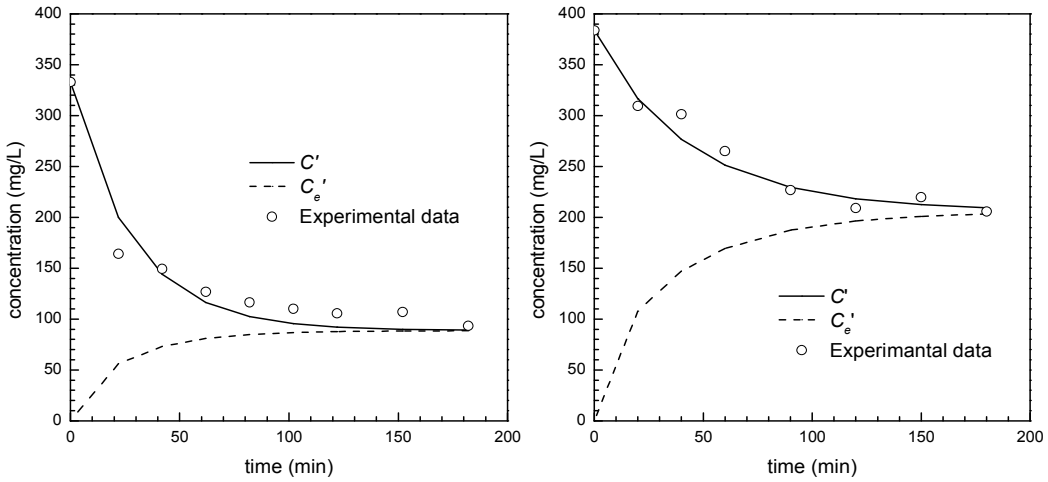

Figure 3-3. Oil concentration as a function of time in a batch kinetic experiment: C' and C_e' are obtained from the linear driving force model: (a) vegetable oil and (b) motor oil.

In solution phase adsorption, the adsorption reaches equilibrium when the adsorption rate is equal to the desorption rate. In other word, the adsorption reaches equilibrium when the bulk concentration of the adsorbate is equal to the concentration at the boundary. In emulsion phase adsorption, the adsorbate molecules are replaced by the colloidal oil droplets. The mass concentration of the oil in the bulk phase is also replaced by the number concentration of the oil particles. Since the experimental conditions for the emulsion preparation are fixed, i.e., the oil concentration, proportion of surfactant, and mixing time, the oil droplet sizes are also fixed in the emulsion, which means that the oil number

concentration in the emulsion is proportional to the oil mass concentration. Therefore, an adsorption equilibrium still exists.

In the oil-in-water emulsion in this study, the surface of the oil droplets is covered with surfactant molecules, Tween 80, which reduces the interfacial tension between oil and water and prevents the coalescence of oil droplets. Tween 80 is an organic compound that is amphiphilic, i.e., containing both hydrophobic groups and hydrophilic groups. When Tween 80 is mixed with oil in the emulsion phase, the hydrophilic groups of the Tween 80 remain in the water phase, while the hydrophobic groups attach to the oil droplets. In this case, the surface of the oil droplets actually become much less hydrophobic and the interaction between oil and Nanogels becomes weak. This might cause the relatively slow adsorption process in the emulsion phase adsorption.

For the adsorption of emulsified oil from oil-in-water emulsion using Nanogel, the relatively slow kinetics results suggest that the possible sorption mechanism might be: (1) migration of the oil droplets into the Nanogel pores, and (2) adsorption of the oil on the surface of the Nanogel pores. Clearly, step (1) should be the rate controlling step, since the surfactant decreases the surface wetting of Nanogel by oil dramatically, and therefore will slow the migration of the oil droplets into the Nanogel pores.

With the mechanism discussed above the sorption of oil from emulsion can be approximated by the linear driving force (LDF) model [Glueckauf et al., 1947], as discussed in *1.3.2*.

As seen Figure 3-3, the solution C' and C_e' can be compared with experimental data to obtain the adsorption rate constant K by means of a least squared regression. The K values for vegetable oil and motor oil with 4% Tween 80 are 5.68×10^{-2} s^{-1} and 2.53×10^{-2} s^{-1}, respectively, which are much lower than K values for the adsorption of organics from solution phase by using Nanogels, around 0.2 s^{-1}, which is discussed in Chapter 2. The low adsorption rate constant K represents the relatively slow adsorption process, i.e., the adsorption of oil from the emulsion phase is slower than the adsorption of organics from the solution phase by using Nanogels, which indicates that the emulsion phase adsorption has a different mechanism than the solution phase adsorption. This is probably due to the presence of the adsorbate (oil) in the form of a colloid, i.e., as very small submicron size droplets, see Figure 3-4, and the effect of the surfactant Tween 80 used to stabilize the emulsion.

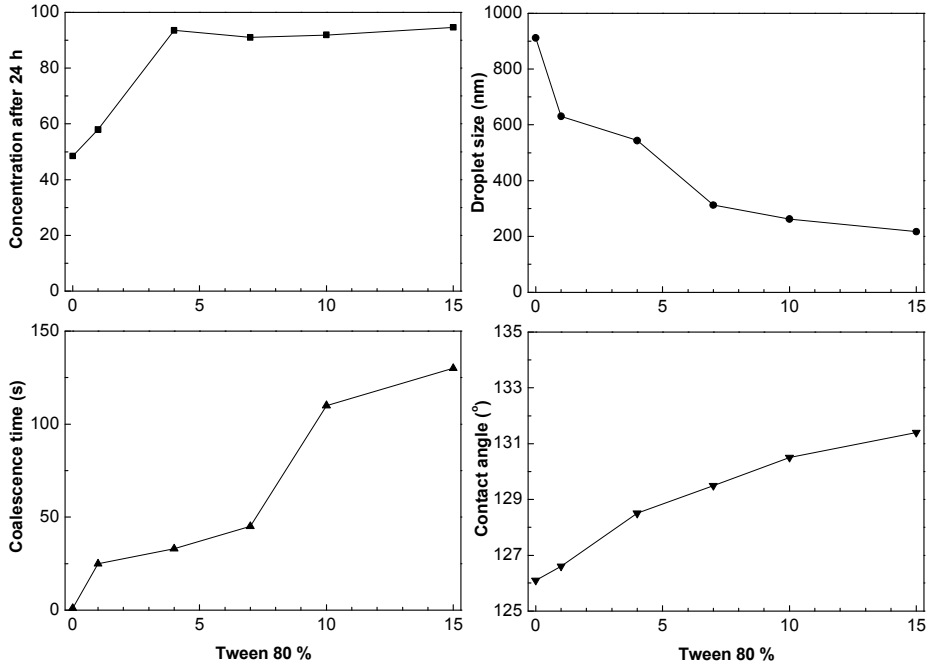

Figure 3-4. The properties of vegetable oil in water emulsion with different proportion of Tween 80: (a) the change of concentration after 24 h (upper left), (b) coalescence time (bottom left), (c) droplet size (upper right), and (d) contact angle between Nanogel and emulsion (bottom right).

3.3.3. The Effect of the Surfactant in the Emulsion Phase Adsorption

As already mentioned in *3.3.2*, the surfactant plays an important role in the emulsion phase adsorption process: the higher the proportion of Tween 80, the lower the adsorption capacity. Therefore, the effect of Tween 80 in the adsorption process is also studied in this work from three aspects: (1) the stability of the emulsion, (2) the oil droplet size in the emulsion and (3) the contact angles between emulsion and Nanogel.

Figure 3-4 shows the change of the stability, the oil droplet size and the contact angle between Nanogel and emulsion with different proportions of Tween 80 in the emulsion. As seen in this figure, it appears that: (1) the stability of the emulsion increases with the increasing amount of Tween 80 in the emulsion, (2)

the oil droplet size decreases with the increasing amount of Tween 80 in the emulsion and (3) the contact angle between Nanogel and emulsion increases with the increasing amount of Tween 80 in the emulsion (the contact angle at high concentration of Tween 80 approaches the contact angle measured using pure water, i.e., no oil present). Therefore, the surfactant might affect the adsorption process through the following two ways: when the amount of surfactant increases, (1) the emulsion becomes more stable, which decreases the adsorption capacity of Nanogel, and (2) the emulsion becomes less hydrophobic (more hydrophilic), and therefore the contact between Nanogel and the emulsion decreases.

3.3.4. Adsorption of Real Oily Wastewater

The organic concentration of the real oily wastewater sample obtained from Williams Air Force Base was measured by using the COD method. Since the calibration relations between COD and the actual mg oil /L concentration of both vegetable oil and motor oil are very similar, the calibration relation between COD and real oily wastewater is assumed to be the same as the calibration relation between COD and vegetable oil, i.e., concentration in mg/L = 0.359 COD concentration. This assumption allows us to define an equivalent concentration instead of the true concentration for the real oily wastewater sample, since the actual oil concentration of the real wastewater sample is unknown.

Using the equivalent concentration as defined above, the Freundlich adsorption model [Freundlich, 1926] was used to fit the adsorption isotherm data for the real wastewater sample (see Figure 3-5), and the k and $1/n$ values are 79

and 1.47, respectively. By comparing the adsorption isotherms between this real oily wastewater sample and the synthetic vegetable oil-in-water emulsion stabilized with Tween 80, it appears that the adsorption capacity of Nanogel is much lower for the real wastewater sample than for the synthetic emulsion, even with as much as 10% Tween 80 added.

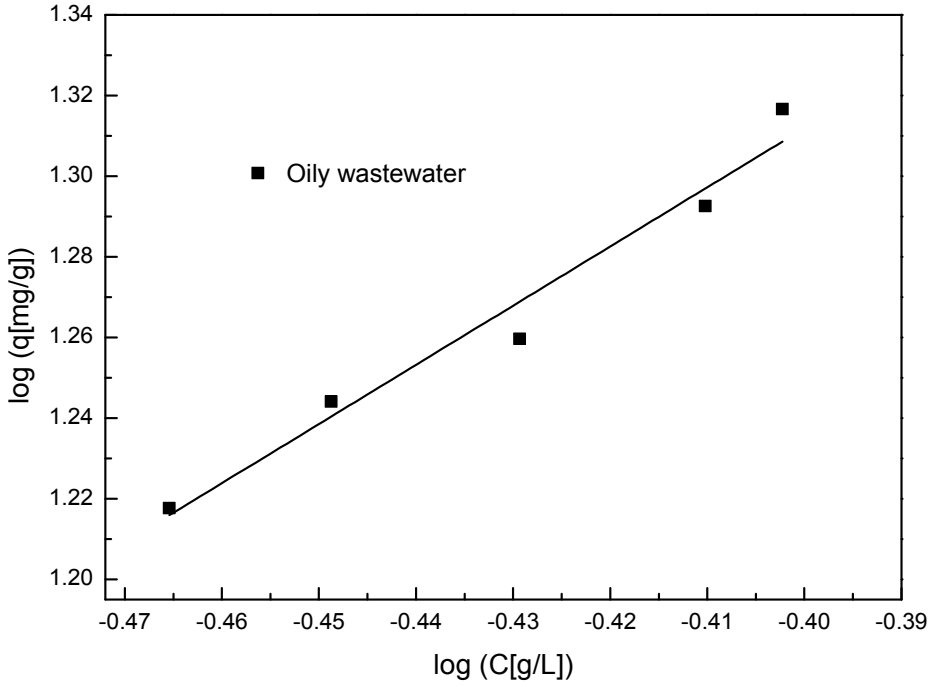

Figure 3-5. Freundlich isotherms for adsorption of real oily wastewater on Nanogel TLD-301.

The relatively low adsorption capacity of Nanogels for the oily wastewater samples as compared to the lab prepared vegetable oil or motor oil emulsions might be due to several reasons: (1) the types of oils present in the wastewater; the main compounds in the oily wastewater samples are JP-4 and JP-8 jet fuels, which consist of a blend of gasoline and kerosene and are quite different in properties from vegetable and/or motor oil; and (2) the existence of one or more

surfactants in the oily wastewater samples might also result in the relatively low adsorption capacity of Nanogels.

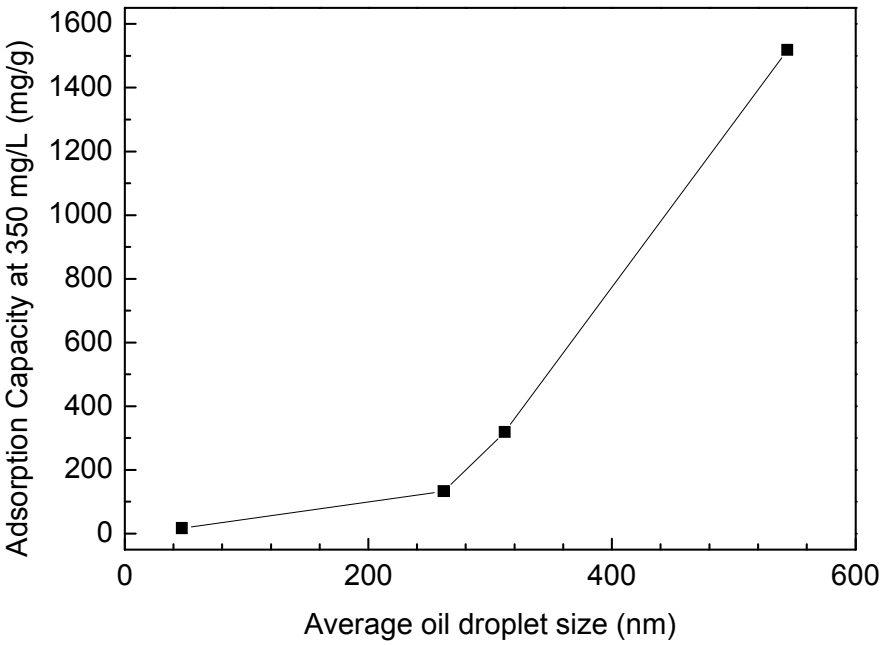

Figure 3-6. The relationship between the oil droplet size and the adsorption capacity of Nanogel. Data points from left to right: real oily wastewater sample, vegetable oil in water emulsion with 4% Tween 80, vegetable oil-in-water emulsion with 7% Tween 80, and vegetable oil-in-water emulsion with 10% Tween 80.

Jet fuel always contains different types of additives to reduce internal engine carbon buildups, improve combustion, and allow easier starting in cold climates. Typical additives include alkylamines and alkyl phosphates at the level of 50-100 ppm. The presence of these additives can make the wastewater samples very stable. Based on previous discussion, the oil droplet size of the emulsion can be used as a metric to represent the stability of the emulsion, i.e., the smaller the oil droplet size, the more stable the emulsion. As seen in Figure 3-6, the average

oil droplet size in the real oily wastewater sample is only 47 nm, much lower than the average oil droplet size in the lab prepared vegetable oil-in-water emulsions with different proportions of Tween 80. Therefore, it appears that this particular wastewater sample has been stabilized by surfactants, which causes the adsorption capacity of Nanogel to be very low. However, for other types of oily wastewater which have less or no surfactants, the adsorption capacity of Nanogel might be improved.

Figure 3-7 shows the adsorption kinetics results for the real oily wastewater samples. As seen in this figure, the adsorption process is very slow. The adsorption rate constant, K, is calculated by LDF model, as 6.95×10^{-3} s^{-1}, which is smaller than the K values for vegetable oil and motor oil emulsions with 4% Tween 80 added as surfactant.

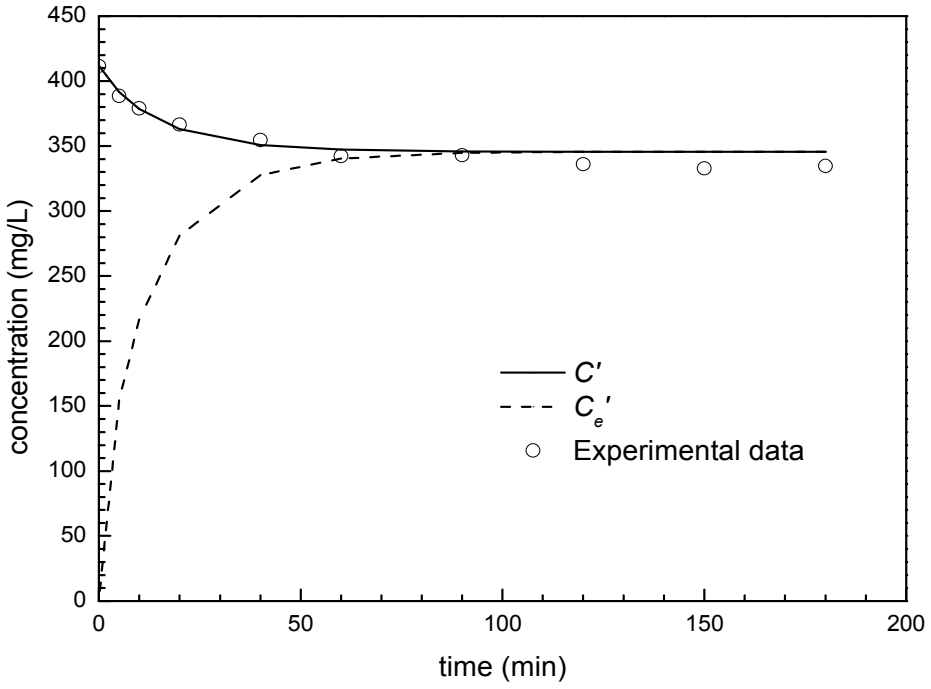

Figure 3-7. Real oily wastewater concentration as a function of time in a batch kinetic experiment: C' and C_e' are obtained from the linear driving force model.

The breakthrough curves using the real oily wastewater for two packed bed experimental runs and one inverse fluidized bed experimental run are obtained from the experiment concentration versus time data and shown in Figure 3-8. Details of these experiments, i.e., the experimental setup, experimental procedure, and data analysis are fully described in Chapter 5 which examines the adsorption of toluene-water solutions in both the packed bed and inverse fluidized bed modes. The inlet concentration of the real oily wastewater was measured by the Hach colorimeter to be around 1100 mg/L COD, and converted to an equivalent oil concentration using the calibration result for vegetable oil as discussed above. As seen in this figure, the breakthrough times in both the packed bed and fluidized bed runs are very short, especially for the fluidized bed where C/C_0 approaches unity in about 10 minutes. Such short breakthrough times are due to slow kinetics for sorption of oil from the oil-in-water emulsion, and low sorption capacity.

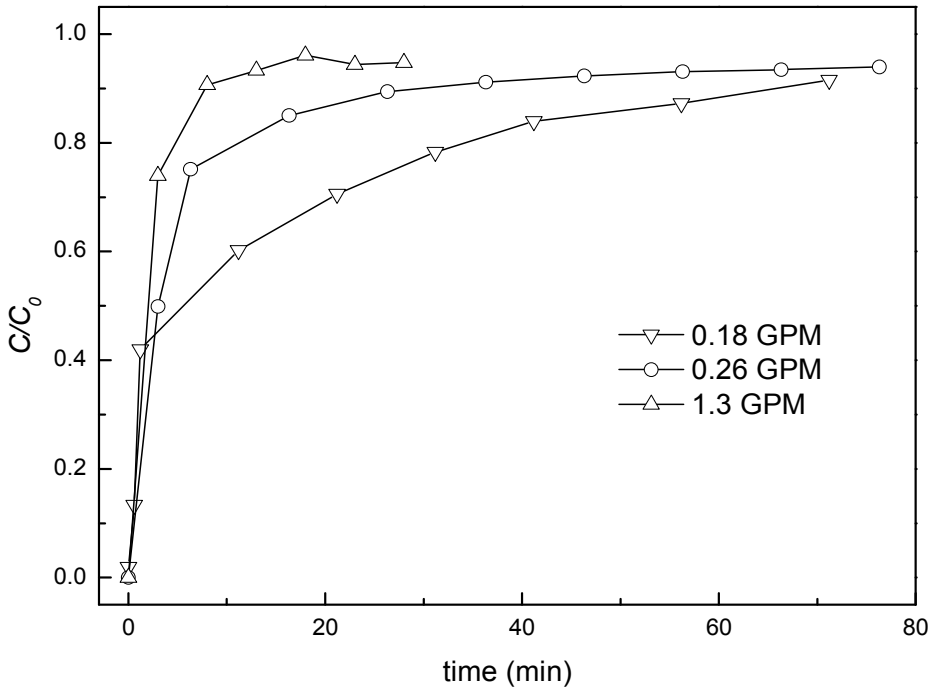

Figure 3-8. Breakthrough curves of oil adsorption on Nanogels from real oily wastewater in the packed bed (flow rate of 0.18 and 0.26 GPM), and fluidized bed (flow rate of 1.3 GPM).

The adsorption capacity q in the packed bed or fluidized bed is given by Equation (3.1).

$$q = \frac{m_{Adsorbed}}{m_{Nanogels}} \tag{3.1}$$

By using Equation (3.1), the adsorption capacities were calculated as 23 mg/g, 21 mg/g and 23 mg/g when the flow rates were 0.18 GPM, 0.26 GPM and 1.3 GPM, respectively. This is in reasonably good agreement with the equilibrium adsorption capacity of 20 mg/g given by Figure 3-5 and indicates that the adsorption capacity of Nanogel is very low for this particular real wastewater sample.

3.4. Conclusions

Sorption of pure oil on Nanogel is governed by the viscous flow in the pores of the Nanogel due to capillary forces. The sorption rate for the three oils on Nanogel decreases as the viscosity of the oil is increased. The volumetric sorption capacities of the three oils on Nanogel are all around 17 mL/g. This very high uptake capacity and high rate of uptake indicates that Nanogel can potentially be effectively used to clean-up oil spills due to accidental spillage during transportation of oils on roads, rivers and sea water, and may even find some applications in mitigating major disasters such as the Deepwater Horizon explosion in the Gulf of Mexico, as long as the oil remains floating on the surface of the water.

For the emulsion phase, the equilibrium adsorption isotherms of vegetable oil and motor oil with different proportion of surfactant, Tween 80, were determined at room temperature. The equilibrium adsorption capacities for these two oils decrease with increasing proportion of Tween 80 in the emulsion. The adsorption rate constant K for these two oils with 4% Tween 80 were calculated by fitting the adsorption kinetic data with the well accepted linear driving force model. The adsorption rate constants were appreciably lower than the rate constants found for the adsorption of organic-water solutions by Nanogel particles. This indicates that the emulsion phase adsorption has relatively slower kinetics compared with solution phase adsorption. The effect of the surfactant during the adsorption was also studied. The higher the proportion of surfactant in the

emulsion, the more stable the emulsion and the poorer the contact between Nanogel and the emulsion.

For the adsorption of oil from the real oily wastewater sample, the adsorption capacity of Nanogel is lower than that of the synthetic emulsion with 10% Tween 80 added as surfactant. This indicates that this particular wastewater is very stable and therefore Nanogel is not a good adsorbent for such a stable wastewater.

CHAPTER4 REMOVAL OF EMULSIFIED OIL FROM WATER BY INVERSE FLUIDIZATION OF HYDROPHOBIC AEROGELS

4.1. Introduction

As discussed in Chapter 1, one of the most challenging environmental problems today is the removal of oil and other organic contaminants from industrial wastewater and storm water. Several types of sorbents have been studied for the removal of dispersed and emulsified oil from water in packed bed filters or adsorbers. Of these materials, only granulated activated carbon (GAC) is commercially used as a sorbent to remove oil and other organics from water [Ayotamuno et al., 2006; Cooney et al., 1999]. However, GAC also displays disadvantages such as slow kinetics and limited removal capacity.

In the work reported in this dissertation, commercially available hydrophobic silica aerogels (Cabot Nanogel®) have been selected as the sorbents for the oil removal and organic separation. Hydrophobic silica aerogels have some unique properties; they are highly porous, nanostructured granules that are available as small particles in a variety of different sizes, and because of their hydrophobicity they attract organic molecules and repel water. Because of these desirable properties, different types of hydrophobic aerogels have been studied for the sorption of oil and other organics from water [Hrubesh et al., 2001; Reynolds et al., 2001; Standeker et al., 2007].

When the density of the particulate material (e.g., silica aerogels) is less than the density of the liquid, inverse fluidization can be applied to disperse the

solid particles in liquid. Since Nanogel granules have a density much lower than water and are robust enough to be fluidized, they can be configured in an inverse fluidized bed, where the oil-contaminated water flows downward through a distributor and through the bed of particles. The benefits of using inverse fluidization as compared to a more simple packed bed of particles are a low and constant pressure drop when operating above the minimum fluidization velocity, excellent mixing between the solid particles and the liquid (approaching CSTR conditions), high heat and mass transfer rate, an adjustable voidage of the fluidized bed by changing the fluid velocity, and the ability for continuous operation.

A recent paper by Quevedo et al. [Quevedo et al., 2009] used an inverse fluidized bed of Nanogels to remove vegetable oil from water. Using a diaphragm pump, they added a small quantity of pure oil to a flowing water stream, the oil-water mixture was then passed through a static mixer made up of steel wire packing to disperse the oil into the water; however, the oil droplets entering the fluidized bed were greater than 20 μm (dispersed oil). They found that an inlet oil concentration of about 1000 mg/L could be reduced to less than 100 mg/L by this method before a significant amount of aerogels became loaded with oil and left the bed at the bottom of the column.

In the work described in this chapter, the objectives are to measure some of the physical properties of Nanogel provided to us by Cabot Corporation, study the hydrodynamics characteristics of the Nanogel granules in the inverse fluidized bed, and determine the feasibility of using Nanogel granules for removing

emulsified oil (droplets less than 20 μm) from stable oil-in-water emulsions using inverse fluidization.

4.2. Experimental Equipment and Methods

4.2.1. Materials

The following materials were used in our experimental work: Nanogel of different size ranges, 0.5-0.85 mm (sieved TLD 101), 0.7-1.2 mm (TLD 301), and 1.7-2.35 mm (sieved TLD 302) was supplied by Cabot Corporation. The contact angles of the hydrophobic Nanogel, as reported by Cabot Corporation, are between 160^{o} and 170^{o}. Using a goniometer in our laboratory, we measured lower contact angles between 130^{o} and 140^{o}. Supermarket vegetable oil (Food Club) stabilized by the surfactant Tween 80 (Aldrich) was mixed with de-ionized water for the inverse fluidized bed experiments.

4.2.2. Surface and Pore Size Analysis

The pore structure (BET surface area, pore size distribution, and pore diameter) of the three size ranges of Nanogel were measured by nitrogen adsorption porosimetry (Micromeritics 2020). Each run was performed using approximately 0.15 g of sample which was pretreated at 120°C under vacuum at 1.5 Pa.

4.2.3. Nanogel Density Measurement

It is difficult to measure the granule density of the Nanogel by using a traditional method such as a liquid pycnometer. This is because the inter-particle forces between the aerogels agglomerate small particles so strongly, that it is difficult to open all the voids around the particles in order to replace the air/gas with a liquid. Hence Cabot Corporation lists the bulk density and the internal porosity of the Nanogel granules to be about 64 kg/m^3 and 0.95, respectively, on their website but only gives a rough estimate of the value of the granule density. In the work in this chapter, the granule density of the Nanogels was measured by an inverse fluidization method, i.e., the pressure drop after the bed was fully fluidized (in the pressure plateau region) was measured and used to calculate the granule density.

4.2.4. IFB Experiments for Measuring Hydrodynamic Characteristics

A schematic diagram of the experimental setup used for inverse fluidization of Nanogel granules by water is shown in Figure 4-1. It consists of a fluidization column, valves and piping, flow meters, a metering pump, static mixers, pressure gauge and a differential pressure transmitter with a display. The fluidization column was made of PVC with an internal diameter (ID) of 0.076 m (3 in.) and an outer diameter (OD) of 0.089 m (3.5 in.). Two different column lengths were used: 1.47 m (58 in.) and 0.77 m (30 in.). The valves and piping were also made of PVC, and the pipe size was 1 in. The flow of de-ionized water was adjusted by ball valves, and flow readings were taken by two calibrated

electronic digital flow meters, one for the range between 0-3 GPM and the other for the range between 3-50 GPM (GPI series A109). The metering pump (Pulsatron series A Plus, 0-6 GPD) and three static mixers (placed in series in the piping after the pump inlet) were used to study the efficiency and removal capacity of emulsified oil in the fluidized bed of Nanogels. Only clean deionized water was used in the hydrodynamics experiments.

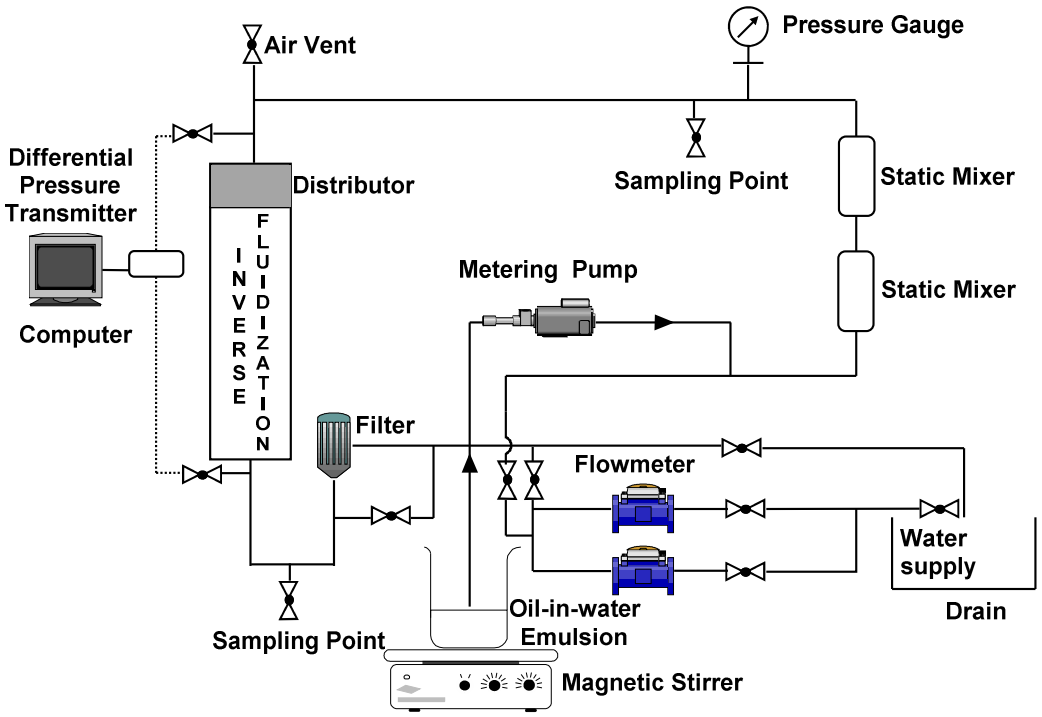

Figure 4-1. Schematic diagram of the inverse fluidization experimental setup.

A typical experimental run is described as follows. First, the pressure drop across the empty column was measured at different water flow rates in order to obtain a correlation that can be used to determine the pressure drop of the fluidized bed alone; this was done by subtracting the empty column pressure drop

from the total fluidized bed pressure drop. Then the particles to be fluidized were loaded into the fluidization column. Next, the column was filled with water from the bottom and air was completely removed by a vent at a high point in the system. Then the water flow was fed at the top of the column through a distributor made up of a packed bed of glass beads supported by a steel wire mesh to prevent channeling. The Nanogel was inversely fluidized by increasing the flow until the drag force on the particles balances the buoyant force less the gravity force (minimum fluidization velocity). The flow rate was then increased significantly above that value and the hydrodynamic parameters, bed height and pressure drop were measured at each flow rate by gradually decreasing the flow of water until the bed defluidizes (packed bed condition) and then increasing the flow again until the bed height had expanded by at least a factor of two. The static pressure before the column was kept constant to ensure consistent readings.

4.2.5. Inverse Fluidized Bed Experiments for Oil Removal

The concentration of oil in water was measured by analyzing chemical oxygen demand (COD) in the sample. Since oil was the dominating organic substance added to the water, it was reasonable to assume that any increase in COD levels was due to the addition of oil. COD was measured by using a HACH DR/890 colorimeter following the procedure indicated in the HACH manual, in particular, Method 8000: reactor digestion method USEPA approved for COD [Jirka et al., 1975; Hach, 2004].

In the inverse fluidized bed experiments to measure the oil removal efficiency and capacity, a constant de-ionized water superficial velocity above the minimum fluidization velocity and a constant static pressure was maintained throughout the duration of the experiment. A high-concentration, stable oil-in-water emulsion was continuously stirred by a magnetic stirrer in a large plastic container and was injected into the piping system by the pump upstream of the static mixers and the fluidization column. By adjusting the pump's stoke displacement and frequency, a desired concentration of oil (1000 ppm COD or less) was obtained when the emulsion was mixed into the flowing water. Samples of water of about 250 ml, upstream and downstream of the inverse fluidized bed, were taken at regular intervals for COD concentration analysis until the expanded bed height reached the bottom of the column and some Nanogel was observed to leave the bed with the water.

Since the oil present in waste water is usually in an emulsified form (oil droplets smaller than 20 μm), we wanted to add a stable oil-in-water emulsion rather than adding pure oil droplets into the inverse fluidized bed as was done by Quevedo et al. [Quevedo et al., 2009]. The oil-in-water emulsion was prepared by adding a small amount of the surfactant Tween 80, about 1 to 4 volume % of the amount of oil added to the water to form the emulsion and the mixture was mixed in a blender for a few minutes. Then, the emulsion was kept stirred by using a magnetic stirrer to keep it stable during the inverse fluidized bed experiment. The size of the oil droplets in the oil-in-water emulsions was measured by using an optical microscope. The stability of the oil-in-water

emulsion was measured by sending the emulsion through the empty column (without any Nanogel present) and comparing the difference between the average value of the inlet and outlet oil concentration.

4.2.6. Batch Equilibrium Measurements for Oil-in-water Emulsion

To measure the adsorption isotherm of the Nanogels, six representative weights of TLD 301 Nanogel, in the range of 20-400 mg, were mixed with 100 mL of around 1000 ppm COD oil-in-water emulsions (using 4% Tween 80) in glass bottles. These bottles were shaken in an Innova 4080 incubator shaker (200 rpm) at room temperature. Upon reaching equilibrium (> 3 hours), all the samples were withdrawn and analyzed by the HACH DR/890 colorimeter.

4.2.7. Batch Kinetic Measurements for Oil-in-water Emulsion

Batch kinetic experiments were conducted at room temperature. A number of glass bottles containing 100 mL of around 1000 ppm COD oil-in-water emulsions were mixed with 100 mg of TLD 301 Nanogel in the Innova shaker at 200 rpm for different time periods. The concentration of each of the liquid samples was measured by the HACH DR/890 colorimeter.

4.3. Theoretical Model

Although some modeling of the adsorption behavior in a liquid-solid fluidized bed has been reported in the literature [Veeraraghavan et al., 1989; Wright et al., 2001; Correa et al., 2007], we would like to compare our inverse

fluidized bed experimental results with a model that is based on the equilibrium and kinetic data for our particular Nanogel-oil-in-water emulsion system. As will be shown below, the breakthrough curves in our inverse fluidized bed absorber are considerably different than those expected in a comparable fixed bed adsorber. This is due to the considerable axial mixing occurring in the solid and liquid phases, especially when the inverse fluidized bed height is relatively short. In order to describe the emulsified oil adsorption in the inverse fluidized bed, a model was developed taking into account hydrodynamic behavior, dispersion, and mass transfer between the liquid and solid phases.

4.3.1. Model Development

The governing equations of the model were derived based on the assumptions listed below: (1) Nanogel particles are monosize and the average particle size is used; (2) radial concentration gradients are negligible for both the liquid and solid phases in the column; (3) rate of adsorption is determined by the linear driving force model (see below) based on the batch kinetic data; (4) adsorption equilibrium is represented by Freundlich equation; (5) the solid phase is completely mixed (short fluidized bed height) and the liquid phase is described by an axial dispersion model; and (6) bed height is expressed as the function of time based on the experimental data.

4.3.2. Derivation of Model Equations

Following Veeraraghavan and Fan [Veeraraghavan et al., 1989], the mass balance with respect to the adsorbate in the liquid phase gives

$$\varepsilon \frac{\partial C}{\partial t} = D_{ax}\varepsilon \frac{\partial^2 C}{\partial z^2} - u\frac{\partial C}{\partial z} - (1-\varepsilon)K(C - C_e) \tag{4.1}$$

where ε the void fraction of the fluidized bed, C is the oil concentration in the liquid phase in the fluidized bed, C_e is the local equilibrium concentration in the liquid phase corresponding to the adsorbate concentration at the Nanogel particle boundary, D_{ax} is the liquid phase axial dispersion coefficient, u is the superficial fluid velocity, and K is the adsorption rate constant.

The initial and boundary conditions for the inverse fluidized bed subject to a switch in the feed from the pure water stream to an oil-in-water emulsion stream are

$$t = 0, \quad C(z,0) = 0, \quad 0 \le z \le H \tag{4.1a}$$

$$z = 0, \quad C = C_0 + \frac{D_{ax}\varepsilon}{u}\frac{\partial C}{\partial z}, \quad t > 0 \tag{4.1b}$$

$$z = H, \quad \frac{\partial C}{\partial z} = 0, \quad t > 0, \text{ (where } H \text{ is a function of t)} \tag{4.1c}$$

where H is the height of the fluidized bed and C_0 is the oil-in-water feed concentration.

The liquid phase axial dispersion coefficient, D_{ax} is calculated using an equation presented by Chung and Wen [Chung et al., 1968].

$$\frac{D_{ax}\rho_l}{\mu} = \frac{\mathrm{Re}}{0.2 + 0.011\mathrm{Re}^{0.48}} \tag{4.2}$$

where ρ_l is the density of fluid, μ is the fluid viscosity, and *Re* is Reynolds number.

There is no convective flow in the solid phase and, in addition, we assume that the solid phase is completely mixed. Hence

$$H\frac{\partial q}{\partial t} = \int_0^H \frac{K}{\rho_P}(C - C_e)dz \tag{4.3}$$

where ρ_P is the density of the particle, and q is the mass of oil per unit mass of Nanogel in the particle.

The initial condition is

$$t = 0, \quad q(0) = 0, \quad 0 \le z \le H \tag{4.3a}$$

Finally, the Freundlich equation, Equation (1.2), is used to relate the amount of oil adsorbed per weight of Nanogel to the concentration of oil in the liquid phase at equilibrium.

The rate constant K in Equations (4.1 and 4.3) is obtained from the batch kinetic experiment by using a linear driving force model, which is defined by Equations (1.4 and 1.5).

Equations (1.2, 1.4, and 1.5) can be solved simultaneously to obtain values of C' at different times by assuming a value of K. The actual value of K can then be obtained by comparing the calculated values of C' with the experimentally measured values of C' using a least squares regression.

4.3.3. Simulation

The governing Equations (4.1 and 4.3) are nonlinear partial differential equations. In these equations, C is a function of t and z, and q is only a function of t because of the assumption that the solid phase is well mixed. The spatial discretization method was used to transform these partial differential equations into a set of ordinary differential equations: these equations were discretized in space using finite differences with 50 evenly spaced finite difference points along the column length. This set of ordinary differential equations was solved using a Runge-Kutta 23 simulation method programmed in Matlab R2008b, the step size in the program was approximately 0.05-0.1 s.

4.4. Results and Discussion

4.4.1. Pore Structure of Nanogels

N_2 adsorption-desorption isotherms for the three different Nanogel size range samples were found to be almost identical and show a type IV isotherm which corresponds to a mesoporous material. The three different particle sized Nanogel also have a similar pore size distribution and the most prevalent pore size is about 15 nm. Specific surface area and pore diameter of the different particle size Nanogel are shown in Table 4-1; the pore volume measurements are inaccurate because of the presence of macropores and are therefore not included in the table. From these results we conclude that the three Nanogel samples of different size ranges have similar pore structures and very high specific surface.

Table 4-1. *Specific surface area and pore diameter results for three different particle size range Nanogel*

Sample	Particle sizes	Surface Properties	
		Specific Surface (m^2/g)	Average pore size (nm)
TLD 101	0.5-0.85 mm	660	15.2
TLD 301	0.7-1.2 mm	686	15.7
TLD 302	1.7-2.35 mm	671	15.6

4.4.2. Hydrodynamics of Inverse Fluidized Beds of Nanogel Granules

The hydrodynamic characteristics of inverse fluidized beds of Nanogel granules are represented by the fluidized bed pressure drop and the bed expansion. Figure 4-2 shows the fluidized bed pressure drop plotted against the superficial fluid velocity for TLD 302, 1.7-2.35 mm Nanogel granules. This plot is used to estimate the minimum fluidization velocity, i.e., the velocity where the particle configuration changes from a packed bed to a fluidized bed and the pressure drop becomes constant.

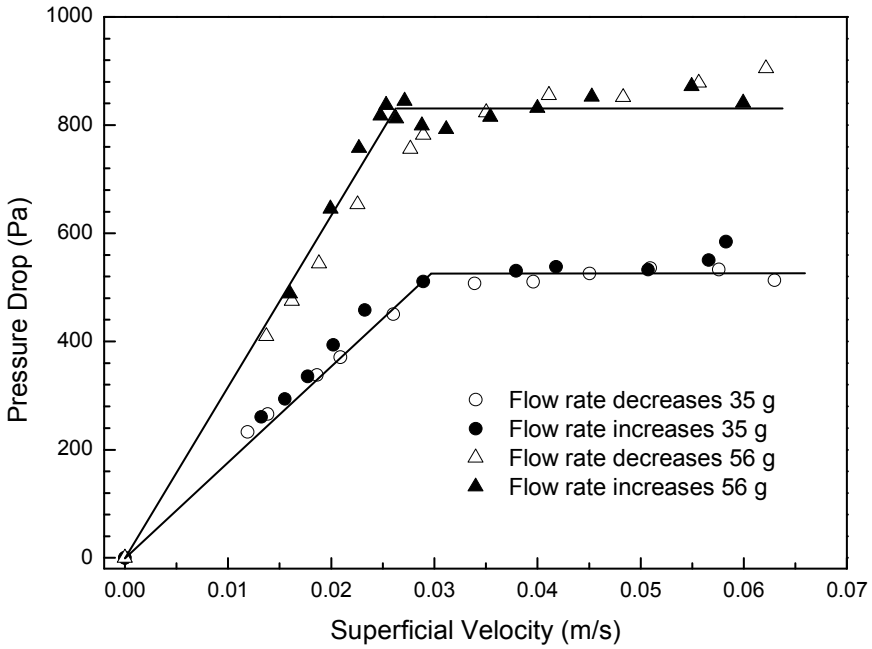

Figure 4-2. Inverse fluidized bed pressure drop vs. superficial fluid velocity of TLD 302, 1.7-2.35 mm Nanogel granules.

Figure 4-3 shows the fluidized bed height as a function of superficial velocity corresponding to Figure 4-2. These two figures show that: (1) the pressure drop rises linearly below minimum fluidization in the packed bed region and then plateaus above minimum fluidization, and (2) the bed height remains relatively constant before minimum fluidization and then expands as the water velocity is increased above minimum fluidization. Table 4-2 shows the minimum fluidization velocity and plateau pressure drop of the three different particle size range Nanogel. As seen in the table, the minimum fluidization velocity is dependent on the granule size and is independent of the amount of the granules fluidized. The larger the granule size, the higher the minimum fluidization velocity.

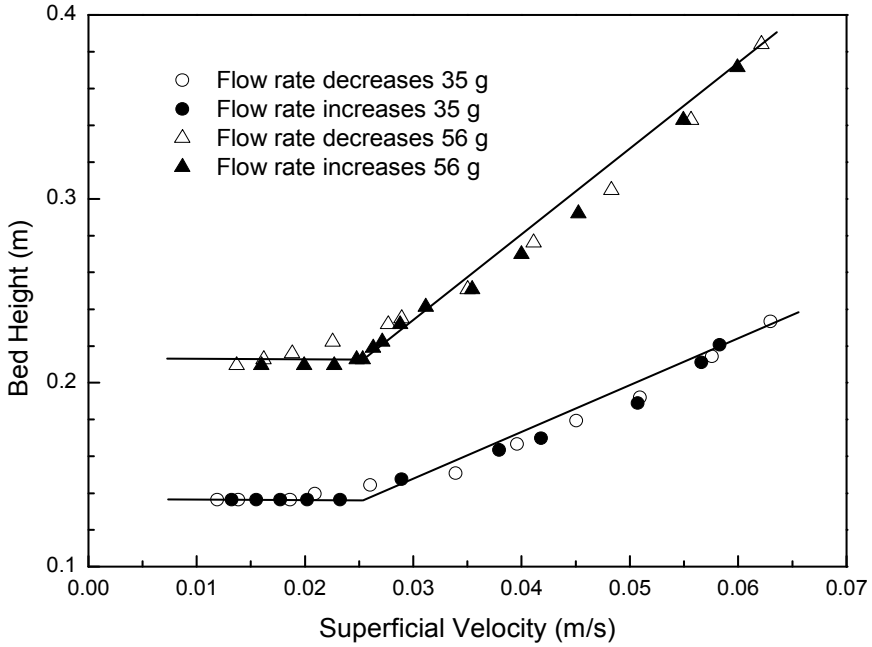

Figure 4-3. Inverse fluidized bed height vs. superficial fluid velocity of TLD 302, 1.7-2.35 mm Nanogel granules.

Table 4-2. *Minimum fluidization velocity and plateau pressure drop results for three different particle size range Nanogel in the inverse fluidized bed*

Particle sizes/ type (mm/type)	Mass (g)	ΔP (Pa)	U_{mf} (m/s)
0.5-0.85 TLD 101	56	876±64	0.015
	70	1046±53	
0.7-1.2 TLD 301	35	492±15	0.017
	70	988±32	
1.7-2.35 TLD 302	35	536±21	0.026
	56	853±27	
	70	1108±36	

4.4.3. Density and the External Porosity of the Granules

The value of the granule density can be calculated from the experimental data by using a force balance. The fluidized granules are acted on by a buoyancy force (F_B), gravity force (F_g) and drag force (F_D). The buoyancy and gravity forces are

$$F_B = \rho_l V_P g \qquad \text{and} \qquad F_g = \rho_p V_P g \tag{4.4}$$

where V_P is the total volume of particles fluidized in the column. The drag force applied on the particles during fluidization (assuming negligible wall effects) is given by the experimental pressure drop (ΔP_{exp}) multiplied by the cross sectional area of the fluidization column (A)

$$F_D = \Delta P_{\exp} A \tag{4.5}$$

A force balance on the particle gives

$$F_B = F_g + F_D = \rho_P V_P g + \Delta P_{\exp} A = \rho_l V_P g \tag{4.6}$$

Since $m_P = \rho_P V_P$, Equation (4.6) can be written as

$$V_P = \frac{(\Delta P_{\exp} A + m_P g)}{\rho_l g} \tag{4.7}$$

and the granule density of the particles is given by $\rho_P = \frac{m_P}{V_P}$ with V_P obtained from Equation (4.7). The void volume can be found by subtracting the volume of the particles (V_P) from the total volume of the fluidized bed (V_b). Hence, the void fraction of the fluidized bed is

$$\varepsilon = \frac{V_\varepsilon}{V_b} = \frac{V_b - V_P}{V_b} = 1 - \frac{V_P}{V_b} = 1 - \frac{m_P}{\rho_P V_b} = 1 - \frac{m_P}{\rho_P A H} \tag{4.8}$$

Equation (4.7) is of the particular significance since it can be used to calculate the particle density if the pressures drop measurement is reliable. It can also be used to predict the pressure drop across the fluidized bed if the particle density is known. The Nanogel density and initial void fraction are calculated and listed in Table 4-3. As seen in the table, the densities of the three different size

ranges of Nanogel vary between 120 kg/m^3 and 133 kg/m^3, and the average granule density of the Nanogel particles is 125±5 kg/m^3.

Table 4-3. *Nanogel density and initial void fraction calculation results from experiment data*

Particle size	Mass (g)	V_P (m^3)	ρ_P (kg/m^3)	Initial bed height (m)	Bulk density (kg/m^3)	Initial void fraction
0.5-0.85 mm	56	(4.6±0.3)E-04	121±8	0.27	46	0.63
	70	(5.6±0.2)E-04	126±6	0.32	48	0.62
0.7-1.2 mm	35	(2.6±0.1)E-04	131±4	0.15	51	0.62
	70	(5.3±0.1)E-04	133±4	0.29	53	0.60
1.7-2.36 mm	35	(3.1±0.1)E-04	123±4	0.14	55	0.51
	56	(4.5±0.1)E-04	123±3	0.21	59	0.53
	70	(6.0±0.2)E-04	120±3	0.27	57	0.51

4.4.4. Mathematical Models of Bed Expansion

The Richardson-Zaki (R-Z) correlation [Richardson et al., 1954] is among the most useful methods to describe the relationship between the void fraction and superficial velocity in a conventional liquid fluidized bed. The R-Z Equation is

$$\varepsilon^n = \frac{U}{U_i} \tag{4.9}$$

where U is the superficial velocity and U_i is the settling velocity of a particle at infinite dilution. The R-Z exponent or index (n) is a function of the particle terminal Reynolds number (Re_t). For the TLD 302 (1.7-2.35 mm) Nanogels

$$n = 4.45\,\mathrm{Re}_t^{-0.1} \qquad for\ 200 < \mathrm{Re}_t < 500 \tag{4.10}$$

$$\text{where, } \mathrm{Re}_t = \frac{U_t \rho_t d_P}{\mu_t} \tag{4.11}$$

The settling velocity at infinite dilution (U_i) and the terminal velocity (U_t) are related by

$$\log\left(U_i\right) = \log U_t - \frac{d_P}{D} \tag{4.12}$$

The R-Z exponent (n) can also be obtained from the experimental data by plotting the logarithm of the superficial velocity against the logarithm of the void fraction

$$\ln U = n \ln(\varepsilon) + \ln(U_i) \tag{4.13}$$

After calculating the void fraction (ε) from Equation (4.8), the experimental data are plotted in Figure 4-4 for three different amounts of fluidized TLD 302, 1.7-2.35 mm Nanogel granules and using our experimental data and the Equations above, the Richardson-Zaki exponent (n), and the terminal velocity (U_t) were calculated and shown in Table 4-4. As seen in the table, the values of the Richardson-Zaki exponent (n), for 1.7-2.35 mm Nanogel granules, calculated from Equation (4-10) are somewhat lower than the experimental values. This may possibly be due to the fact that the data were obtained in an inverse fluidized bed rather than a conventional fluidized bed.

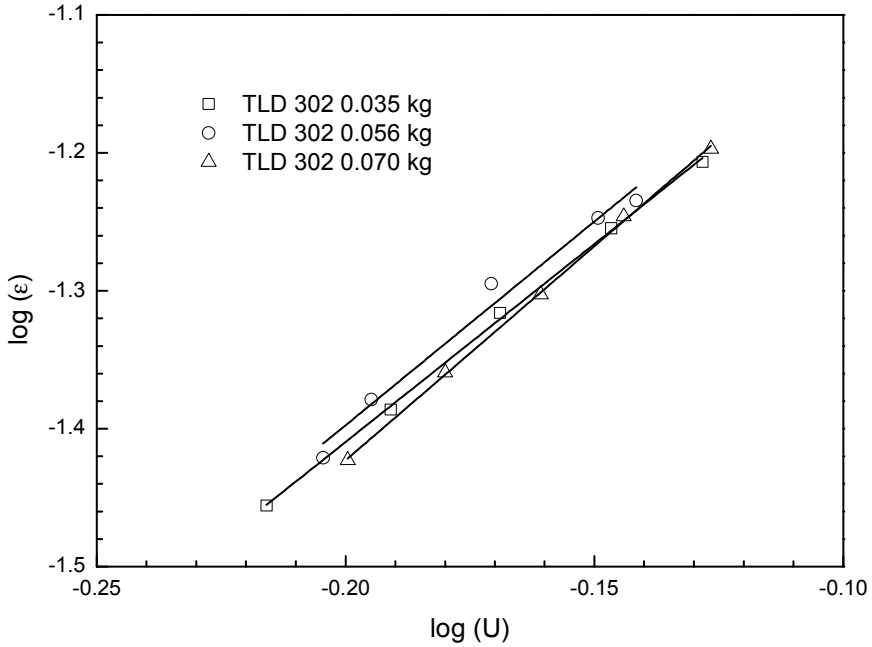

Figure 4-4. Relationship between the superficial velocity and the void fraction ε for three different amounts of TLD 302 Nanogels accordingly to the R-Z Equation.

Table 4-4. *Richardson-Zaki bed expansion parameters for 35 g, 56 g and 70 g TLD 302 Nanogel particles from experiment data and calculated using Equations (4.10-4.12)*

Mass (g)	R-Z (exp) (n)	R-Z (exp) (U_i) (m/s)	U_t Eq. (4.12) (m/s)	Re_t Eq. (4.11)	R-Z Eq. (4.10) (n)
35	2.87	0.145	0.154	310	2.52
56	2.95	0.155	0.164	333	2.49
70	3.10	0.158	0.169	340	2.48

There are very few correlations for an inverse fluidized bed, though several models are available for correlating bed expansion with fluid superficial velocity in a conventional liquid-solid fluidized bed (such as the R-Z model above). Fan et al. [Fan et al., 1982] proposed a model based on a drag force function, f, which can be used to describe the bed expansion in an inverse fluidized bed. This correlation expressed in terms of the void fraction of the

inverse fluidized bed ε, Archimedes number $Ar = d_P^3(\rho_l - \rho_P)\rho_l g / \mu_l^2$, Reynolds number $\mathrm{Re} = \frac{U\rho_l d_P}{\mu_l}$ and the ratio of the particle size to the bed diameter is

$$f = 3.21\varepsilon^{-4.05} Ar^{-0.07} \exp(3.5\frac{d_P}{D}) \tag{4.14}$$

In this model, a drag force function, *f,* defined as the ratio of the drag force of fluid on particles in a multi-particle system to that in a single particle system, is a function of the Archimedes number and the Reynolds number. This drag force function for the inverse fluidization system taken from Fan et al. [Fan et al., 1982] is

$$f = \frac{Ar}{13.9\,\mathrm{Re}^{1.4}} \qquad for\ 2 < \mathrm{Re} < 500 \tag{4.15}$$

$$f = \frac{3Ar}{\mathrm{Re}^2} \qquad for\ \mathrm{Re} > 500 \tag{4.16}$$

where the Archimedes number and the Reynolds number at different flow superficial velocities can be calculated from the experimental data. The void fraction of the inverse fluidized bed ε at different flow superficial velocities can be calculated from Equation (4.8).

By plotting the logarithm of the drag force function *f* against the logarithm of the void fraction ε, the slope of the straight line (see Equation (4.14)) can be obtained, which should be close to -4.05 according to Fan et al. [Fan et al., 1982]. After calculating the void fraction (ε) from Equation (4.7) and the drag force function *f* from Equation (4.14), the experimental data are plotted in Figure 4-5 for 35 g of TLD 301 0.7-1.2 mm Nanogel granules and three different amounts of

TLD 302 1.7-2.35 mm Nanogel granules. As seen in the figure, straight lines are obtained for all these three experimental runs; the slope of -4.04 for TLD-301 Nanogels and the average slope of -4.15 for TLD 302 Nanogels closely agree with the value of -4.05 suggested by Fan et al. [Fan et al., 1982].

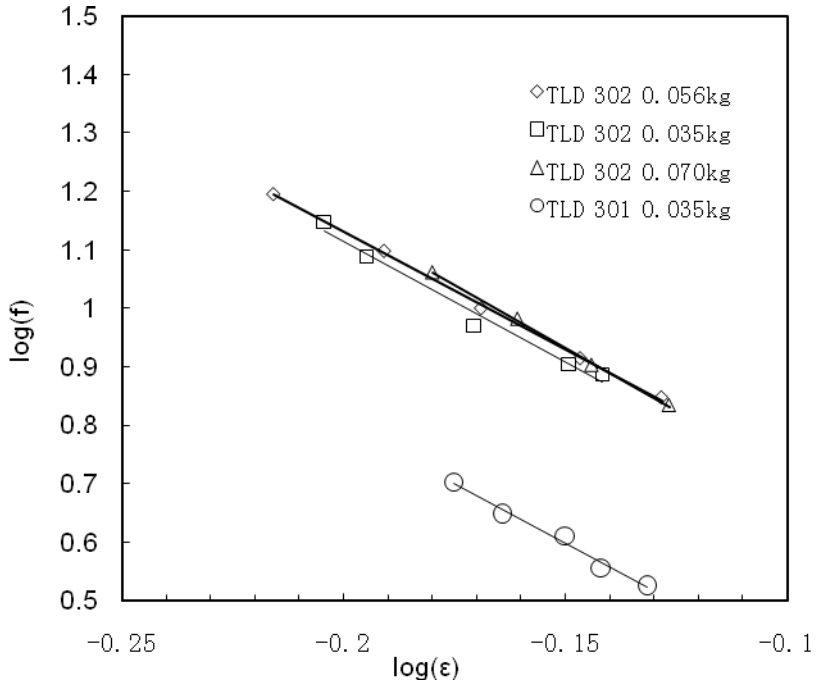

Figure 4-5. Relationship between the drag force '*f*' as defined by Fan et al. [Fan et al., 1982] and the void fraction ε for TLD 301, 0.7-1.2 mm and TLD 302 sieved, 1.7-2.35 mm.

4.4.5. Removal of Oil from Water in an Inverse Fluidized Bed and an Inverse Packed-Fluidized Bed of Nanogel Granules

Figure 4-6 (a) and (b) shows the size of the oil droplets in oil-in-water emulsions with 1% and 4% Tween 80 added. As seen in this figure, the size of most of the oil droplets is less than 20 μm, which indicates that the oil droplets

produced in our experiments can be classified as emulsified oil. Without adding the Tween 80 stabilizer, the oil droplets are much larger than 20 μm (see Figure 4-6 (c)) indicating the presence of dispersed oil.

Table 4-5 shows the emulsion stability experiment results. The addition of 4% by volume (or higher) of Tween 80 as compared to the amount of oil added produces an emulsion that remains stable without stirring for 1 hour. That is, the average inlet concentration (COD) (after being mixed with deionized water) measured at 10 minute intervals differed from the average outlet concentration by less than 5% when passed through the empty column (without Nanogel present). Before starting an inverse fluidized bed experiment, the Tween 80 stabilized oil-in-water emulsion is mixed in a blender for a few minutes and the emulsion is kept stirred with a magnetic stirrer to keep it stable during the duration of the experiment.

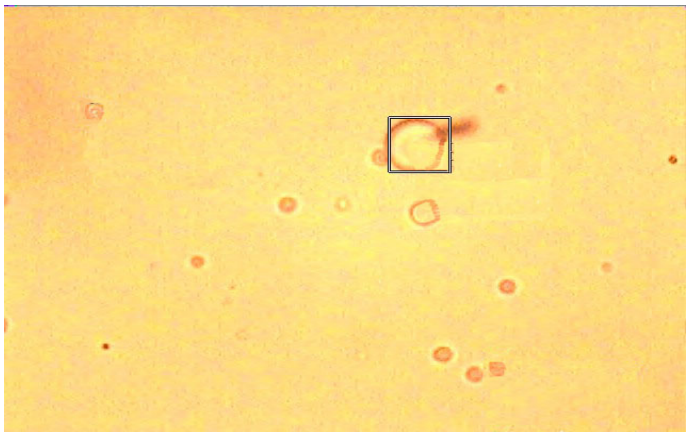

(a)

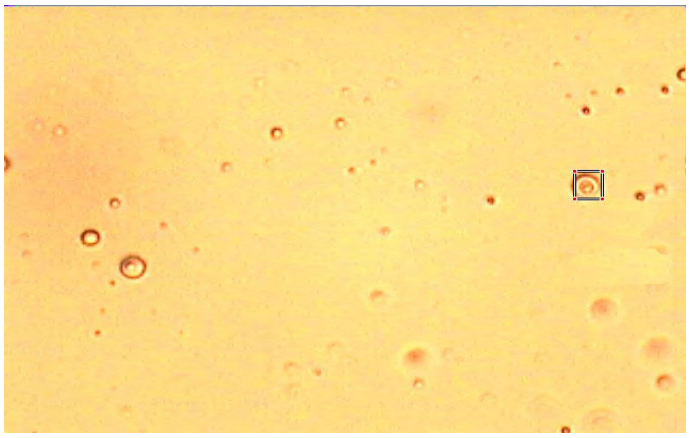

(b)

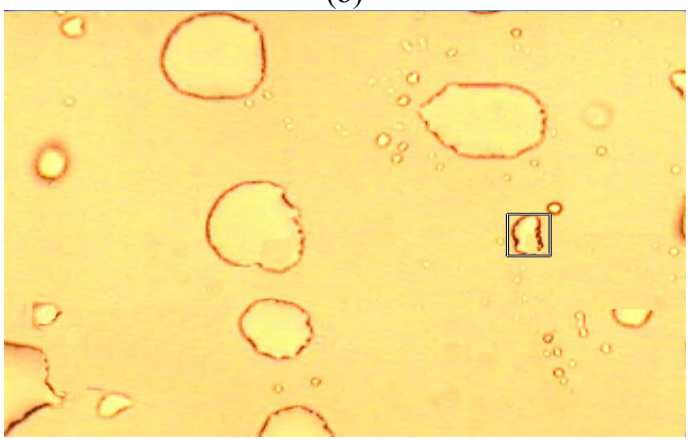

(c)

Figure 4-6. Marked oil droplet size with different amount of Tween 80: (a) 1% Tween 80, height 12.4 µm, width 11.9 µm, in the range of emulsified oil, (b) 4% Tween 80, height 5.7 µm, width 5.8 µm, in the range of emulsified oil, and (c) 0% Tween 80, height 95.6 µm, width 83.5 µm, in the range of dispersed oil.

Table 4-5. *Oil-in-water emulsion stability results for different proportion of emulsifier (Tween 80)*

Proportion of Tween 80	0.5%	1%	3%	4%	5%
Inlet average COD concentration (mg/L)	1092	1091	1065	1085	1104
Outlet average COD concentration (mg/L)	687	966	978	1058	1065
Decrease	37%	11%	8.2%	2.3%	3.6%

The oil removal efficiency and capacity of the Nanogel granules is studied by measuring both the inlet and exit concentrations of oil as a function of time and plotting a breakthrough curve. Ideally, the inlet oil concentration should remain constant throughout the experiment, but small changes in the water pressure, oil pump flow rate and stability of the emulsion result in somewhat different inlet concentrations with time; hence an average value is used. From the breakthrough curve, the amount of oil removed by the inverse fluidization process is given by

$$m_{\mathrm{Re}moval} = F\overline{C_{in}}t - F\int_o^t C_{out}dt \tag{4.17}$$

where $m_{Removal}$ is the weight of oil removed by the aerogel granules, F is the flow rate during the experiment, $\overline{C_{in}}$ is the average inlet oil concentration, C_{out} is the outlet oil concentration, t is the time when the fluidized bed is no longer stable and Nanogel granules begin to leave the column due to their decrease in buoyancy as they adsorb/absorb oil.

The inlet and outlet concentrations of oil are monitored by analyzing the chemical oxygen demand (COD) at several time intervals during the experiments. A calibration curve relating the measured COD concentration to the actual oil concentration in mg/l is shown in Figure 4-7.

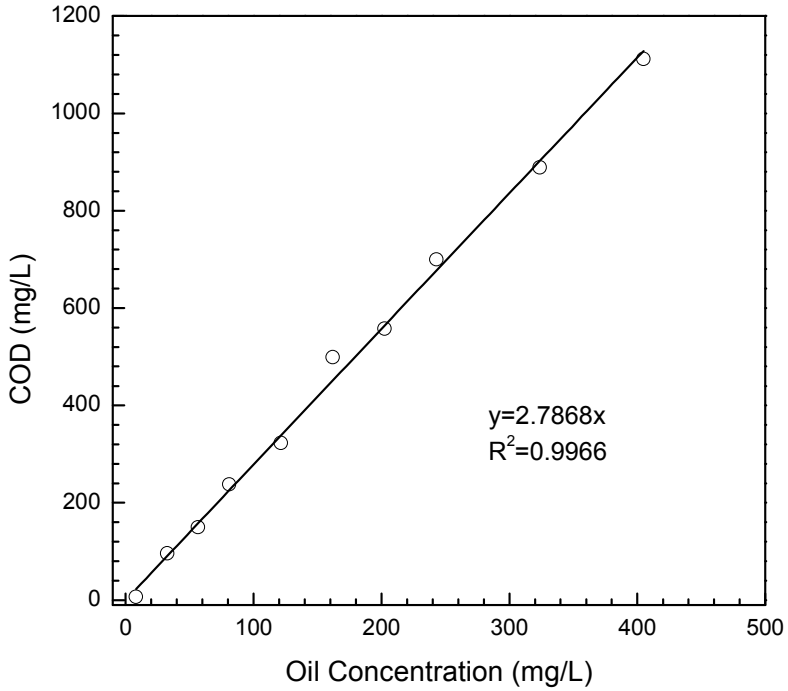

Figure 4-7. Correlation between the oil concentration in water and COD levels measured by HACH DR/890 colorimeter.

The breakthrough curve in each experimental run is obtained from the experiment concentration versus time data. Table 4-6 shows the operating conditions for each experiment. The following parameters are changed to compare the oil removal efficiency: the proportion of Tween 80 in the oil-in-water emulsion, fluid superficial velocity, particle (granule) size range, and amount of particles. The breakthrough curves under different operating conditions are shown in Figures 4-8, 4-9, and 4-10 for inverse fluidization and Figure 4-11 for an inverse packed-fluidized bed. Here we have started the experiment at a flow rate (water velocity) which is below the minimum fluidization velocity so that the bed remains in the packed bed mode until the Nanogel granules adsorb/absorb sufficient oil to decrease the net buoyancy force (buoyancy minus gravity) acting on them and the bed fluidizes.

Table 4-6. *Summary of experimental conditions and oil removal capacity from water by an inverse fluidized bed, packed-fluidized bed or fluidized-packed bed of Nanogel*

Nanogel type	Particle size (mm)	Figure #	% Tween 80	Nanogel Mass (g)	Flow Rate (GPM)	U/U_{mf} ratio	Entrance COD (mg/L) (average)	q (g oil / g Nanogel)
301	0.7-1.2	4-8	4	55	1.3	1.1	1052±30	1.43
301	0.7-1.2	4-8	4	110	1.3	1.1	1076±67	1.35
301	0.7-1.2	4-8	4	200	1.3	1.1	1032±49	1.26
301	0.7-1.2	4-9	1	55	1.3	1.1	1094±51	2.13
301	0.7-1.2	4-9	1	110	1.3	1.1	1075±81	1.75
301	0.7-1.2	4-9	1	200	1.3	1.1	1163±102	1.51
302	1.7-2.3	4-10	4	110	2.0	1.1	1104±51	1.84
302	1.7-2.3	4-11	4	55	1.2	0.67	1198±118	2.26*
302	1.7-2.3	4-11	4	55	1.0	0.56	1211±51	2.77*
302	1.7-2.3	4-12	1	110	2.0-1.2	1.1-0.67	1007±32	1.91#

* Packed–fluidized bed # fluidized-packed bed

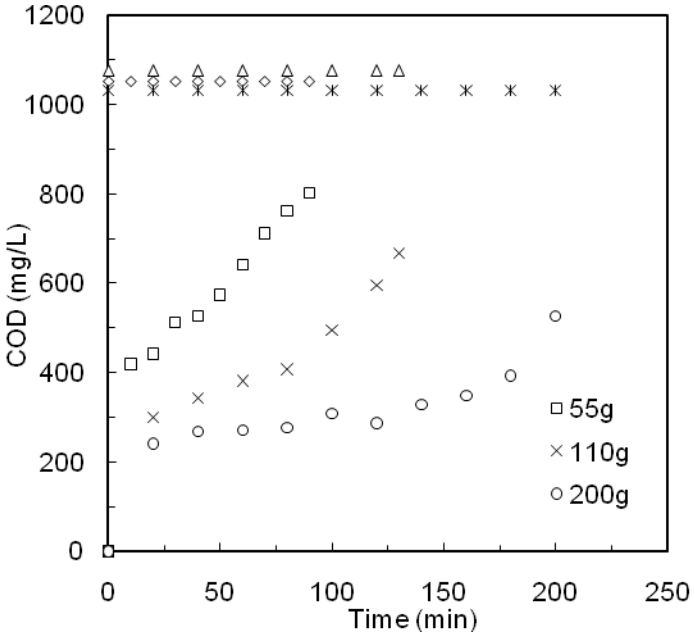

Figure 4-8. Breakthrough curve in fluidized bed for 55 g, 110 g and 200 g TLD 301, 0.7-1.2 mm Nanogel granules when the proportion of Tween 80 is 4%, the inlet COD is around 1000 mg/L and U/U_{mf} is 1.1.

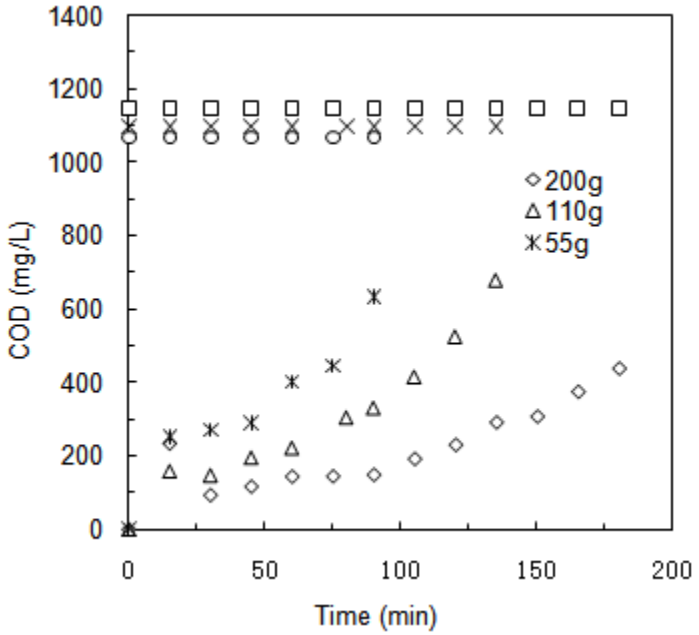

Figure 4-9. Breakthrough curve in fluidized bed for 55 g, 110 g and 200 g TLD 301, 0.7-1.2 mm Nanogel granules when the proportion of Tween 80 is 1%, the inlet COD is around 1100 mg/L and U/U_{mf} is 1.1.

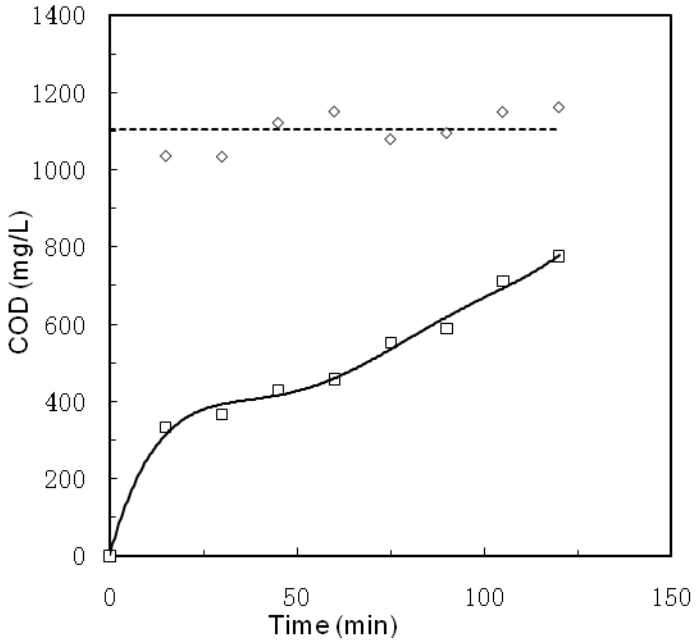

Figure 4-10. Breakthrough curve in fluidized bed for 110 g TLD 302, 1.7-2.35 mm Nanogel granules when the proportion of Tween 80 is 4%, the average inlet COD is around 1100 mg/L and U/U_{mf} is 1.1.

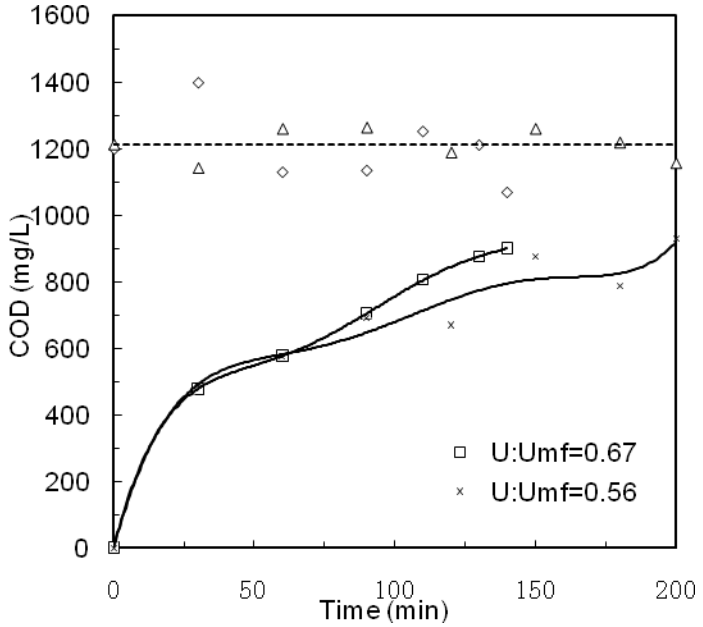

Figure 4-11. Breakthrough curve in packed-fluidized bed for 55 g TLD 302, 1.7-2.35 mm Nanogel granules when the proportion of Tween 80 is 4%, the average inlet COD for both runs is around 1200 mg/L and U/U_{mf} are 0.56 and 0.67, respectively.

We also started a run using an emulsion stabilized by 1% Tween 80 as a fluidized bed (U/U_{mf} = 1.1) and when the bed expanded, but before any Nanogels left the column, we decreased the flow rate below minimum fluidization (U/U_{mf} = 0.67) and ran as a packed bed. This allowed us to continue the experiment without losing Nanogel granules from the bottom of the column. The breakthrough curve for this experimental run is shown in Figure 4-12.

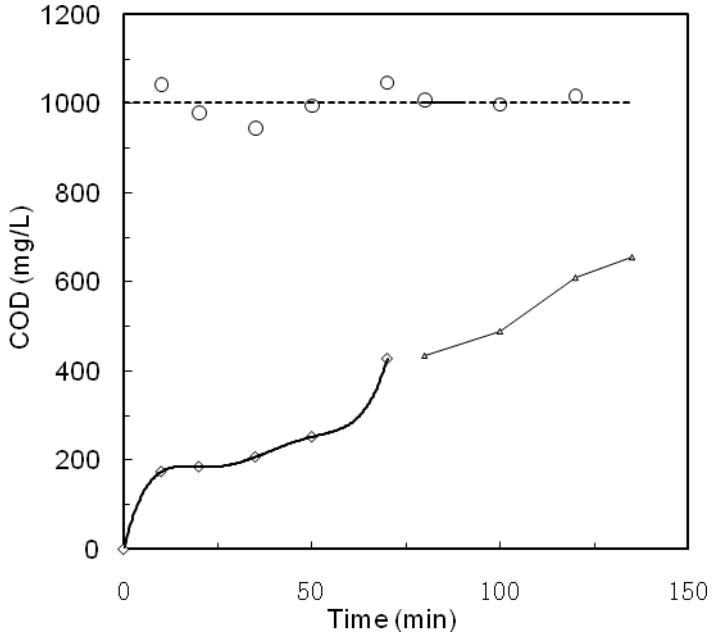

Figure 4-12. Breakthrough curve in fluidized-packed bed for 110 g TLD 302, 1.7-2.35 mm Nanogel granules when the proportion of Tween 80 is 1%, the average inlet COD is around 1000 mg/L and U/U_{mf} is 1.1 during the fluidized bed process and 0.67 during the packed bed process.

The removal capacity (kg oil/kg Nanogel) using Equation (4.20) based on the breakthrough curves is also shown in Table 4-6 and varied between 1.2 to 1.84 for the fluidized bed and 2.26-2.77 for the packed-fluidized bed mode when the proportion of Tween 80 in the emulsion is 4% and varied between 1.51-2.13 for the fluidized bed when Tween 80 in emulsion is reduced to 1%.

The shape and sharpness of the breakthrough curve for a given adsorbent mainly depend on such factors as the adsorption isotherm at equilibrium, the mass transfer rate, and hydrodynamic factors such as bed height and contact (residence) time. As already mentioned, the breakthrough time in a fluidized bed adsorber is considerably shorter than in a fixed bed adsorber due to the large axial mixing in the fluidized bed. In our experiments, the outlet oil concentrations in the beginning of the experiment are high and the oil removal efficiencies are relatively low. There are several possible reasons for these results: (1) the contact time through the fluidized bed or packed-fluidized bed is too short (less than 1 min) and is not long enough for the Nanogels to absorb the oil passing through them and (2) while the presence of the emulsifier, Tween 80, greatly increases the stability of the oil-in-water emulsion, it may also hinder the adsorption/absorption of oil by the Nanogel surfaces.

According to Hrubesh et al. [Hrubesh et al., 2001], solvents that are insoluble in water are separated by selectively wetting the surfaces of the aerogels, entering the pores and subsequently absorbed into the porous structure. Even though very little Tween 80 is present (only 1% or 4% of the weight of oil in the emulsion), since the surfactant can physically interact with both oil and water, the hydrophilic end of the Tween 80 may allow some water molecules to attach to the surface and enter the Nanogel particles thus reducing the Nanogel adsorption/absorption capacity for oil. In Chapter 3, we have already shown that as the amount of Tween 80 is increased and the oil-in-water emulsion becomes more stable, the adsorption capacity decreases.

To check whether the Tween 80 has an effect on the adsorption/absorption capacity of the Nanogels, we also did runs using only 1% of Tween, as seen in Figures 4-9 and 4-12. If we compare Figures 4-8 and 4-9 for TLD 301 Nanogel, Figure 4-8 shows outlet concentrations at short times that are almost twice as large as the outlet concentrations at short times in Figure 4-9. A similar result is found when comparing Figures 4-10 and 4-12 for the larger TLD 302 Nanogel granules. Hence it appears that adding 4% Tween is inhibiting the Nanogels from adsorbing/absorbing oil more than adding 1% Tween similar to what was observed in the batch experiments described in Chapter 3.

The oil removal results from Table 4-6 also show that: (1) for the same type of Nanogel, when the flow rates are the same, the oil removal capacities become lower as the weight of the Nanogel granules increases. This is probably due to a decrease in the axial mixing of the solid phase as the bed height increases. (2) for the same U/U_{mf} ratio and the same weight of Nanogel granules, it appears that the larger the particle size, the higher the oil removal capacity, and (3) the oil removal capacities for the same type of Nanogel are higher in the packed-fluidized bed mode than those in the fluidized bed. This latter result can be explained from the force balance Equation (4.4). As Nanogels begin to absorb oil, the net buoyancy force acting on the particles decreases, (the buoyancy force is constant and the gravity force increases) and therefore the drag force (ΔPA) needed to fluidize the particles decreases and the bed begin to expand due to the increase of the gravity force. At the moment, when the length of the bed reaches the entire column or the sum of the gravity force and drag force is larger than the

buoyancy force, the Nanogel particles begin to leave the column. For Nanogel particles which adsorb/absorb the same amount of oil in a fluidized bed or in a packed-fluidized bed, both will have the same gravity force and buoyancy force, but the former has the larger drag force due to the larger fluid velocity. Therefore it is much easier for the particles in the fluidized bed to leave the column when they adsorb/absorb the same amount of oil compared with the same particles in the packed-fluidized bed.

By decreasing the flow rate during an experiment (Figure 4-12), the drag force is reduced (fluidized-packed bed mode) and the Nanogel granules will remain in the column for a longer time. This mode of operation will also result in a higher oil removal capacity.

4.4.6. Comparison of Modeling Results with Experimental Measurements

A Freundlich isotherm for oil adsorbed onto TLD 301 Nanogel from the oil-in-water emulsion using 4% Tween 80 as the stabilizer at room temperature is shown in Figure 4-13. The Freundlich constants, k and $1/n$, are calculated from the slope and intercept of the curve and are equal to 6133 and 1.33, respectively. One set of batch kinetic data fitted to the linear driving force model is shown in Figure 4-14; the adsorption rate constant K in Equation (1.4) is obtained using a least squares regression. An average value of K, based on two separate batch kinetic experiments, is 5.68×10^{-2} s^{-1}.

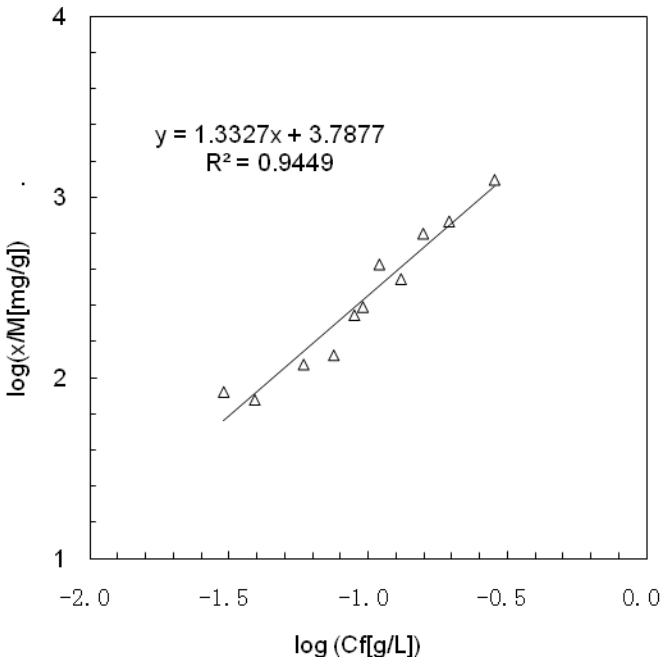

Figure 4-13. Freundlich isotherm for adsorption of oil from oil-in-water emulsion by TLD 301 Nanogel granules.

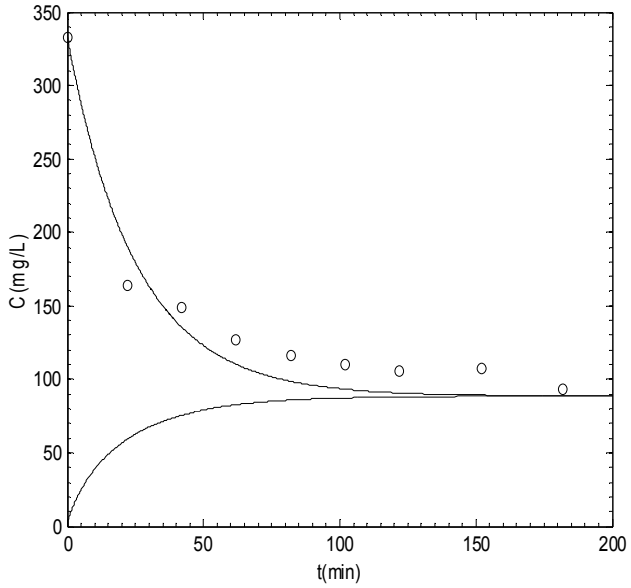

Figure 4-14. Oil concentration as a function of time in a batch kinetic experiment: circles represent experimental data and solid lines C' and C_e' are obtained from the linear driving force model when K is 5.68×10^{-2} s^{-1}.

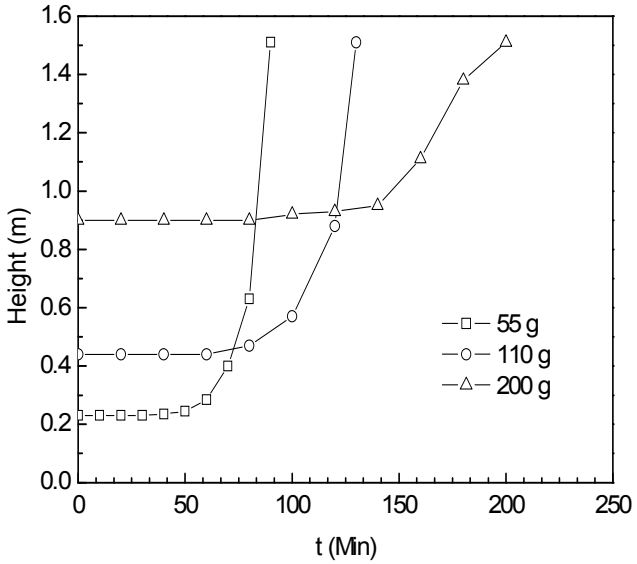

Figure 4-15. Bed height as a function of time for 55 (□), 110 (○) and 200 (△) grams of TLD 301. For 55g TLD 301, data was fit by a horizontal line for t < 30 Min and a sixth order polynomial for t > 30 Min; for 110g TLD 301, data was fit by a horizontal line for t < 60 Min and a fifth order polynomial for t > 60 Min; for 200g TLD 301, data was fit by a horizontal line for t < 80 Min and a sixth order polynomial for t > 80 Min.

Unlike experiments in fluidized bed adsorbers reported in the literature, the expanded fluidized bed height in our experiments changes as a function of time. The fluidized bed height remains relatively constant at the beginning of the experiment until some of the Nanogels have adsorbed/absorbed an appreciable amount of oil. These particles become heavier and can no longer be suspended by the buoyancy force of the fluid, and the bed begins to expand downward towards the bottom of the column until the expanded bed height is equal to the physical length of the column at which point the experiment is stopped. Figure 4-15 shows the expanded bed height data as a function of the time of the experiment for 55,

110, and 200 grams of TLD 301 Nanogel. This adds an additional complication to the simulations.

The experimentally observed concentration of oil in the exit stream (breakthrough curve) is compared with the model predictions in Figures 4-16, 4-17 and 4-18. Here we have plotted the oil concentrations as actual mg/l rather than as COD mg/l using the calibration curve, Figure 4-7, to convert from one to the other. All of the experimental runs in these three figures were made at the same conditions except for the weight of Nanogel used (height of the bed). As seen in the figures, the results of the simulations and experiments are not in good agreement when using the value of $K = 5.68 \times 10^{-2}$ s^{-1} as obtained from the batch kinetic experiments. We suspect that the K value from the batch kinetic experiments is appreciably lower than the real K value for adsorption in the fluidized bed, because the Nanogel particles are much better mixed in the fluidized bed than in the batch experiments performed in a bottle stirred by a shaker.

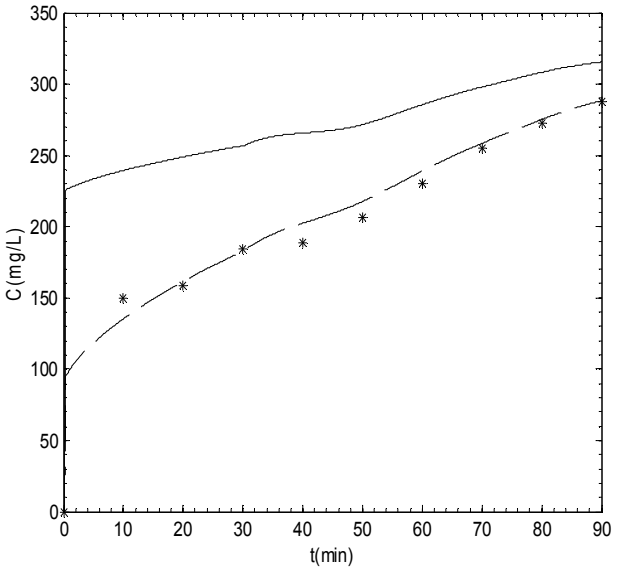

Figure 4-16. Model results for the breakthrough curve using 55 g TLD 301: (a) measured *K* (solid line) (b) 2.75 *K* (dashed line) compared to experimental data.

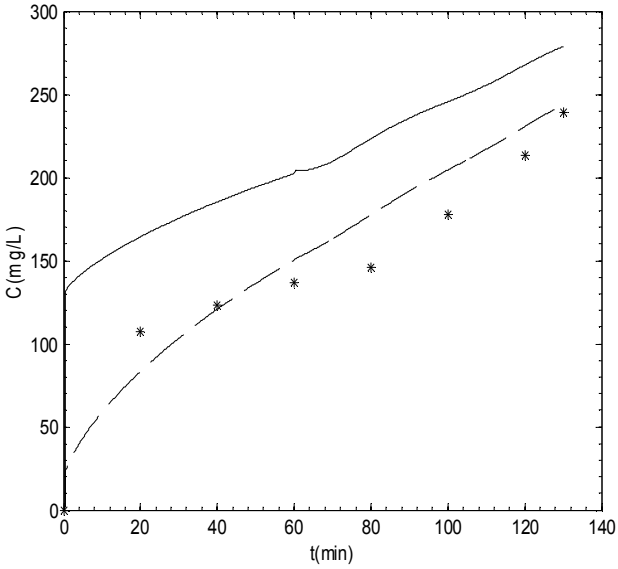

Figure 4-17. Model results for the breakthrough curve using 110 g TLD 301: (a) measured *K* (solid line) (b) 2.75 *K* (dashed line) compared to experimental data.

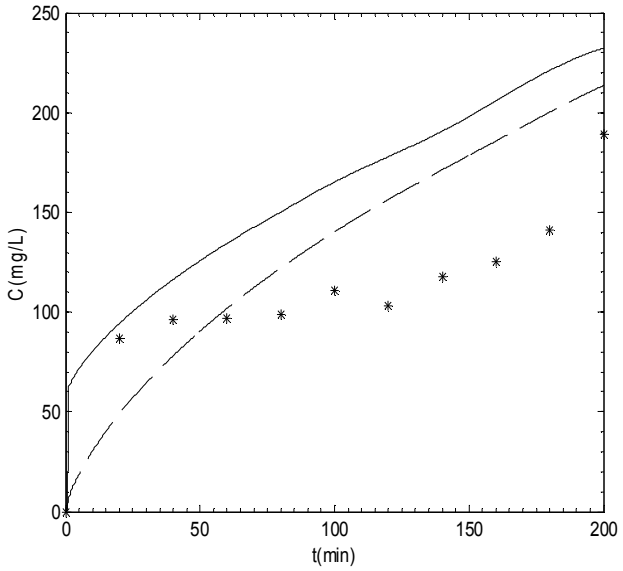

Figure 4-18. Model results for the breakthrough curve using 200 g TLD 301: (a) measured K (solid line) (b) 2.75 K (dashed line) compared to experimental data.

In the experimental run shown in Figure 4-16 (55 g Nanogel, and the shortest bed height used), the value of K which gives the best fit of the experimental breakthrough curve in the inverse fluidized bed was calculated by the method of least squares and is about 2.75 times larger (1.56×10^{-1} s^{-1}) than the original K value. This new K value is also used to fit the experimental data in Figures 4-17 and 4-18, with poorer results observed as the bed height (amount of Nanogel granules) becomes larger. When less granules are used in the inverse fluidized bed (shorter bed), the Nanogel granules tend to saturate more uniformly because of the CSTR-like mixing. When more granules are fluidized in the bed, since the bed height is larger, it is more difficult for the granules to mix well. In this case, the assumption made in the model that the solid phase is completely mixed is not very accurate.

4.5. Conclusions

The granule density and hydrodynamic characteristics of the Nanogels was calculated by measuring the pressure drop and bed expansion of clean water in the inverse fluidized bed. The experimental results are in good agreement with previous models used for liquid-solid fluidized beds. The main factors which affect the oil removal capacity of the Nanogel granules in the inverse fluidized bed and inverse packed-fluidized bed are the size of the granules, the bed height, and the fluid velocity. The use of Tween 80 to stabilize the oil-in-water emulsions used in the experiments appears to decrease the adsorbing/absorbing capability of the Nanogels and the use of another type of stabilizer, perhaps a nanopowder (Pickering emulsion), should be investigated. A model was developed to predict the inverse fluidized bed experimental results based on equilibrium and kinetic batch measurements using the Nanogel and oil-in-water emulsion. The model assumed complete axial mixing in the solid phase, but variable bed height as a function of time. Good agreement between the model and experimental results are obtained for short bed heights using an equilibrium rate constant about 2.75 times larger than that measured in the batch system.

CHAPTER 5 AQUEOUS PHASE ADSORPTION OF TOLUENE IN A PACKED AND FLUIDIZED BED OF HYDROPHOBIC AEROGELS

5.1. Introduction

In Chapter 4, Nanogel was used as the sorbent for the removal of emulsified oil from oil-in-water emulsion in the inverse fluidized bed mode. As discussed, the Nanogel particles can adsorb as much as 2.8 times their weight of emulsified oil by the inverse fluidization process. In the work in this chapter, the adsorption performance of Nanogel in the inverse fluidized bed or the packed bed for the removal of toluene from aqueous phase was studied.

Toluene is a monoaromatic hydrocarbon with a wide variety of uses in industry, primarily as a gasoline component and as a solvent for paints, thinners, coatings, adhesives, inks, gums, oils and resins [Buikema et al., 1980; Irwin et al., 1997]. Sources contributing to the occurrence of toluene in wastewater can be broadly characterized as: toluene emissions associated with these industries, commercial establishments that use toluene, household and consumer products, surface runoff, and chemical and biogenic reactions that occur during water and wastewater treatment [Tata et al., 2003]. Toluene discharged into the aquatic ecosystem is dangerous to aquatic life and will result in fouling of the shoreline. Also, toluene can cause disease in humans such as skin disease, respiratory system disorders, heart disease, and kidney and liver damage [Irwin et al., 1997].

Current technologies for toluene removal from wastewater include biological treatment [Ahmadvand et al., 1995; Enright et al., 2007], chemical

treatment, and adsorption or absorption by a variety of sorbents. However, the biological treatment approach introduces new problems such as secondary pollution from remaining nutrients and a risk of microbial contamination [Bouwer et al., 1988; Lemoine et al., 1991]. Chemical treatment is currently used in many drinking water plants in the United States; however, it is difficult to maintain the reaction conditions in the treatment and some chemically decomposed byproducts can be introduced in the water [Yue et al., 2001].

Several types of sorbents have been studied for the removal of toluene from water in packed bed filters or adsorbers. They include activated carbon [Chatzopoulos et al., 1995; Yue et al., 2001; Wibowo et al., 2007; Choi et al., 2009], diatomite [Aivalioti et al., 2010], zeolite [Ranck et al., 2005; Choi et al., 2009], and tires crumb rubber [Alamo-Nole et al., 2010]. Of these materials, only granulated activated carbon (GAC) is commercially used as a sorbent to remove toluene and other organics from water. However, GAC displays disadvantages such as slow kinetics and limited removal capacity. As proposed in Chapter 1, hydrophobic silica aerogels have been studied for the sorption of several organic solvents from water [Hrubesh et al., 2001; Standeker et al., 2007]. They have some desirable properties and might be used as sorbent for the removal of toluene from water.

In the work described in this chapter, Nanogel granules about 1 mm in size were used to remove trace amounts of toluene (~200 ppm) from aqueous solutions configured either as a packed bed or fluidized bed. The objectives of this work

are to investigate the performance of Nanogel granules for removing low concentrations of toluene from aqueous solutions in both packed bed and inverse fluidized bed modes, and to simulate packed bed and fluidized bed adsorption behavior by models taking into account, hydrodynamics, mass transfer, and adsorption at equilibrium.

5.2. Experimental Equipment and Methods

5.2.1. Materials

The following materials were used in our experimental work: TLD-301 (0.7-1.2 mm) Nanogels supplied by Cabot Corporation and anhydrous reagent grade toluene supplied by Sigma-Aldrich. Ordinary tap water was used to prepare the dilute toluene solutions.

5.2.2. Packed Bed and Inverse Fluidized Bed Experiments for Toluene Adsorption

A schematic diagram of the experimental setup used in the toluene adsorption experiment is shown in Figure 5-1. It consists of a tank with cover, a high speed mixer, a magnetic drive pump, a fluidization column, valves and piping, flow meters, a pressure gauge and a differential pressure transmitter with a display. The tank has a volume of 100 gallons and is made of high-density polyethylene (HDPE). The cover was also made of HDPE and used to prevent toluene volatilization, i.e., to ensure that the influent toluene concentrations remained within 2-3% of its average value throughout the course of the adsorption

experiments. To minimize any adsorption of toluene by the HDPE tank, the dilute toluene solution only remained in the HDPE tank for the duration of the experiment and the tank was rinsed with clean water after each experiment. A high speed mixer (WingertC-2-0-PRP/316) was used to prepare the feed toluene solution and a magnetic drive pump (March BC-4C-MD) was employed to transfer the feed solution into the piping system. The fluidization column was made of PVC with an internal diameter (ID) of 0.076 m (3 in.) and an outer diameter (OD) of 0.089 m (3.5 in.). The length of the column was 1.47 m (58 in.). The valves and piping were also made of PVC, and the pipe size was 1 in. The flow of water was adjusted by ball valves, and flow readings were taken by two calibrated electronic digital flow meters, one for the range between 0-3 GPM and the other for the range between 3-50 GPM (GPI series A109).

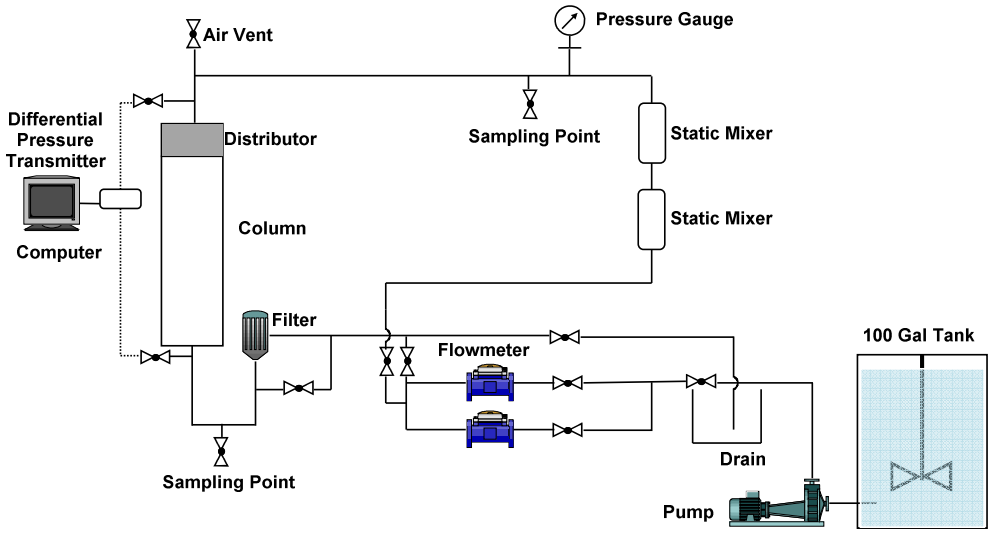

Figure 5-1. Schematic diagram of the packed bed and inverse fluidized bed experimental setup.

For both the packed bed and inverse fluidized bed experiments to measure the toluene adsorption efficiency and capacity, a typical experimental run is described as follows. First, the toluene solution was prepared in the tank by mixing a certain amount of toluene into tap water and stirred by using the high speed mixer for several minutes until toluene was totally dissolved in the water. Then, the solution was injected into the piping system upstream of column by the pump. By adjusting the flow rate with ball valves, a desired flow rate of solution was obtained. If the fluid superficial velocity was lower than the particle minimum fluidization velocity in the column, the experiment was operated in the packed bed mode; if the fluid superficial velocity was larger than the particle minimum fluidization velocity, the experiment was operated in the fluidized bed mode. Samples of solution of about 100 ml, upstream and downstream of the packed bed or fluidized bed, were taken at regular intervals and analyzed for toluene concentration by using a gas chromatograph (GC) equipped with the flame ionization detector (SRI 8610C) until the concentrations of the downstream sample was equal to the concentrations of the upstream sample, i.e., breakthrough occurred.

5.2.3. Batch Equilibrium and Kinetic Measurements for Toluene Solution

To determine the adsorption isotherm of the Nanogels, 100 mg TLD-301 Nanogel was mixed with 100 mL toluene solutions of different initial concentrations in sealed glass bottles to prevent toluene vapor from escaping.

The concentrations of these toluene solutions were lower than the solubility limit of toluene in water (470 mg/L). These bottles were shaken in an Innova 4080 incubator shaker (200 rpm) at room temperature. Upon reaching equilibrium (> 3 hours), all the samples were withdrawn and analyzed by the GC.

Batch kinetic experiments were also conducted at room temperature. A sealed glass bottle containing 100 mL toluene solution of concentration around 350 mg/L, was continuously mixed with 100 mg of TLD-301 Nanogel using a magnetic stirrer (Cimarec). The toluene concentration of the liquid sample was measured by the GC at different time intervals. The experiment was stopped when the concentration approached the equilibrium concentration.

5.3. Theoretical Models

Although modeling of the adsorption behavior in a liquid-solid packed bed or fluidized bed has been reported in the literature [Lin et al., 1989; Veeraraghavan et al., 1989; Lin et al., 1990; Cooney, 1998; Wright et al., 2001; Correa et al., 2007; Wang et al, 2010], we wanted to compare our packed bed or fluidized bed experimental results with models that are based on equilibrium and kinetic data for our particular Nanogel-toluene-water solution system. As will be shown below, the breakthrough curves in our inverse fluidized bed absorber are considerably different than those expected in a comparable fixed bed adsorber. In order to describe the toluene adsorption in aqueous phase in the packed bed or inverse fluidized bed, two somewhat different model equations and boundary

conditions were used, taking into account hydrodynamic behavior, dispersion, and mass transfer between the liquid and solid phases.

5.3.1. Assumptions

The governing equations of the models were derived based on the assumptions listed below: (1) Nanogel particles are mono-size and an average particle size of 0.95 mm is used; (2) wall effects are negligible since the column-to-particle-diameter ratio is ~80; (3) radial concentration gradients are negligible for both the liquid and solid phases in the column; (4) rate of adsorption is determined by the linear driving force model (see below) based on batch kinetic data; (5) adsorption equilibrium is represented by the Freundlich equation; (6) the solid phase is immobile and there is no dispersion of the adsorbate (toluene) in the solid phase in the packed bed mode; (7) the solid phase is completely mixed in the fluidized bed mode; and (8) the liquid phase is described by an axial dispersion model.

5.3.2. Derivation of Packed Bed Model Equations

Following Lin et al. [Lin et al, 1989; Lin et al, 1990], the mass balance with respect to the adsorbate in the liquid phase gives

$$\varepsilon \frac{\partial C}{\partial t} = D_{ax}\varepsilon \frac{\partial^2 C}{\partial z^2} - u\frac{\partial C}{\partial z} - (1-\varepsilon)K(C - C_e) \tag{5.1}$$

where ε is the void fraction of the packed bed or fluidized bed, C is the toluene concentration in the liquid phase in the packed bed or fluidized bed, C_e is the local equilibrium concentration in the liquid phase corresponding to the adsorbate concentration at the Nanogel particle boundary, D_{ax} is the liquid phase axial dispersion coefficient, u is the superficial fluid velocity, and K is the adsorption rate constant.

The initial and boundary conditions for the packed bed subject to a switch in the feed from a pure water stream to a toluene solution stream are

$$t = 0, \quad C(z,0) = 0, \quad 0 \le z \le H \tag{5.1a}$$

$$z = 0, \quad C = C_0 + \frac{D_{ax}\varepsilon}{u}\frac{\partial C}{\partial z}, \quad t > 0 \tag{5.1b}$$

$$z = H, \quad \frac{\partial C}{\partial z} = 0, \quad t > 0 \tag{5.1c}$$

where H is the height of the packed bed or fluidized bed and C_0 is the toluene feed concentration.

The liquid phase axial dispersion coefficient, D_{ax} is calculated using Equation (4.2), presented by Chung and Wen [Chung et al., 1968].

A mass balance with respect to the adsorbate in the solid phase gives

$$\frac{\partial q}{\partial t} = \frac{K'(C - C_e)}{\rho_P} \tag{5.2}$$

where ρ_P is the density of the particle, and q is the mass of toluene per unit mass of Nanogel in the particle.

The initial condition is

$$t = 0, \quad q(z,0) = 0, \quad 0 \le z \le H \tag{5.2a}$$

Finally, the Freundlich equation, Equation (1.2), is used to relate the amount of toluene adsorbed per weight of Nanogel to the concentration of toluene in the liquid phase at equilibrium.

The rate constant K' in Equation (3.1 and 3.2) is obtained from the batch kinetic experiments by using a linear driving force model, which is defined by Equations (1.4 and 1.5).

5.3.3. Derivation of Fluidized Bed Model Equations

The equations used to simulate the adsorption behavior of Nanogels in the inverse fluidized bed are proposed in *4.3.2*, Equations (4.1, 4.2, and 4.3).

5.3.4. Numerical Calculations

The governing Equations (4.1, 4.3, 5.1, and 5.2) are nonlinear partial differential equations. The spatial discretization method was used to transform these partial differential equations into a set of ordinary differential equations: these equations were discretized in space using finite differences with 50 evenly

spaced finite difference points along the column length. This set of ordinary differential equations was solved using a Runge-Kutta 23 simulation method programmed in Matlab R2008b; the step size in the program was approximately 0.05-0.1 s.

5.4. Results and Discussion

5.4.1. Adsorption Isotherms and Kinetics

A Freundlich isotherm for toluene adsorbed onto TLD 301 Nanogel from a toluene solution at room temperature is shown in Figure 5-2. The Freundlich constants, k and $1/n$, are calculated from the slope and intercept of the curve and are equal to 223 and 1.15, respectively. One set of batch kinetic data fitted to the linear driving force model is shown in Figure 5-3; the adsorption rate constant K is obtained using a least squares regression. An average value of K, based on two separate batch kinetic experiments, is 0.284 s^{-1}.

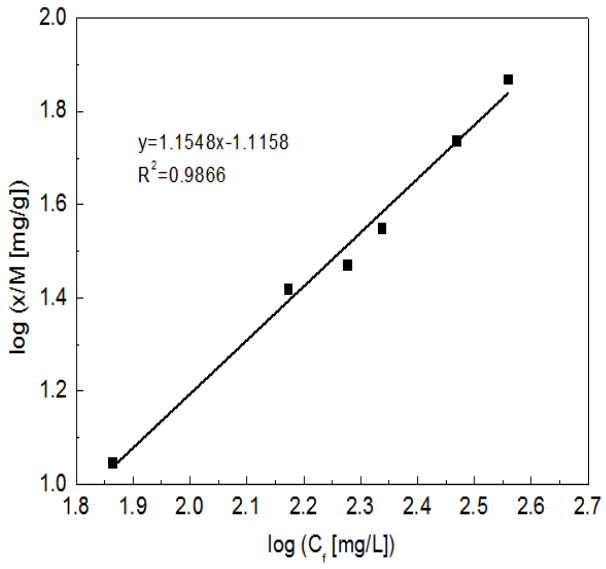

Figure 5-2. Freundlich isotherm for adsorption of toluene from toluene solution by TLD 301, 0.7-1.2 mm Nanogel granules.

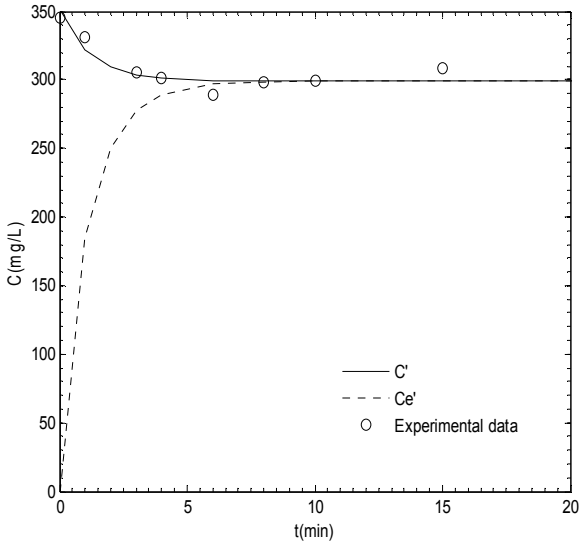

Figure 5-3. Toluene concentration as a function of time in a batch kinetic experiment: C' and C_e' are obtained from the linear driving force model when K is 0.284 s^{-1}.

The equilibrium toluene adsorption capacity of Nanogel compared with other sorbents for a concentration of 200 mg/L, are shown in Table 5-1. It should be noted that the values listed for the Freundlich constants for GAC, crumb rubber and diatomite are different than the values quoted in the original references because the units of k in Table 5-1 are mg g^{-1} $(g/L)^n$ instead of mg g^{-1} $(mg/L)^n$. As can be seen in this table, the adsorption capacity of Nanogel is lower than that of GAC, somewhat lower than that of MTMS aerogel, close to that of crumb rubber, and higher than that of diatomite. In reference [Hrubesh et al., 2001], the authors list a much lower value of k for GAC than that in Table 5-1 although the units of k are the same as in the table; thus the adsorption capacity of toluene of their fluorinated aerogel appears to be much higher than that of GAC. However if the correct value of k (as listed in Table 5-1, and based on reference [Dobbs et al., 1980]) is used instead, the adsorption capacities of GAC and fluorinated aerogel are about the same order of magnitude.

Table 5-1. *Comparison of toluene equilibrium adsorption capacity for Nanogel and other sorbents*

Sorbents	Freundlich Constants		Adsorption Capacity q (g/g) when C_e = 200 mg/L
	k (mg g^{-1} $(g/L)^n$)	$1/n$	
Nanogel	223	1.15	0.037
MTMS aerogel [Standeker et al., 2007]	1344	1.7	0.087
GAC [Dobbs et al., 1980]*	545	0.44	0.268
Crumb rubber [Alamo-Nole et al., 2010]*	208	0.98	0.043
Diatomite [Aivalioti et al., 2010]*	0.019	1.33	2×10^{-6}

* The value of k is different than the original value reported in the reference because of the different k units used, mg g^{-1} $(g/L)^n$ instead of mg g^{-1} $(mg/L)^n$.

5.4.2. Adsorption of Toluene from Water in a Packed Bed or an Inverse Fluidized Bed of Nanogel Granules

The toluene adsorption efficiency and capacity of the Nanogel granules in a packed bed or an inverse fluidized bed is obtained by measuring both the inlet and exit concentrations of toluene as a function of time and plotting a breakthrough curve. Ideally, the inlet toluene concentration should remain constant throughout the experiment. However, small changes in the water pressure and toluene pump flow rate result in somewhat different inlet concentrations with time; hence an average value is used. From the breakthrough curve, the toluene adsorption capacity q is defined as Equation (3.1).

The breakthrough curves for each experimental run are obtained from the experiment concentration versus time data and are shown in Figures 5-4, 5-5, 5-6 and 5-7 for different operating conditions, i.e., changing the fluid superficial velocity and the amount of particles added to the column (bed height). The experiments were operated at a flow rate (water velocity) that was either below the minimum fluidization velocity (packed bed mode) or above the minimum fluidization velocity (fluidized bed mode). The toluene adsorption capacity (kg toluene/kg Nanogel) using Equation (3.1) based on the breakthrough curves is shown in Table 5.2 and is also compared with the toluene adsorption capacity based on the adsorption isotherm from the batch equilibrium experiments (Equation (1.2)). Theoretically, when the Nanogel granules are saturated in the packed bed or the fluidized bed, the toluene adsorption capacity only depends on the value of the inlet toluene concentration and should agree with the adsorption

capacity at the corresponding concentration from the adsorption isotherm. As can be seen in Table 5.2, the toluene adsorption capacity in most experiments is close to its theoretical value, within an error range of +/- 20%.

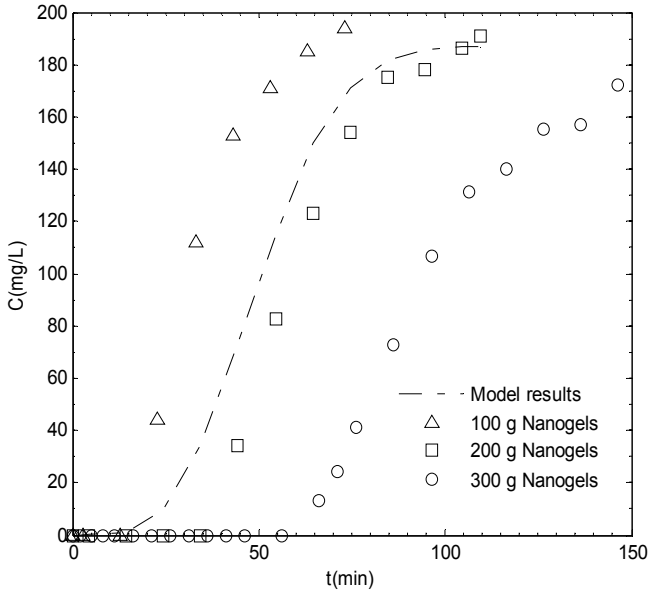

Figure 5-4. Breakthrough curve in packed bed for 100 g, 200 g and 300 g TLD 301, 0.7-1.2 mm Nanogel granules. Average inlet concentrations are 187 mg/L for 100 g, 187 mg/L for 200 g and 171 mg/L for 300 g, respectively, and the flow rate is 0.2 GPM. Dashed line is the model results for 200 g TLD 301.

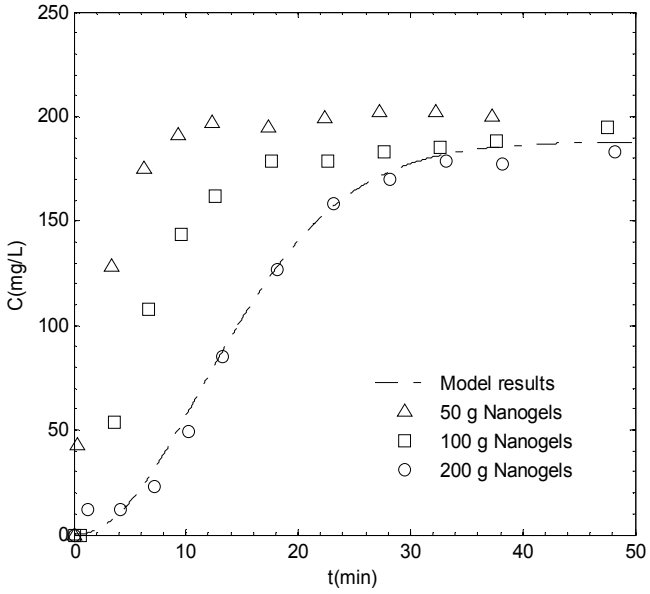

Figure 5-5. Breakthrough curve in packed bed for 50g, 100 g, and 200 g TLD 301, 0.7-1.2 mm Nanogel granules. Average inlet concentrations are 201 mg/L for 50 g, 200 mg/L for 100 g and 188 mg/L for 200 g, respectively, and the flow rate is 0.6 GPM. Dashed line is the model results for 200 g TLD 301.

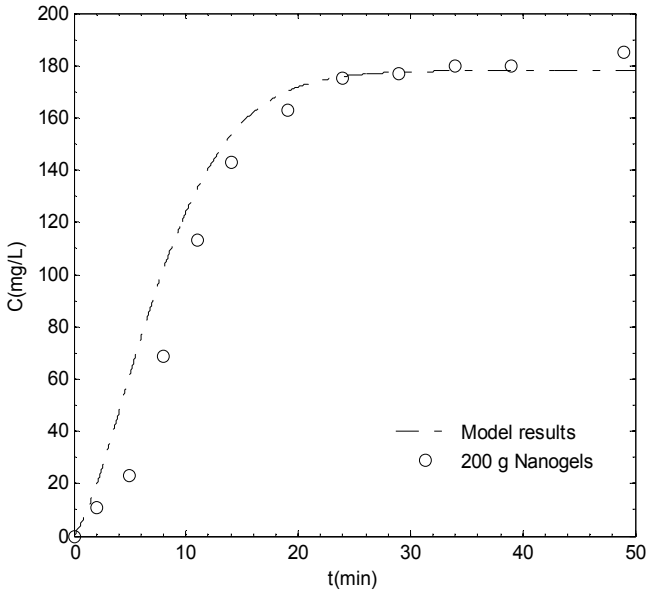

Figure 5-6. Breakthrough curve in packed bed for 200 g TLD 301, 0.7-1.2 mm Nanogel granules. Average inlet concentration is 178 mg/L, and the flow rate is 1.1 GPM. Dashed line is the model results for 200 g TLD 301.

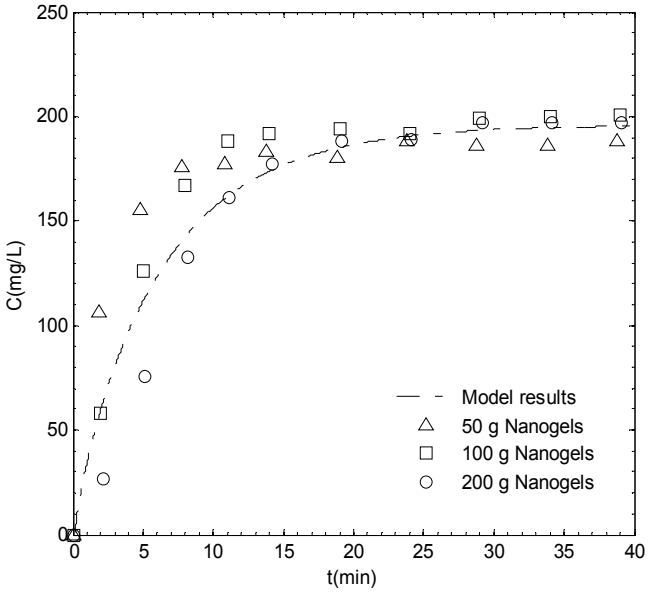

Figure 5-7. Breakthrough curve in inverse fluidized bed for 50 g, 100 g, and 200 g TLD 301, 0.7-1.2 mm Nanogel granules. Average inlet concentrations are 189 mg/L for 50 g, 199 mg/L for 100 g and 196 mg/L for 200 g, respectively, and the flow rate is 1.3 GPM. Dashed line is the model results for 200 g TLD 301.

Table 5-2. *Summary of experimental conditions and toluene adsorption capacity from water by a packed bed or inverse fluidized bed of TLD 301 Nanogel granules*

No. #	Nanogel Mass (g)	Flow Rate (GPM)	$C_0^{\#}$ (mg/L)	q, Eq. (3-1) (g/g)	q, Eq. (1-2) (g/g)
1	100	0.19	187	0.041	0.034
2	200	0.19	187	0.038	0.034
3	300	0.18	171	0.036	0.030
4	50	0.6	201	0.031	0.037
5	100	0.6	200	0.044	0.037
6	200	0.6	188	0.034	0.034
7	200	1.1	178	0.036	0.032
8*	50	1.3	189	0.043	0.034
9*	100	1.3	199	0.039	0.036
10*	200	1.3	196	0.035	0.035

* Fluidized bed experiment; # Average value

The shape and sharpness of the breakthrough curve for a given adsorbent mainly depend on such factors as the equilibrium adsorption isotherm, the mass

transfer rate, and hydrodynamic factors such as bed height and contact (residence) time. As can be seen in Figures 5-4, 5-5 and 5-6, for the breakthrough curves in the packed bed, (1) when the flow rates are the same, the breakthrough time becomes longer as the amount (weight) of the Nanogel granules increases (bed height increases), and (2) for the same weight of the Nanogel granules in the column, the lower the flow rate, the longer the breakthrough time.

As seen in Figure 5-7, the breakthrough time in a fluidized bed adsorber is considerably shorter than in a fixed bed adsorber, which is due to the large axial mixing in the fluidized bed. In our experiments, the outlet toluene concentrations in the fluidized bed in the beginning of the experiment are high and the toluene adsorption efficiencies are relatively low. The breakthrough curves of toluene adsorption on Nanogels in the packed bed mode (Figure 5-4) and fluidized bed mode (Figure 5-7) are compared as dimensionless concentration (C/C_0) versus dimensionless time (tu/L) in Figure 5-8. As can be seen in this figure, the breakthrough curve is much more like a step function in the packed bed mode as compared to the fluidized bed mode. If the dimensionless breakthrough time is arbitrarily defined as the time when $C/C_0 = 0.1$, it can be seen from Figure 5-8 that the dimensionless breakthrough time is 11 in the packed bed mode compared to 1 in the fluidized bed mode, which indicates that, the dimensionless breakthrough time is much longer in the packed bed mode than in the fluidized bed mode, and the toluene adsorption efficiency is higher in the packed bed mode than in the fluidized bed mode.

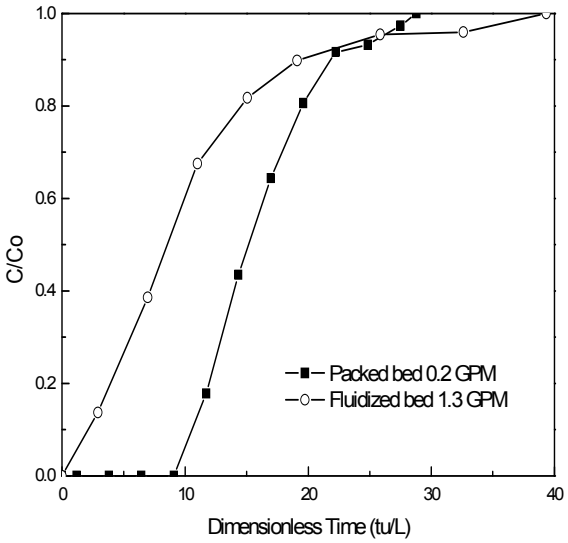

Figure 5-8. Comparison of the breakthrough curves of toluene adsorption on Nanogels in the packed bed and fluidized bed mode.

The toluene adsorption capacity before the breakthrough time (when C/C_0 = 0.1) is also calculated for the two curves in Figure 5-8. The adsorption capacity is 0.027 in the packed bed mode compared with 0.005 in the fluidized bed mode, which indicates that the toluene adsorption capacity is much higher in the packed bed mode than in the fluidized bed mode when the breakthrough time occurs.

5.4.3. Comparison of Modeling Results with Experimental Measurements

The parameters used in the modeling calculation are shown in Table 5-3. The concentrations of toluene in the exit stream (breakthrough curve) in both the packed bed and fluidized bed modes predicted by the model are compared with the experimentally observed concentrations for the same weight of Nanogels (200

g) in Figures 5-4 to 5-7. As seen in the figures, the results of the simulations and experiments are in good agreement when using the value of k = 223 and $1/n$ =1.15 as obtained from the batch equilibrium experiments and K = 0.284 s^{-1} as obtained from the batch kinetic experiments.

Table 5-3. *Parameters used in the modeling calculation*

d_P (m)	ρ_p (g/ml)	μ (N · m · s^{-2})	K' (s^{-1})	k	$1/n$	A(m^2)
9.5×10^{-4}	0.125	1.005×10^{-3}	0.284	223	1.15	0.0046

Flow Rate (GPM)	0.19	0.6	1.1	1.3
D_{ax} (m^2/s)	1.1×10^{-5}	3.4×10^{-5}	6.0×10^{-5}	7.4×10^{-5}

5.4.4. Parametric Sensitivity Analysis

A parametric sensitivity analysis was also performed to assess the contribution of the following parameters on breakthrough behavior for both the packed bed mode and the fluidized bed mode: the adsorption rate constant K, the Freundlich constant k, and the liquid phase axial dispersion coefficient D_{ax}. In performing the sensitivity analysis of the adsorption process, it is important to choose parameter values in the normal operating range in order to understand the influence of the parameters on its performance. In this study, each parameter was increased and decreased by a factor of 2 to study the effect on the breakthrough curve. The sensitivity analysis was performed by perturbing each of the parameters while holding the rest of the parameters constant. Based on the parametric sensitivity analysis, it appears that (1) the toluene outlet concentrations

at the initial stage of the breakthrough curve increase as K is decreased in both the fluidized bed mode and packed bed mode, (2) the toluene outlet concentrations at the initial stage of the breakthrough curve increase as k is decreased in both the fluidized bed mode and packed bed mode, and (3) the effect of changing the axial dispersion in the liquid phase (D_{ax}) is negligible in both fluidized bed mode and packed bed mode. These results are in agreement with results previously reported in the literature [Wen et al., 1975; Carberry et al., 1976; Veeraraghavan et al, 1989].

5.5. Conclusions

The toluene adsorption efficiency and capacity of the Nanogel granules in a packed bed or fluidized bed was studied by measuring both the inlet and exit concentrations of toluene as a function of time and plotting a breakthrough curve. Assuming equilibrium adsorption is reached, the toluene adsorption capacity only depends on the inlet toluene concentration and for an inlet concentration of about 200 ppm, the adsorption capacity is about 4%. The main factors which affect the toluene adsorption efficiency of the Nanogel granules in the packed bed and inverse fluidized bed are the weight of the Nanogel granules (height of the bed) and the fluid superficial velocity. In the fluidized bed adsorber the breakthrough time is considerably shorter than that in the packed bed adsorber due to solids mixing in the fluidized bed; the outlet toluene concentrations at short times are also much higher and the toluene adsorption efficiencies are relatively low.

Simple models were used to predict the packed bed and inverse fluidized bed experimental results based on equilibrium and kinetic batch measurements using Nanogel and toluene-water solutions. The packed bed model neglects dispersion in the solid phase and the fluidized bed model assumed complete axial mixing in the solid phase. Good agreement between the models and experimental results are obtained when using the k and $1/n$ values from the batch equilibrium experiments and the K value obtained from the batch kinetic experiments. Based on a parametric sensitivity analysis, the results show that a two-fold change in the adsorption rate constant K and the Freundlich constant k will dramatically affect the breakthrough curves, while changes in the liquid phase axial dispersion coefficient D_{ax} have a negligible effect.

CHAPTER 6 HYDRODYNAMICS AND DENSITY MEASUREMENT OF HYDROPHOBIC AEROGELS USING AN INVERSE FLUIDIZED BED

6.1. Introduction

As described in Chapter 4, it is difficult to measure the granule density of the Nanogel by using a traditional method such as a liquid pycnometer. This is because the inter-particle forces between the aerogels agglomerate small particles so strongly, that it is difficult to open all the voids around the particles in order to replace the air/gas with a liquid. In the work described in this chapter, the hydrodynamics characteristics of Nanogels in the inverse fluidized bed were further investigated. The granule density of Nanogel granules with different densities and sizes was studied by using the inverse fluidization method.

When the density of the particle material is less than the density of the fluid, inverse fluidization can be applied to disperse the solid particles in liquids. Since Nanogels have a density much lower than water, they can be inversely fluidized. Figure 6-1 shows the typical plot of pressure drop as a function of liquid velocity in a fluidized bed [Epstein, 2003]. In this figure, the path AB corresponds to the pressure drop across the immobile fixed bed as the velocity increases; the path BC is caused by loosening up the densely packed particles with each incremental velocity increase; from C to D, the bed continues to expand in the mobile fluidized state, during which the pressure drop remains constant; beyond D, all particles are carried out of the column by the flow. The path DCE

shows the defluidization process. The bed settles at its random loose packing condition in the defluidization process.

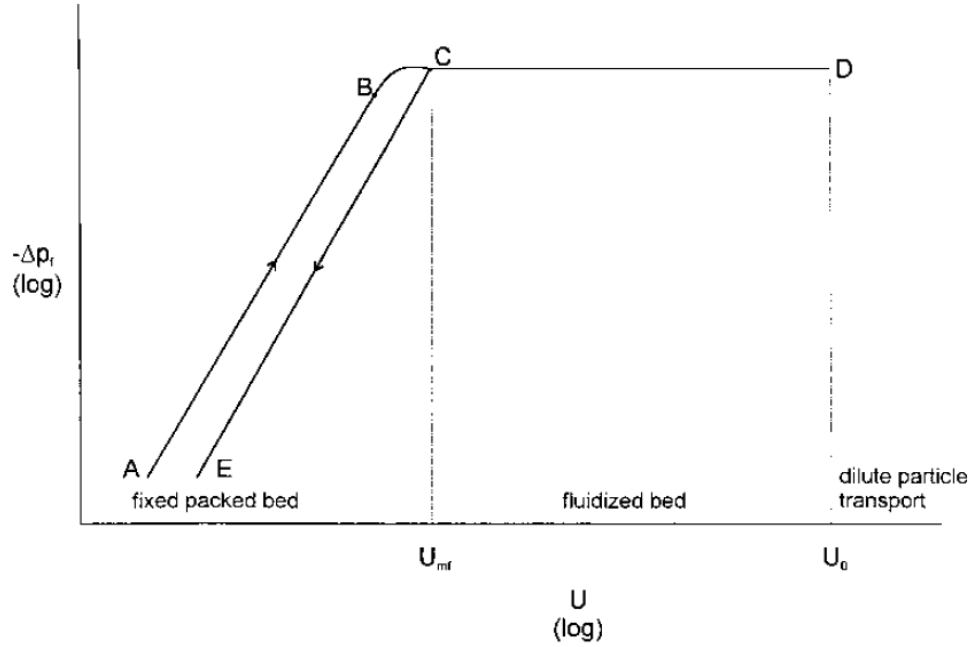

*Figure 6-19***.** Frictional pressure drop as a function of liquid superficial velocity for monodispersed particles [Epstein, 2003].

As seen in Figure 6-1, the pressure drop remains constant when particles in the fluidization bed are fully fluidized. This pressure drop can be used to calculate the granule density of the particles based on the force balance. The objectives of the work in this chapter are to investigate the feasibility of using the inverse fluidization method to determine the granule density of different Nanogel, granules, taking into account the effect of particle size, material density, particle shape, and particle mass.

6.2. Experimental Equipment and Methods

6.2.1. Materials

The following materials were used in our experimental work: Nanogel of different densities and size ranges, TLD 302-N2677 (0-0.7 mm, 0.7-1.2 mm, and 1.2-4 mm), TLD 302-9321108 ID1 (1.2-4 mm), TLD 302-93210928 ID31 (1.2-4 mm), TLD 302-832821 ID1 (1.2-4 mm), TLD 302-816512 ID2 (1.2-4 mm), TLD 302-832511 ID4 (1.2-4 mm), OBD 301 (0.7-1.2 mm), OBD 351 (0.7-1.2 mm), and Nanogel Fine Particles (0-0.2 mm) supplied by Cabot Corporation; OBD 351 (0.5-0.7 mm) prepared by crushing the big spherical OBD 351 Nanogel particles into small irregular particles and sieving into a 0.5-0.7mm size range; Glass Bubbles K1 supplied by 3M corporation and Inert Polymer IP4 supplied by Purolite Corporation, which were used as known density control samples.

6.2.2. Inverse Fluidized Bed Experiments for Measuring Hydrodynamics Characteristic

The experimental setup used for inverse fluidization of Nanogel granules by water is the same as shown in Figure 4-1. The upstream pressure tap is located right below the distributor so that the pressure drop across the distributor will not affect the measured pressure drop across the bed of Nanogel. A typical experimental run for an inverse fluidization experiment is described in Chapter 6, *6.2.4*.

6.3. Theoretical Models

In the inverse fluidization method, the value of the granule density can be calculated from the experimental data (the plateau pressure drop between C and D in Figure 6-1) by using a force balance. The detailed derivation of the expression of the granule density has been described in Chapter 4, *4.4.3*.

6.4. Results and Discussion

6.4.1. Density of Nanogels

Figures 6-2, 6-3 and 6-4 show the fluidized bed pressure drop plotted against the superficial fluid velocity for TLD 302-832821 ID1, TLD 302-816512 ID2, and TLD 302-832511 ID4 Nanogel granules. These three figures show that the pressure drop rises linearly below minimum fluidization in the packed bed region and then plateaus above minimum fluidization. The hysteresis observed in these figures when increasing the flow rate as compared to decreasing the flow rate is agreement with the theory that the packing of the particles in the bed is looser upon defluidization.

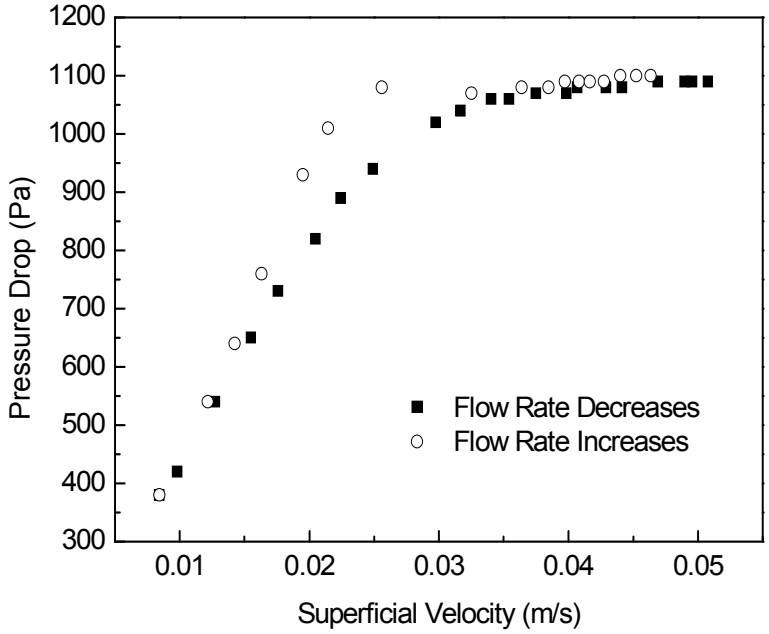

Figure 6-20. Inverse fluidized bed pressure drop vs. superficial fluid velocity of TLD 302-832821 ID1 Nanogel granules.

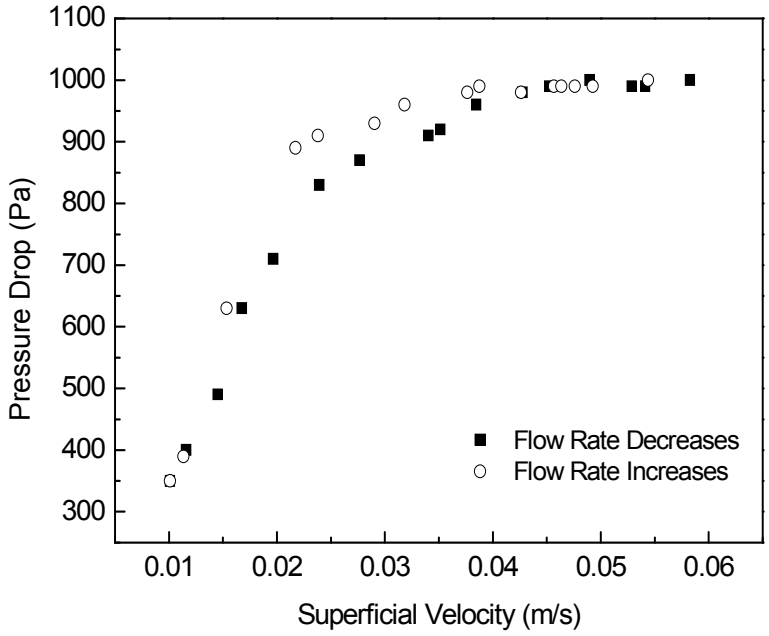

Figure 6-21. Inverse fluidized bed pressure drop vs. superficial fluid velocity of TLD 302-816512 ID2 Nanogel granules.

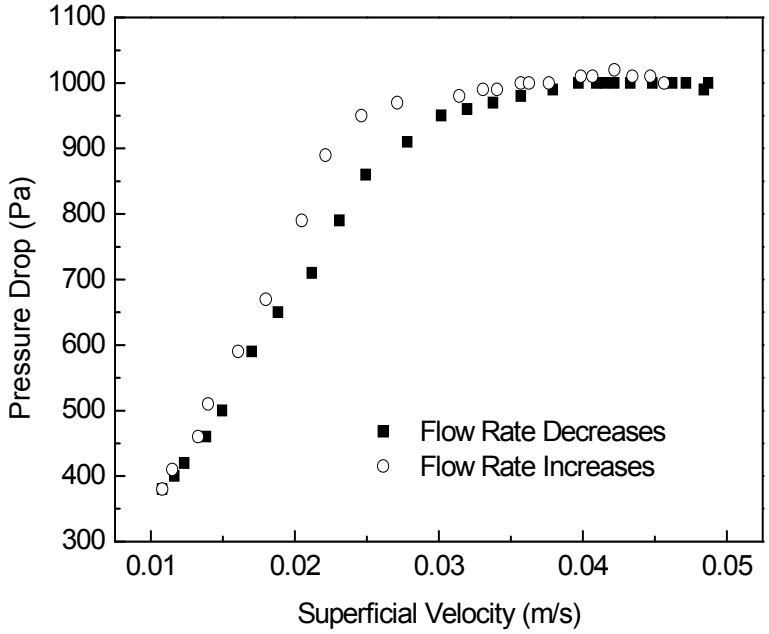

Figure 6-22. Inverse fluidized bed pressure drop vs. superficial fluid velocity of TLD 302-832511 ID4, 1.2-4 mm Nanogel granules.

6.4.1.1. Effect of Mass of Particles on the Density Results

Figures 6-5 and 6-6 show the fluidized bed pressure drop plotted against the superficial fluid velocity for TLD 302-93210928 ID31 and TLD 302-9321108 ID1 Nanogel granules. For these two Nanogels, both 30 g and 70 g samples were used in the measurement. As seen in these two figures, the larger the amount of Nanogels fluidized in the column, the higher the pressure drop values. For TLD 302-93210928 ID31, the plateau pressure drop values for 30g and 70 g samples were 360 Pa and 840 Pa, respectively; while for TLD 302-9321108 ID1, the plateau pressure drop values for 30g and 70 g samples were 440 Pa and 1030 Pa, respectively. As seen in Equation (4.10), the particle density ρ is a function of $(\Delta P_{exp}/m)$. If the $(\Delta P_{exp}/m)$ values are constant for the same Nanogel particles, it

means that the mass of Nanogels doesn't affect the density results. For TLD 302-93210928 ID31, the ($\Delta P_{exp}/m$) values were 12.0 in both the 30 g and 70 g experimental runs; while for TLD 302-9321108 ID1, the ($\Delta P_{exp}/m$) values were 14.7 in both experimental runs, which indicate that the mass of Nanogels used in the experiments doesn't affect the density result.

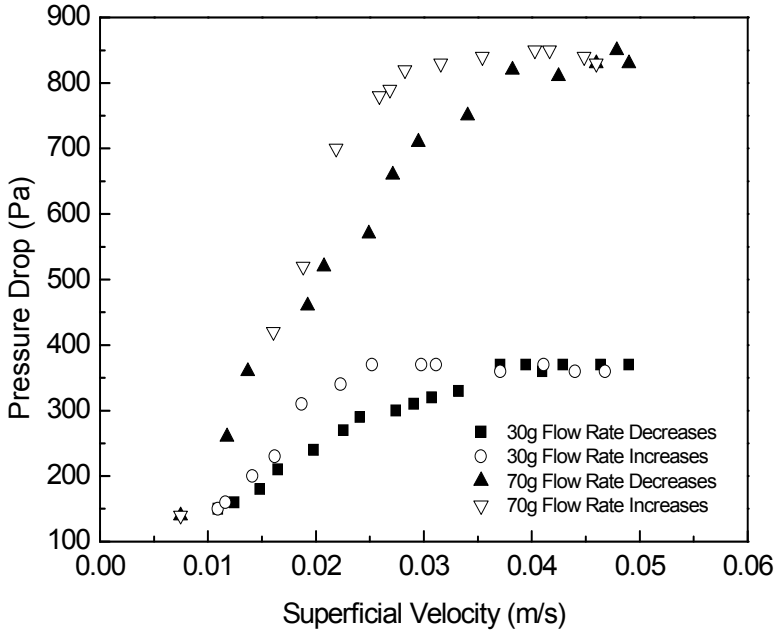

Figure 6-23. Inverse fluidized bed pressure drop vs. superficial fluid velocity of TLD 302-9321108 ID1, 1.2-4 mm Nanogel granules.

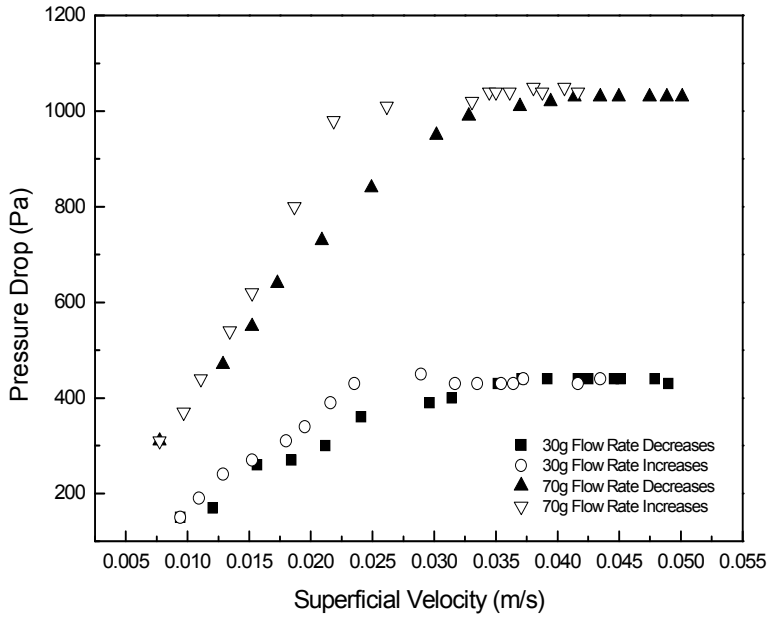

Figure 6-24. Inverse fluidized bed pressure drop vs. superficial fluid velocity of TLD 302-93210928 ID31, 1.2-4 mm Nanogel granules.

6.4.1.2. Effect of Size of Particles on the Density Results

Figures 6-7, 6-8 and 6-9 show the fluidized bed pressure drop plotted against the superficial fluid velocity for three different particle size range TLD 302-N2677 Nanogel granules. By comparing the density results in Table 6-1, it appears that the smaller the particle size, the higher the density value. This is probably because the smaller particles are more likely to be carried out of the column with the increase of flow rate during the experiment which will lower the amount (weight) of fluidized particles and cause a decrease in the pressure drop.

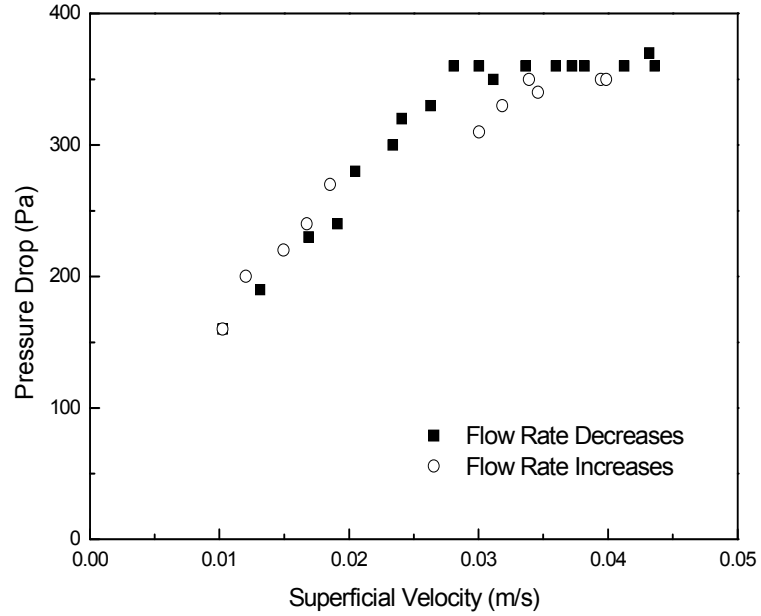

Figure 6-25. Inverse fluidized bed pressure drop vs. superficial fluid velocity of TLD 302-N2677, 0-0.7 mm Nanogel granules.

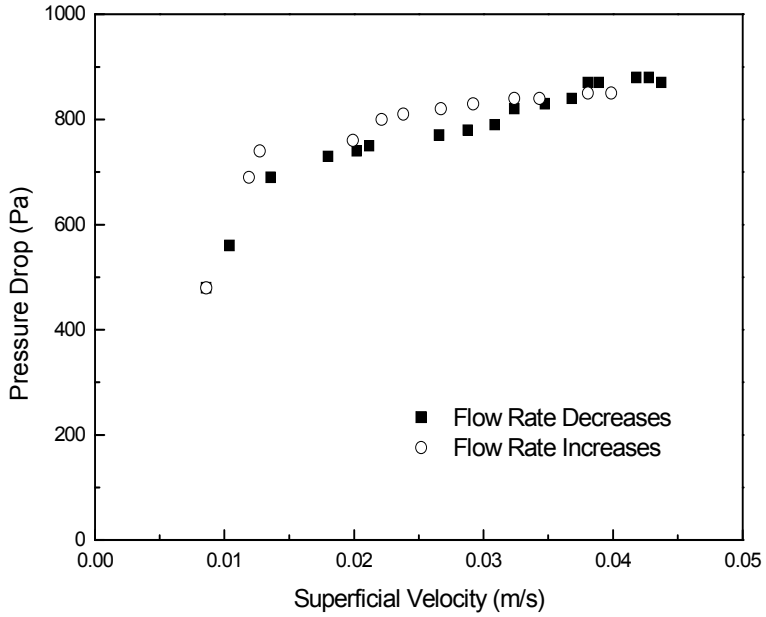

Figure 6-26. Inverse fluidized bed pressure drop vs. superficial fluid velocity of TLD 302-N2677, 0.7-1.2 mm Nanogel granules.

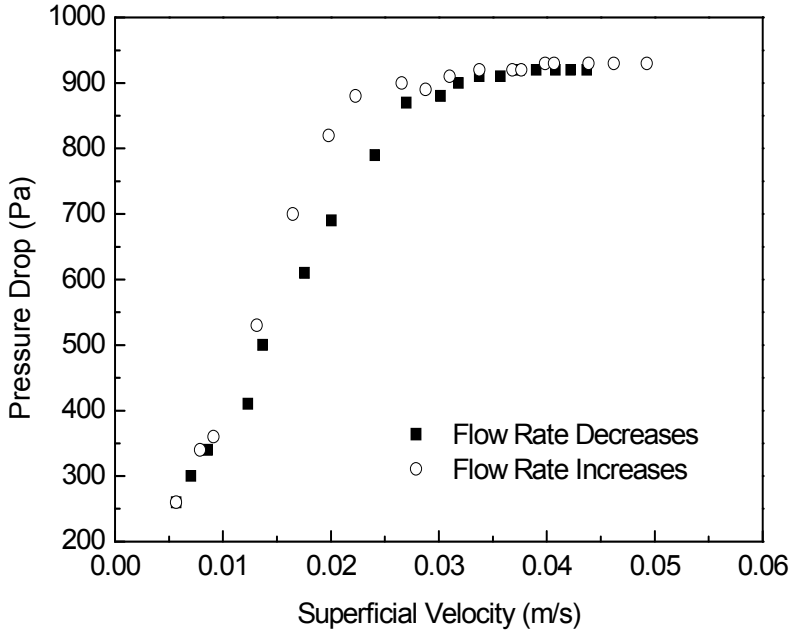

Figure 6-27. Inverse fluidized bed pressure drop vs. superficial fluid velocity of TLD 302-N2677, 1.2-4 mm Nanogel granules.

Table 6-7. *Comparison of the density measurement results*

Sample	Fraction (mm)	Density: Fluidized Bed (kg/m^3)		Density: GeoPyc (kg/m^3)
		30g	70g	
N2677	1.2-4		140	141
N2677	0.7-1.2		147	
N2677	0-0.7	152		
832821 ID1	1.2-4		121	129
816512 ID2	1.2-4		131	124
9321108 ID1	1.2-4	150	152	150
93210928 ID31	1.2-4	129	127	131
832511 ID4	1.2-4		131	128
OBD 301	0.7-1.2	145		120
OBD 351	0.7-1.2	166 (14.8g)		143
OBD 351	0.5-0.7	171		
Purolite IP4	1.1-1.5	890 (300g)		800-900*

* Data from Purolite

The Richardson-Zaki correlation [Richardson et al., 1954], as described in Chapter 4, *4.4.4.*, was used to predict the expansion of a liquid fluidized bed. In Equation (4.12), the terminal velocity U_t for spherical particles is given by

$$U_t = \sqrt{\frac{4gd(\rho_l - \rho_P)}{3\rho_l C_D}} \tag{6.1}$$

where C_D is the drag coefficient. In Equation (6.1), at low Reynolds number (<0.1), the terminal velocity U_t can be simplified from Stokes' law

$$U_t = \frac{d^2(\rho_l - \rho_P)g}{18\mu_l} \tag{6.2}$$

For higher particle Reynolds numbers, a number of empirical correlations are available in the literature to calculate the C_D value. Karamanev [Karamanev, 1996] provided a correlation for C_D for rising light solid spheres in terms of the Archimedes number, $Ar = d_P^3 \rho_l (\rho_P - \rho_l) g / \mu_l^2$.

$$\begin{aligned} C_D &= \frac{432}{Ar}(1 + 0.0470 Ar^{2/3}) + \frac{0.517}{1 + 154 Ar^{-1/3}} \quad Ar < 13000 \\ C_D &= 0.95 \quad Ar > 13000 \end{aligned} \tag{6.3}$$

The R-Z exponent or index (n) is a function of the particle terminal Reynolds number (Re_t) and the particle to column diameter ratio as given below

$$\begin{aligned} n &= (4.35 + 17.5\frac{d}{D})\,\mathrm{Re}_t^{-0.03} && for\ 0.2 < \mathrm{Re}_t < 1 \\ n &= (4.45 + 18\frac{d}{D})\,\mathrm{Re}_t^{-0.1} && for\ 1 < \mathrm{Re}_t < 200 \\ n &= 4.45\,\mathrm{Re}_t^{-0.1} && for\ 200 < \mathrm{Re}_t < 500 \\ n &= 2.4 && for\ \mathrm{Re}_t > 500 \end{aligned} \tag{6.4}$$

In these equations, the Reynolds number at terminal velocity is defined by Equation (4.11).

Combining Equations (4.8-4.13, 6.1-6.4), the bed height H can be expressed as a function of the superficial velocity U and the particle size d when the bed is fluidized.

$$H = \frac{m_P}{[1-(\frac{U}{U_t})^{1/n}]A\rho_P} \tag{6.5}$$

On the basis of the equations above, Richardson-Zaki bed expansion parameters, U_t, Ar, C_D, Re_t and n for TLD 302-N2677 0-0.7 mm Nanogels were calculated as shown in Table 6-2. The diameters of the particles used in the calculation are 0.1 mm, 0.2 mm, 0.3 mm, 0.4 mm, 0.5 mm, 0.6 mm and 0.7 mm, respectively.

Table 6-8. *Richardson-Zaki bed expansion parameters for TLD 302-N2677 0-0.7mm Nanogels*

Particle size (mm)	0.1	0.2	0.3	0.4	0.5	0.6	0.7
Ar	8.34	66.75	225.30	534.04	1043.04	1802.38	2862.11
C_D	61.79	11.49	5.27	3.34	2.45	1.95	1.62
U_t (m/s)	0.004	0.014	0.025	0.036	0.047	0.058	0.068
Re_t	0.42	2.78	7.55	14.61	23.83	35.14	48.47
n	4.49	4.26	4.16	4.10	3.33	3.22	3.13

The bed expansion data (when the bed is fluidized, i.e., at superficial velocities above the minimum fluidization velocity), was calculated using Equation (4.9) after calculating C_D from Equation (6.3) and U_t from Equation (6.1). The values of H could then be calculated at different superficial velocities using Equation (6.5) for 30 g TLD 302-N2677 0-0.7 mm Nanogels, and are plotted against the superficial velocity in Figure 6-10. As can be seen from this plot, the bed expands much more quickly for the smaller particles than for the

larger ones. For 0.1 mm particles, the bed expands to its full length (1.47 m) at very low velocity (0.0025 m/s). This indicates that some very fine particles are lost during the process of increasing the flow rate, even at low velocities before the bed becomes fluidized for the TLD 302-N2677 0-0.7 mm Nanogels, which could be the reason that the pressure drop value for small particles is lower than for large particles and the density value for small particles is higher than for large particles. Based on these calculations, if the particle size distribution of TLD 302-N2677 0-0.7 mm Nanogels was known, the amount of particles lost in the experiment could be estimated and the density value could also be revised.

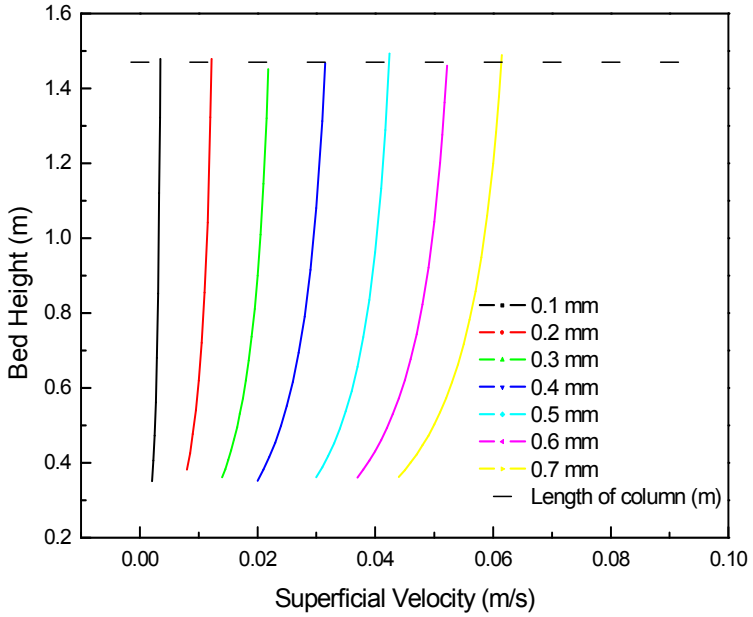

Figure 6-28. Inverse fluidized bed height vs. superficial fluid velocity of 30 g TLD 302-N2677, 0-0.7 mm Nanogel granules based on the Richardson-Zaki equation.

6.4.1.3. Effect of Shape of Particles on the Density Results

Figures 6-11 and 6-12 show the fluidized bed pressure drop plotted against the superficial fluid velocity for two OBD 351 Nanogel granules with different particle sizes and shapes. As seen in the density results in Table 6-1, the density for 0.7-1.2 mm particles is 166 kg/m^3 while the density for 0.5-0.7 mm particles is 171 kg/m^3. Since the smaller size particles usually give slightly higher density values as discussed in *6.4.1.2*, it appears that the shape of Nanogels doesn't affect the density results. However, more experiments with different sizes and shapes of particles are needed to confirm this conclusion.

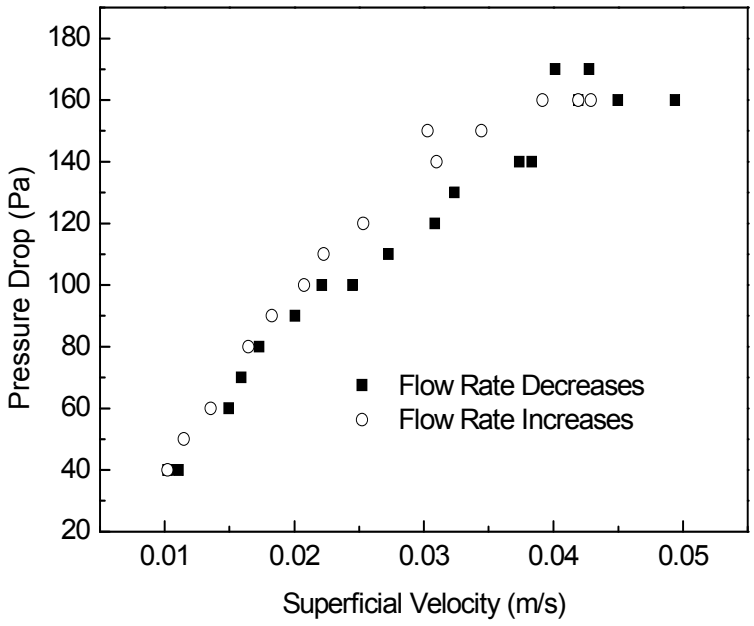

Figure 6-29. Inverse fluidized bed pressure drop vs. superficial fluid velocity of OBD 351, 0.7-1.2 mm Nanogel granules.

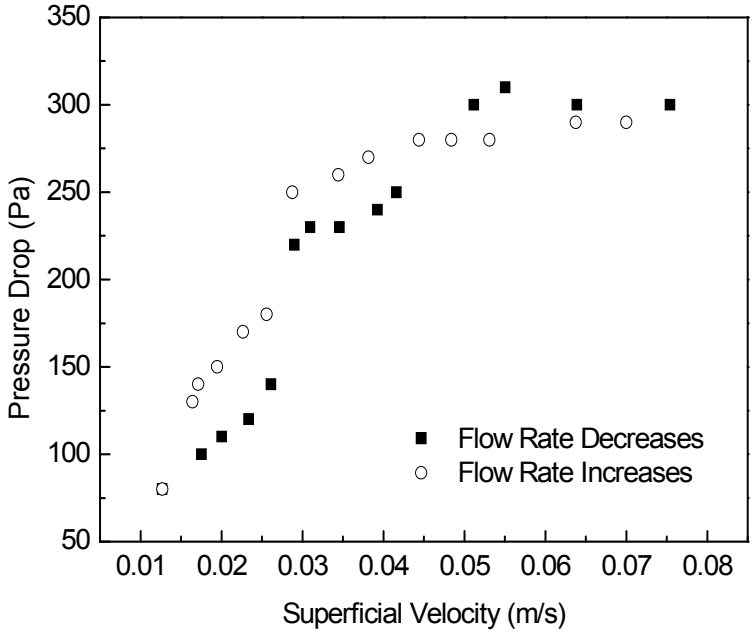

Figure 6-30. Inverse fluidized bed pressure drop vs. superficial fluid velocity of OBD 351, 0.5-0.7 mm Nanogel granules.

6.4.2. Density Results of Control Samples

6.4.2.1. Density Results of Purolite IP4

Figure 6-13 shows the fluidized bed pressure drop plotted against the superficial fluid velocity for Purolite IP4 particles. As seen in the density results from Table 6-1, the density value is 890 kg/m^3, which is in the range of 800 to 900 kg/m^3 provided by Purolite.

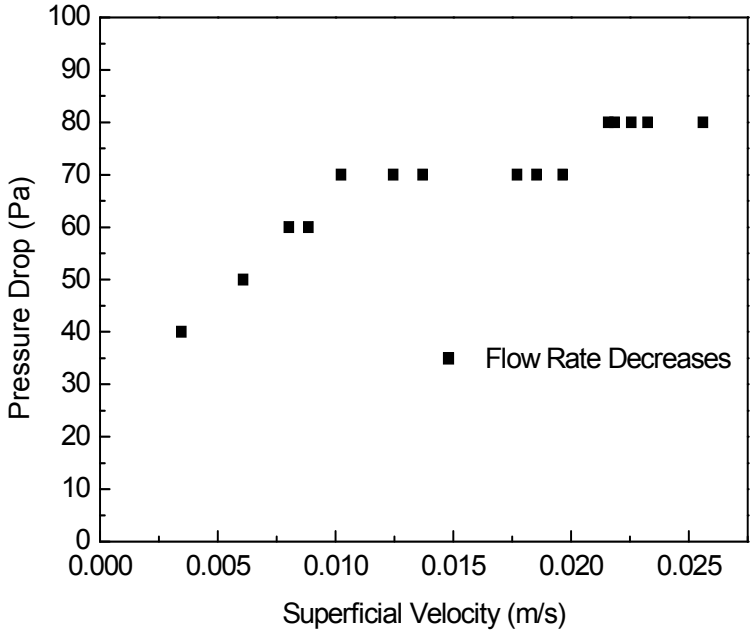

Figure 6-31. Inverse fluidized bed pressure drop vs. superficial fluid velocity of Purolite IP4.

6.4.2.2. Density Results of 3M K1

For 3M K1 particles, there were some problems in the measurement. Since the K1 particles are very small (65 μm), the particles were very easily fluidized and carried out of the column even at a very low flow rate.

There are a number of empirical equations used to determine the minimum fluidization velocity in a fluidized bed, U_{mf}, for hard, non-porous particles of different size, shape, and density. One widely accepted equation is the Ergun equation [Ergun, 1952]:

$$\frac{-dp_f}{dz} = (1-\varepsilon_{mf})(\rho_P - \rho_l)g = \frac{150U_{mf}\mu_l(1-\varepsilon_{mf})^2}{\varphi^2 d_p^2 \varepsilon_{mf}^3} + \frac{1.75U_{mf}^2\rho_l(1-\varepsilon_{mf})}{\varphi d_p \varepsilon_{mf}^3} \qquad (6.6)$$

Algebraic manipulation and rearrangement of this equation results in

$$\mathrm{Re}_{mf}^2 + \frac{150}{1.75}\frac{1-\varepsilon_{mf}}{\varphi}\mathrm{Re}_{mf} - \frac{\varphi\varepsilon_{mf}^3 Ar}{1.75} = 0 \tag{6.7}$$

where $\mathrm{Re}_{mf} = d_p U_{mf}\rho_l / \mu_l$, $Ar = d_P^3\rho(\rho_P - \rho_l)g / \mu_l^2$ and φ is the sphericity which depends on the shape of the particles. The solution of the quadratic Equation (6.7) can be written as

$$\mathrm{Re}_{mf} = (C_1^2 + C_2 Ar)^{1/2} - C_1 \tag{6.8}$$

This equation should also be applicable to inverse fluidization as well as conventional gas fluidization assuming that the drag force of the fluid moving with superficial velocity (U_{mf}) is equal to the buoyancy force less the weight of the particles as described by Karamanev et al. [Karamanev et al., 1992]. In this case, $Ar = d_P^3\rho(\rho_l - \rho_P)g / \mu_l^2$. For the parameters C_1 and C_2, many investigators have proposed different combinations of the values [Wen et al., 1966; Saxena et al., 1977; Babu et al., 1978; Grace et al., 1982; Thonglimp et al., 1984; Tannous et al., 1994] mostly based on empirical fits to experimental data of U_{mf}. In this chapter, the parameters C_1 and C_2 used were introduced by Wen and Yu [Wen et al., 1966] who considered them to be applicable for various particle shapes. The values of C_1 and C_2 are 33.7 and 0.0408, respectively. Table 6-3 shows the theoretical minimum fluidization velocity for 3M K1 particles. In this table, the theoretical minimum fluidization velocity is 0.000022 m/s, which indicates that this particle is easily fluidized at a very low flow rate.

Table 6-9. *The theoretical minimum fluidization velocity for 3M K1*

Particle Size (mm)	*Ar*	Re_{mf}	U_{mf}(m/s)
0.65	2.33	0.0014	0.000022

The bed expansion data for 30 g 3M K1 particles were calculated by using Equations (4.8-4.13, 6.1-6.4) and plotted in Figure 6-14. As can be seen from this plot, the bed expands very quickly for this particle at very low velocity.

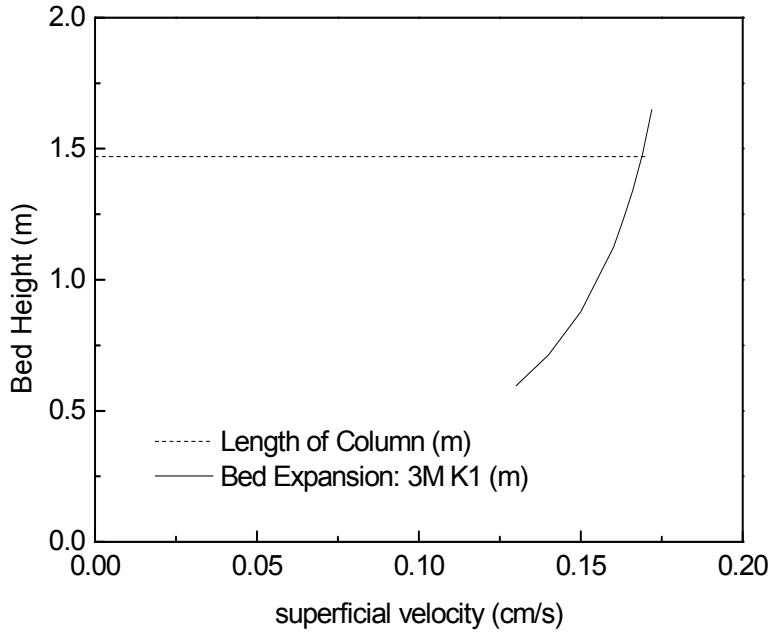

Figure 6-32. Inverse fluidized bed height vs. superficial fluid velocity of 30 g 3M K1 particles based on Richardson-Zaki equation.

6.4.3. Density Results of Nanogel Fine Particles

For the measurement of Nanogel fine particles, there was another problem, i.e., the particles agglomerated at the top of the column no matter what flow rate was used (see Figure 6-15). This is probably because the size of the Nanogel fine

particles was so small that the interparticle interactions among these small particles，such as van der Waals forces，and liquid bridges were very strong. Even though the Nanogels are hydrophobic, some water (3-4%) will adsorb on the surface.

Figure 6-33. Photo showing severe particle agglomeration with fluidizing fine Nanogel particles.

6.4.4. Comparison of the Results between Fluidization Method and GeoPyc Method

In Figure 6-16 and Table 6-1, the density results measured by using the fluidization method are compared against the results from the GeoPyc Method [Micromeritics]. It appears that the density data for most materials is similar by using both the fluidized bed method and the GeoPyc method. For OBD 301 and OBD 351, the reason the value from the fluidization method is larger than the

GeoPyc method is probably because since the size of these particles is smaller than 2 mm, so the result from the GeoPyc method is lower than its real value.

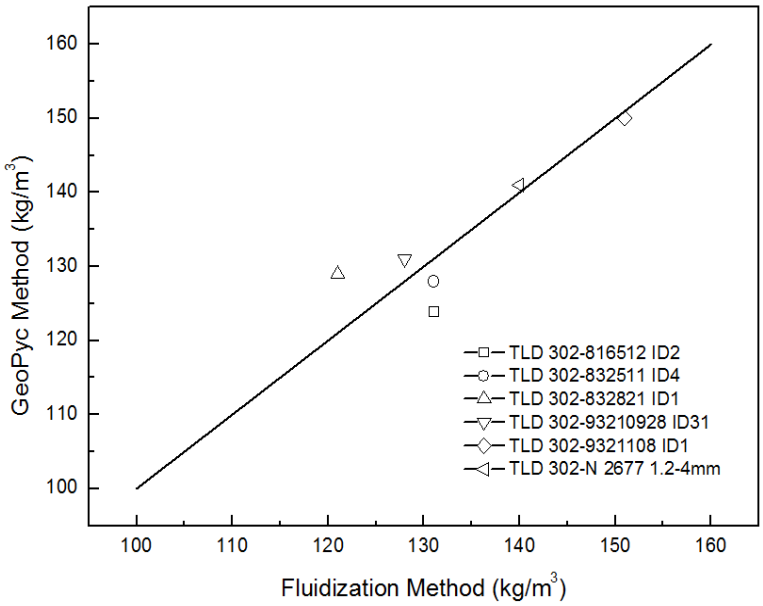

Figure 6-34. Comparison of the density measurement results between the fluidization method and the GeoPyc method.

6.5. Conclusions

The granule density of the Nanogels was calculated by measuring the pressure drop of clean water in the inverse fluidized bed. The density results are in good agreement with the GeoPyc method, especially for the large particles. The experimental results show that the mass and shape of Nanogels used in the measurement don't affect the density results. However, the smaller the particle size, the higher the density value. This is probably because the smaller particles are more likely to be carried out of the column as flow rate is increased during the experiment and causes a decrease in the pressure drop. In summary, this method can be used for measuring the density of Nanogel particles with reasonable

accuracy for a particle size down to about 0.7 mm. This is much better than the GeoPyc method, which is suitable only for particles larger than 2 mm [Micromeritics]. However, for very fine particles, this method still has some drawbacks such as elutriation and agglomeration of particles.

CHAPTER 7 SUMMARY AND RECOMMENDATIONS FOR FUTURE WORK

7.1. Summary

This work is the first systematic study experimentally and theoretically detailing the sorption properties of commercially available hydrophobic silica aerogel (Cabot Nanogel) for oil removal and organic separation. Additionally, this is the first work demonstrating the application of packed bed and inverse fluidized bed technologies on the adsorption process by using Nanogel. The information presented in this study will be valuable in gaining a deeper understanding of the sorption mechanisms of oil and organics on Nanogel, the hydrodynamics characteristics of Nanogel in a liquid-solid inverse fluidized bed, and the adsorption behavior of Nanogel in a liquid-solid packed bed and an inverse fluidized bed.

The adsorption capacity and efficiency of Nanogel granules for removing laboratory prepared emulsified oil, oil from real oily wastewater, and toluene at low concentrations, in both packed bed and inverse fluidized bed modes were studied. For the removal of oil from laboratory prepared emulsions, several factors, i.e., the granule size, the bed height, and the fluid velocity, will affect the adsorption capacity and efficiency of the Nanogel granules in the inverse fluidized bed and the packed bed. Under the same experimental conditions, the slower the flow rate, the higher the oil adsorption capacity and efficiency. Higher oil adsorption capacity in the inverse fluidized bed at low flow rate is due to the

lower drag force and longer remaining time of the Nanogel granules in the column.

For the removal of oil from real oily wastewater and toluene at low concentrations, it was found that the adsorption capacity is only dependent on the inlet concentration of the sample. The adsorption efficiency, however, depended on the flow rate through the column; the lower the flow rate, the higher the adsorption efficiency. By comparing the adsorption capacity and efficiency in both the packed bed and fluidized bed modes for these three cases, it appears that the use of a packed bed to remove oil or VOCs from water may give better capacity and efficiency than using an inverse fluidized bed. The high rate of mixing of the solid phase in the fluidized bed (CSTR conditions) actually is detrimental to the adsorption process since all of the particles in the bed become loaded with the contaminant at about the same time.

The hydrodynamics characteristics of the Nanogel granules with different size ranges, shape, and density in the inverse fluidized bed were studied by measuring the pressure drop and bed expansion of clean water in the inverse fluidized bed. As expected, the pressure drop increased with the increasing flow rate before fluidization and then reached a plateau. The bed height remained constant before fluidization and then increased with increasing flow rate. Based on these inverse fluidized bed flow characteristics, a new density measurement method for Nanogels was developed by measuring the plateau pressure drop value of the fluidized bed when Nanogel particles were fully fluidized. The density

results are in good agreement with results from the GeoPyc method [Micromeritics], especially for large particles.

The density measurement results show that the mass and shape of Nanogels do not affect the density results, whereas the size of Nanogels does affect the results. The smaller the particle size, the higher the density value measured. This is probably because the smaller particles are more likely to be carried out of the column as flow rate is increased during the experiment and causes a decrease in the pressure drop. The experimental results show that the inverse fluidization method can be used for measuring the density of Nanogel particles with reasonable accuracy for a particle size down to about 0.7 mm. This is much better than the GeoPyc method, which is suitable only for particles larger than 2 mm. However, for very fine particles, this method still has some drawbacks such as elutriation and agglomeration of particles.

The sorption capacity, equilibria, and kinetics of oil in liquid and emulsion phases, real oily wastewater and VOCs in vapor, liquid and solution phases on Nanogels were experimentally and theoretically investigated. The Nanogels have high sorption capacities, i.e., 12-23 g/g and fast sorption kinetics, i.e., 25-1200 s for three different free oils and six VOC liquids. This indicates that Nanogels can be used advantageously to clean up spills of VOC liquids and oils.

For sorption of oil from oil-in-water emulsions stabilized with a surfactant and real oily wastewater, the adsorption capacity of Nanogel decreases with increasing proportion of the surfactant. The particular oily wastewater sample studied here showed an even lower sorption capacity and slower sorption kinetics

due to the high stability of the real oily wastewater, which indicates that Nanogels probably should not be used to capture highly dispersed emulsified oil with very small droplet sizes.

For the sorption of five VOC vapors on Nanogels, the "half time," defined as the time when weight of organic adsorbed is equal to half of the equilibrium adsorption capacity, varies from about 30 minutes for benzene to over 3 hours for p-xylene indicating that the adsorption rate is relatively slow. We believe this is due to the extremely low thermal conductivity of Nanogel compared to other sorbents which results in a poor dissipation of heat and subsequent increase in temperature which hinders adsorption. The adsorption capacity of Nanogels was compared with two other hydrophobic aerogels that were synthesized in the laboratory using supercritical drying and two other commercial sorbents (silica gel and activated carbon) [Standeker et al., 2009]. The results show that the adsorption capacity of Nanogel is higher than that of the two other hydrophobic aerogels, and much higher than that of silica gel and activated carbon for toluene and xylene, and lower than that of the two other hydrophobic aerogels and silica gel but higher than that of activated carbon for benzene.

In the solution phase adsorption, the Freundlich isotherm [Freundlich, 1926] and LDF model [Glueckauf et al., 1947] were used to fit the equilibrium and kinetics data. The adsorption capacities of benzene and toluene at the concentrations below their aqueous solubility on Nanogel were compared with other two hydrophobic aerogels, activated carbon, and polymeric resin. The comparison shows that the adsorption capacity of Nanogel is slightly lower than

that of the MTMS-aerogel and TMES-aerogel [Standeker et al., 2007; Novak et al., 2005] and much lower than that of GAC (AC-F400) and polymeric resin (XAD2) [Simpson et al., 1993]. These results again indicate that hydrophobic silica aerogels may not be the best choice sorbent for removing organic contaminants from water.

The sorption mechanisms of free oil, emulsified oil and VOCs in vapor, liquid or solution phases onto Nanogel were investigated based on the sorption capacity, equilibria, and kinetics. Sorption of free oil and organic liquids on Nanogel is governed by the viscous flow in the pores of the Nanogel due to capillary forces. As mentioned above, the adsorption for organic vapor appears to be controlled by the slow dissipation of the heat generated during adsorption due to the extremely low thermal conductivity of the aerogel. The adsorption for organics in the solution phase is considered to include the following three steps [Hrubesh et al., 2001]: (1) mass transfer of the organic across the liquid-vapor interface to organic vapor, (2) diffusion of organic vapor into the aerogel pores, and (3) adsorption of the organic on the surface. For the adsorption of emulsified oil from oil-in-water emulsions using Nanogel, the relatively slow kinetics that was observed suggests that the possible sorption mechanism might be: (1) migration of the oil droplets into the Nanogel pores, and (2) adsorption of the oil on the surface of the Nanogel pores.

7.2. Recommendations for Future Work

Based on the experimental and theoretical studies in this dissertation, the following recommendations are made for future research using Nanogels or other hydrophobic silica aerogels to adsorb/absorb organic compounds.

7.2.1. Continuous Operation Mode of the Inverse Fluidized Bed

As discussed in Chapter 2, the inverse fluidized bed adsorption experiments were operated in a batch mode, i.e., the experiment was stopped when Nanogel became heavier due to the adsorption of oil and was observed to leave the bed with the water. For an industrial application, it is highly desirable to design and operate the inverse fluidized bed in a continuous mode, i.e., water containing an organic contaminant is fed to the top of the bed and clean water, carrying a certain amount of saturated Nanogels, is removed from the bottom. To replace the Nanogels leaving the bed, fresh Nanogels could be continuously fed to the bottom of the bed, adsorbing some organic as they rise up due to their buoyancy and mix into the bed.

The rising motion of the fresh Nanogels should also improve liquid mixing in the bed, acting somewhat like gas bubbles in a gas fluidized bed, and might also improve adsorption capacity since the downward flowing organic contaminated solution would always encounter relatively fresh Nanogels at the top of the bed. Some of the benefits of using a continuous operation mode as compared to a batch operation mode are better process control, lower running costs, and increased adsorption efficiency since the sorbent is continuously

replaced. Though some biofilm reactors operate continuously [Kryst et al., 2001], this type of continuous inverse fluidized bed has not been studied before. Therefore, it would be interesting to conduct such a study to determine whether adsorption capacity and efficiency can be appreciably increased.

In addition to continuous fluidized bed experiments, a model for the operation of a continuous inverse fluidized bed is needed for the design and scale up of the separation process. A simple model can be constructed based on: 1. the liquid phase flowing downwards, 2. the fresh solid phase fed into the bottom of the adsorber flowing upwards, and 3. the solid phase adsorbed with organic contaminant flowing downwards. The equations and boundary conditions that need to be solved for this model are given in Appendix D.

7.2.2. Sorption of Oil Spill with Nanogel under Ocean Oil Spill Conditions

As discussed in Chapter 5 and Chapter 6, Nanogel has a very high uptake capacity and high rate of uptake for the removal of free oil and liquid organics. In future research, it would be interesting to evaluate the Nanogel sorption capacity and sorption kinetics for crude oil and weathered crude oil (crude oil that has been exposed to water and air for some time) under ocean oil spill conditions.

To this end, crude oil and salty water of similar concentration to ocean water will be prepared and characterized. Since the physical properties of the crude oil continue to evolve as it is weathered after environmental exposure, both fresh crude oil and crude oil which has been weathered to various extent will be investigated. Fresh crude oil samples can be obtained from the major US oil

companies and artificially weathered oil samples through controlled evaporation can prepared in a range of viscosities.

Since the physical properties of the oil, such as density, viscosity, and surface tension will most likely play a significant role in the sorption kinetics, the density, viscosity, and surface tension of the as-received and weathered crude oils will be measured. The chemical composition of the crude oil can be analyzed through gas chromatography (GC) and Fourier Transform Infrared Spectroscopy (FTIR).

Waters with salinities ranging from 0-35 ppm and containing natural organic materials ranging from 0-2 g/L should be investigated, as these are representative of the variety of water types that are found in coastal and estuarial areas. These synthetic waters can be fabricated by adding sea salts to de-ionized water, and water pH tuned between 5 and 9. Since real coastal waters have many organic components other than salts and minerals, some synthetic waters will be prepared with alginic acid (at concentrations of up to 2 g/L), as a representative natural organic foulant material. Samples of the prepared waters will be characterized for color, turbidity, conductivity, pH, and total organic carbon content both prior to and after the addition of the oil.

The effect of water motion on the sorption properties of Nanogel also needs to be studied to simulate water motion in the oceans and rivers. This can be done using a wave generator in an aquarium tank filled with salt water, as shown in Figure 7-1. The impact of wave period and amplitude on contact interaction

between the water, the oil, and Nanogel particles of different size ranges will be investigated.

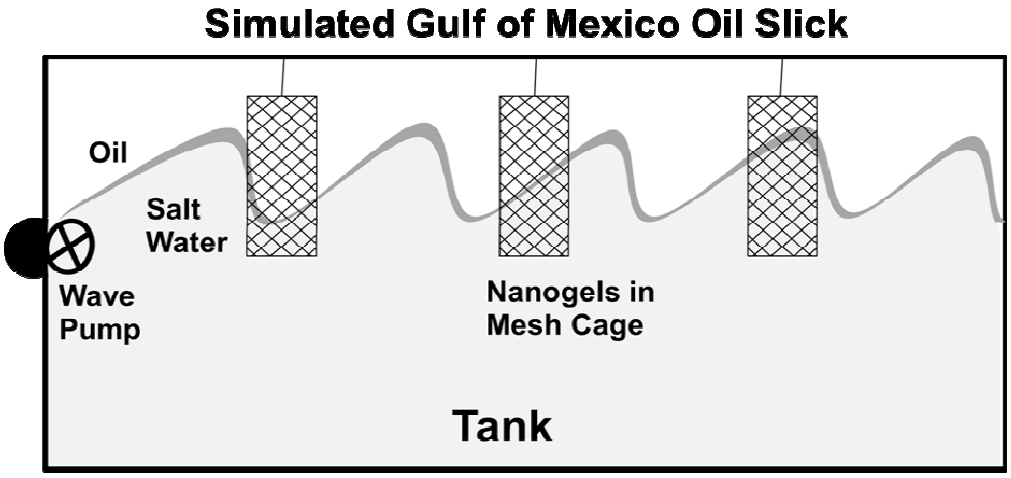

Figure 7-1. Schematic diagram of lab crude oil sorption study.

Sorption capacity and kinetics experiments will be conducted by adding a specific amount of crude oil to the surface of the salt water. The wave pump will be programmed to create different wave actions. A specific mass of Nanogel will then be added to the surface of the oil slick. After sorption has occurred, the saturated Nanogel will be skimmed off, dried, and weighed in order to determine how much oil was removed from the water. These particular experiments are already in progress by Elisabeth McLaughlin, an undergraduate chemical engineering honors student, as part of her research for her honors thesis.

In addition to determining the capacity of Nanogel to adsorb/absorb crude oil under different conditions, it is important to develop a knowledge of the kinetics of the sorption process and the time required to fully utilize the Nanogel

material. The kinetics or the rate of oil capture in various Nanogel samples can be measured by using the microbalance apparatus, as described in *5.2.4*, and verified by the Washburn equation or a modification thereof.

7.2.3. The Recovery of used Nanogel and Sorbed Organics

It has been reported that hydrophobic aerogels saturated with liquid or vapor VOCs can be regenerated by simply heating at high temperature (100^{o}C) under inert gas atmosphere [Standeker et el., 2007; Standeker et el., 2009]. However, it is difficult to regenerate and reuse conventional oil saturated sorbents and even more difficult to regenerate aerogels because of their complex pore structure. One method for regenerating conventional oil saturated sorbents was recently reported by Wei et al. [Wei et al., 2005] using a biodegradable biosurfactant, but it is unknown whether this will work for aerogels. Therefore most sorbents currently used for oil removal end up in landfills or are incinerated after a single use [Wei et al., 2005].

In future research that uses Nanogel as a sorbent for oil, the possibility of converting the captured oil into useful products, rather than emitting CO_2 and particulate matter to the atmosphere during burning should be investigated. Since the oil is strongly trapped within the pores of the hydrophobic Nanogel, the best way to desorb it is to convert the oil into a gas or into liquids such as gasoline and aviation fuel.

One method to recover the absorbed oil is by the thermal pyrolysis [Vogel, 1964]. The oil saturated Nanogels can be heated in vacuum at various

temperatures and the effluent gas examined by GC/MS. The recovered Nanogels can be weighted to determine the residual oil.

If there is significant residual oil after the thermal pyrolysis, steam reforming of the crude oil absorbed in the Nanogel at elevated temperature in a fixed bed can also be investigated. The spent Nanogel can be packed in a ceramic tubular reactor, and pure steam (or a steam/N_2 mixture) sent through the reactor at a high temperature (700-900^{o}C). In the case of catalytic reforming, porous ceramic membrane tubes within which a reforming catalyst, such as Ni/alumina, is packed, will be inserted in the reactor. Such an arrangement will prevent the mixing of the solid catalyst with the Nanogel particles, but allow for interaction of gas and liquid during the reactions. The effluent from the reactor can be analyzed by GC/MS for H_2, CO, CO_2 and possible hydrocarbons.

Another possibility for recovering the absorbed oil from the spent Nanogel is to feed the oil saturated Nanogel particles directly into a fluid catalytic cracking (FCC) unit. The high temperature of the cat cracker will volatilize the oil and the CH_3 groups on the surface of the Nanogel forming useful products such as gasoline and aviation fuel, leaving behind the silica nanoparticles that formed the aerogel. These will probably form large agglomerates in the fluidized bed catalytic cracker of the order of 100 microns due to van der Waals forces [Zhu et al., 2005], and simply become part of the FCC catalyst. Whether this addition of silica nanoagglomerates will eventually degrade the catalyst will need to be studied.

REFERENCES

Ahmadvand, H., German, G., Gandee, J.P., Buehler, V.T. (1995). Utilizing the fluidized bed to initiate water treatment on site. In Hinchee, R.E., Sayles, G.D., Skeen R.S. (Eds.), *Biological Unit Processes for Hazardous Waste Treatment* (pp. 47-53). Columbus, OH: Battelle Press.

Aivalioti, M., Vamvasakis, I., Gidarakos, E. (2010). BTEX and MTBE adsorption onto raw and thermally modified diatomite. *J. Hazard. Mater., 178*, 136-143.

Alamo-Nole, L.A., Perales-perez, O., Roman-Velazquez, F.R. (2010). Sorption study of toluene and xylene in aqueous solutions by recycled tires crumb rubber. *J. Hazard. Mater., 185*, 107-111.

Alther, G.R. (1995). Organically modified clay removes oil from water. *Waste Manage.*, *15*, 623-628.

Annunciado, T.R., Sydenstricker, T.H.D., Amico S.C. (2005). Experimental investigation of various vegetable fibers as sorbent materials for oil spills. *Marine pollution bulletin, 50*, 1340-1346.

Ayotamuno, M.J., Kogbara, R.B., Ogaji, S.O.T., Probert, S.D. (2006). Petroleum contaminated ground-water: remediation using activated carbon. *Appl. Energ.*, *83*, 1258-1264.

Babu, S.P., Shah, B., Talwalkar, A. (1978). Fluidization correlations for coal gasification materials — minimum fluidization velocity and fluidized bed expansion ratio. *AIChE Symp. Ser., 74*, 176-186.

Bastani, D., Safekordi, A.A., Alihosseini, A., Taghikhani, V. (2006). Study of oil sorption by expanded perlite at 298.15 K. *Sep. Purif. Technol., 52*, 295-300.

Berkeley lab. In Berkeley lab website, from http://eetd.lbl.gov/ecs/aerogels/images/aerogel-tem.html

Bendict, R.J.F., Kumaresan, G., Velan, M. (1998). Bed expansion and pressure drop studies in a liquid-solid inverse-fluidized bed reactor. *Bioprocess Eng., 19*, 137-142.

Bennett, G.F. (1988). The removal of oil from wastewater by air flotation: a review. *CRIT. Rev. ENV. CONTR., 18*, 189-253.

Bouwer, E.J., Crowe P.B. (1988). Biological process in drinking water treatment. *J.AWWA, 80*, 82-91.

Brunauer, S., Emmett, P.H., Teller, E. (1938). Adsorption of gases in multimolecular layers. *J. Am. Chem. Soc., 60*, 309-319.

Buikema, A.L., Hendricks, A.C., (1980). *Benzene, xylene, and toluene in aquatic systems: a review*. Washington, D.C.: American Petroleum Institute.

Butt, J.B., (2000). *Reaction kinetics and reactor design*. New York: M. Dekker.

Cabot. In Cabot website, from http://www.cabot-corp.com/Aerogel?WT.mc_id=AE-HP

Cambiella, A., Ortea, E., Rios, G., Benito, J.M., Pazos, C., Coca, J. (2006). Treatment of oil-in-water emulsions: performance of a sawdust bed filter. *J. Hard. Mater. B*, *131*, 195-199.

Carberry, J.J., (1976). *Chemical and catalytic reaction engineering*. New York: McGrew-Hill.

Carmody, O., Frost, R., Xi, Y., Kokot, S. (2007). Adsorption of hydrocarbons on organo-clays: implications for oil spill remediation. *J. Colloid Interface Sci., 305*, 17-24.

Ceylan, D., Dogu, S., Karacik, B., Yakan, S.D., Okay, O.S., Okay, O. (2009). Evaluation of butyl rubber as sorbent material for the removal of oil and polycyclic aromatic hydrocarbons from seawater. *Environ. Sci. Technol.*, *43,* 3846–3852.

Chatzopoulos, D.; Varma, A. (1995). Aqueous-phase adsorption and desorption of toluene in activated carbon fixed beds: experiments and model. *Chem. Eng. Sci.*, *50*, 127-141.

Chilton, T.H., Colburn, A.P. (1931). II — Pressure drop in packed tubes. *Ind. Eng. Chem., 23*, 913-919.

Cho, Y.J., Park, H.Y., Kim, S.W., Kang, Y., Kim, S.D. (2002). Heat Transfer and Hydrodynamics in two and three phase inverse fluidized beds. *Ind. Eng. Chem. Res., 41*, 2058-2063.

Choi, J.W., Choi, N.C., Lee, S.J., Kim, D.J. (2007). Novel three-stage kinetic model for aqueous benzene adsorption on activated carbon. *J. Colloid Interface Sci., 314*, 367-372.

Choi, J., Yang, K., Kim, D., Lee, C.E. (2009). Adsorption of zinc and toluene by alginate complex impregnated with zeolite and activated carbon. *Current Applied Physics, 9*, 694-697.

Chung, S.F., Wen, C.Y. (1968). Longitudinal dispersion of liquid flowing through fixed and fluidized beds. *AICHE J. 14*, 857-866.

Cojocaru, C., Macoveanu, M., Cretescu, I. (2011). Peat-based sorbents for the removal of oil spills from water surface: application of artificial neural network modeling. *Colloids Surface A*, *384*, 675-684.

Cooney, D.D., (1998). *Adsorption design for wastewater treatment*. New York: Lewis.

Correa, R.A., Calcada, L.A. Pecanha, R.P. (2007). Development of a fluidized bed system for adsorption of phenol from aqueous solutions with commercial macroporous resins. *Braz. J. Chem. Eng., 24*, 15-28.

Crittenden, J.C., Liu, J.B., Hand, D.W., Perram, D.L. (1997). Photocatalytic oxidation of chlorinated hydrocarbons in water. *Water Res., 31*, 411-418.

Cussler, E.L., (1997). *Diffusion Mass Transfer in Fluid Systems*. USA: Cambridge University Press.

Dobbs, R.A., Cohen, J.M., (1980). *US EPA Report 600. 880-023*: Cincinnati.

Eckenfelder, W.W., (2000). *Industrial water pollution control*. New York: McGraw-Hill.

Enright, A., Collins, G., O'Flaherty, V. (2007). Low-temperature anaerobic biological treatment of toluene-containing wastewater. *Wat. Res.*, *41*, 1465-1472.

Epstein, N. (2003). Applications of Liquid-Solid Fluidization. **International Journal of Chemical Reactor Engineering, 1,** R1.

European Communities. (2003). *European union risk assessment report: toluene*.

Fan, L.S., Muroyama, K., Chern, S.H. (1982). Hydrodynamic Characteristics of Inverse Fluidization in Liquid-Solid and Gas-Liquid-Solid Systems. *Chem. Eng. J., 24*, 143-150.

Farhadian, M., Duchez, D., Vachelard, C., Larroche, C. (2008). Monoaromatics removal from polluted water through bioreactors — a review. *Water Res., 42*, 1325-1341.

Faust, S.D., Aly, O.M., (1987). *Adsorption Processes for Water Treatment*, Stoneham, UK: Butterworths Publishers.

Fingas, M. F., (2010). *The basics of oil spill cleanup*. London: Lewis Publishers.

Freundlich, H., (1926). *Colloid and capillary chemistry*. London: Methuen.

Fricke, J., Tillotson, T. (1997). Aerogels: production, characterization, and applications. *Thin solid films, 297*, 212-223.

Furnas, C.C., (1929). *Flow of gases through beds of broken solids*. Bill 307. US Bureau of Mines.

Garcia-Calderon, D., Buffiere, P., Moletta, R., Elmaleh, S. (1998). Influence of biomass accumulation on bed expansion characteristics of a down-flow anaerobic fluidized-bed reactor. *Biotechnology and bioengineering, 57*, 136-144.

Glueckauf, E., Coates, J.I. (1947). Theory of chromatography. Part IV. The influence of incomplete equilibrium on the front boundary of chromatograms and on the effectiveness of separation. *J. Chem. Soc.*, *41*, 1315.

Grace, J.R. (1982). *Fluidized bed hydrodynamics.* In: Hetsroni G, ed. Handbook of Multiphase Systems. New York: Hemisphere and McGraw-Hill.

Hach Co. (2004). *Method 8000: Reactor digestion method USEPA approved for oxygen chemical demand wastewater analysis, DR/890 Datalogging Colorimeter Handbook*, Lovelanf, CO.

Hand, D.W., Crittenden, J.C., Thacker, W.E. (1984). Simplified models for design of fixed-bed adsorption systems. *J. Environ. Eng-ASCE., 110*, 440–456.

He, X., Iasmin, M., Dean, L.O., Lappi, S.E., Ducoste, J.J., De Los Reyes, F.L. (2011). Evidence for fat, oil, and grease (FOG) deposit formation mechanisms in sewer lines. *Environ. Sci. Technol., 45*, 4385-4391.

Ho, Y.S., McKay, G. (1999). Pseudo-second order model for sorption process. *Process Biochem., 34*, 451-465.

Holth, T.F., Beylich, B.A., Munilla, I., Skarphéðinsdóttir, H., Liewenborg, B., Grung, M., Hylland, K. (2009). Genotoxicity of environmentally relevant concentrations of water-soluble oil components in cod (gadus morhua). *Environ. Sci. Technol.*, *43*, 3329–3334.

Hrubesh, L.W. (1998). Aerogel applications. *J. Non-Cryst. Solids, 225*, 335-342

Hrubesh, L.W., Coronado, P.R., Satcher Jr., J.H. (2001). Solvent removal from water with hydrophobic aerogels. *J. Non-Cryst. Solids*, *285*, 328-332.

Ibrahim, Y.A.A., Briens, C.L., Margarities, A., Bergongnou, M.A. (1996). Hydrodynamics characteristics of a three-phase inverse fluidized-bed column. *AICHE J., 42*, 1889-1900.

Irwin, R.J., van Mouwerik, M., Stevens, L., Seese, M.D., Basham,W., (1997). *Environmental Contaminants Encyclopedia*. Fort Collins, Colorado: National Park Service, Water Resources Division.

Jian, W., Kitanaka, A., Nishijima, W., Baes, A.U., Okada, M. (1996). Removal of oil pollutants in seawater as pretreatment of reverse osmosis desalination process. *Wat. Res., 33*, 1857-1863.

Jirka, A.M.; Carter, M.J. (1975). Micro semiautomated analysis of surface and wastewaters for chemical oxygen demand. *Anal. Chem.*, *47*, 1397-1402.

Johnson, R.F., Manjrekar, T.G., Halligan, H.R. (1973). Removal of oil from water surface by sorption on unstructured fibers. *Environ. Sci. Technol.*, *7*, 439-443.

Karamanev, D.G., Nikolov, L.N. (1992). Bed expansion of liquid-solid inverse fluidization, *AICHE J. 38*, 1916-1922.

Karger, J., Ruthven, D.M., (1992). *Diffusion in zeolites and other microporous solids*. New York: Wiley.

Koh, S.M., Dixon, J.B. (2001). Preparation and application of organo-minerals as sorbents of phenol, benzene and toluene. *Appl. Clay Sci.*, *18*, 111-122.

Kryst, K., Karamanev, G. (2001). Aerobic phenol biodegradation in an inverse fluidized bed biofilm reactor. *Ind. Eng. Chem. Res., 40*, 5436-5439.

Lagergren, S. (1898). About the theory of so-called adsorption of soluble substances. *Kungliga Svenska Vetenskapsakademiens. Handlingar, 24*, 1-39.

Lakshmi, A.C.V., Balamurugan, M., Sivakumar, M., Samuelm, T.N., Velan, M. (2000). Minimum fluidization velocity and friction factor in a liquid-solid inverse fluidized bed reactor. *Bioprocess Eng., 22*, 461-466.

Langmuir, I. (1916). The constitution and fundamental properties of solids and liquids. part i. solids. *J. Am. Chem. Soc. 38*, 2221-95.

Lapidus, L., Amundsen, N.R. (1952). Mathematics of adsorption in beds. IV. The effect of longitudinal diffusion in ion exchange and chromatographic columns. *J. Phys. Chem., 56*, 984-988.

Lemoine, D., Jouenne, T., Junter, G.A. (1991). Biological denitrification of water in a two-chambered immobilized-cell bioreactor. *Appl. Microbial Biot.*, *36*, 257-264.

Leva, A. (1949). Pressure drop correlation for a single incompressible fluid. *Chem. Eng., 56*, 115-117.

Lin, S.H., Huang, C.Y. (1999). Adsorption of BTEX from aqueous solution by macroreticular resins. *J. Hazard. Mater., 70,* 21-37.

Lin, Y.S., Ma, Y.H. (1989). A comparative chromatographic study of liquid adsorption and diffusion in microporous and macroporous adsorbents. *Ind. Eng. Chem. Res., 28*, 622-630.

Lin, Y.S., Ma, Y.H. (1990). Analysis of liquid chromatography with nonuniform crystallite particles. *AIChE J., 36*, 1569-1576.

Liu, H., Sha, W., Cooper, A.T., Fan, M. (2009). Preparation and characterization of a novel silica aerogel as adsorbent for toxic organic compounds. *Colloids Surface A*, *347*, 38-44.

Ma, Y.H., Lin, Y.S. (1985). Adsorption of liquid hydrocarbons in silicalite. *AIChE Symp. Seri.*, *242*, 39-44.

Manual on disposal of refining wastes, America Petroleum Institute, Washington. D. C., 1969, vol. 5, pp. 5-15.

Mathavan, G.N., Viraraghavan, T. (1989). Use of peat in the treatment of oily waters. *Wat. Air Soil Pollut., 45*, 17-26.

Mattson, J.S., Mark, H.B., Malbin, M.D., Weber, W.J., Crittenden, J.C. (1969). Surface chemistry of activate carbon: specific adsorption of phenols. *J. Colloid Interface Sci., 31*, 116-130.

McKay, G. (1983). The adsorption of dyestuffs from aqueous solution using activated carbon: analytical solution for batch adsorption based on external mass transfer and pore diffusion. *Chem. Eng. J., 27*, 187-196.

Micromeritics. In Micromeritics website, from http://www.micromeritics.com/Product-Showcase/GeoPyc-1360-Envelope-Density-Analyzer.aspx.

Miller, J.W. Jr., McGinley, J.J., Yaws, C.L. (1976). Correlation constants for liquids- thermal conductivities. *Chem. Eng.*, *83*, 133-135.

Moulai-Mostefa, N., Brou, A., Ding, L., Joffrin, M.Y. (2005). Ultrafiltration of oil in-water emulsions and cyclohexane microemulsions using a rotating disk system. *Mecanique & Industries, 6*, 203–210.

Moura, C.P., Vidal, C.B., Barros, A.L., Costa L.S., Vasconcellos, L.C.G., Dias, F.S., Nascimento, R.F. (2011). Adsorption of BTX (benzene, toluene, o-xylene, and p-xylene) from aqueous solutions by modified periodic mesoporous organosilica. *J. Colloid Interface Sci., 363*, 626-634.

Mysore, D., Viraraghavan, T., Jin, Y.C. (2005). Treatment of oily waters using vermiculite. *Water Res.*, *39*, 2643-2653.

Nielsen, L.E., Wall, R., Adams, G. (1958). Coalescence of liquid drops at oil-water interface. *J. Colloid Sci.*, *13*, 441-458.

Nikov, I., Karamanev, D. (1991). Liquid-solid mass transfer in inverse fluidized bed. *AICHE J., 37*, 781-784.

Nikov, I., Nikolov, D., Dimitrov, D. (1999). Biodegradation of aniline using light carriers with optimized surface in TPIFB. *Bioprocess Eng., 21*, 547-552.

Noll, K.E., Gounaris, V., Hou, W.S., (1992). *Adsorption technology for air and water pollution control*, US: Lewis Publication.

Pasila, A. (2004). A biological oil adsorption filter, *Mar. Pollut. Bull., 49*, 1006-1012.

Paterson, J.W., (1975). *Wastewater treatment technology*, Stoneham, MA: Ann Arbor Science.

Paterson, J.W., (1985), 3rd ed. *Industrial wastewater treatment technology*. Stoneham: Butterworth Publishers.

Pelech, R., Milchert, E., Bartkowiak, M. (2006). Fixed-bed adsorption of chlorinated hydrocarbons from multicomponent aqueous solution onto activated carbon: Equilibrium column model. *J. Colloid Interf. Sci., 296*, 458-464.

Novak, Z., Černcic, S., Knez, Z. (2005). Hydrophobic silica aerogel-solvent removal from water. *Proceedings of 10th European Meeting on Supercritical Fluids*, Colmar, France.

Quemeneur, M., Marty, Y. (1994). Fatty acids and sterols in domestic wastewaters. *Water Res.*, *28*, 1217-1226.

Quevedo, J.A., Patel, G., Pfeffer, R. (2009). Removal of oil from water by inverse fluidization of aerogels. *Ind. Eng. Chem. Res.*, *48*, 191-201.

Ranck, J.M., Bowman, R.S., Weeber, J.L., Katz, L.E., Sullivan, E.J. (2005). BTEX removal from produced water using surfactant-modified zeolite. *J. Environ. Eng., 131*, 434-442.

Rao, A.V., Hegde, N.D., Hirashima, H. (2007). Absorption and desorption of organic liquids in elastic superhydrophobic silica aerogels. *J. Colloid Interf. Sci.*, *305*, 124-132.

Rengannathan, T., Krishnaiah, K. (2003). Prediction of minimum fluidization velocity in two and three phase inverse fluidized beds. *Can. J. Chem. Eng., 81*, 853-860.

Rengannathan, T., Krishnaiah, K. (2004). Stochastic simulation of hydrodynamics of a liquid-solid inverse fluidized bed. *Ind. Eng. Chem. Res., 43*, 4405-4412.

Rengannathan, T., Krishnaiah, K. (2005). Voidage characteristics and prediction of bed expansion in liquid-solid inverse fluidized bed. *Chem. Eng. Sci., 60*, 2545-2555.

Reynolds, J.G., Coronado, P.R., Hrubesh, L.W. (2001). Hydrophobic aerogels for oil-spill cleanup — intrinsic absorbing properties. *Energ. Source*, *23*, 831-843.

Reynolds, J.G., Coronado, P.R. (2001). Hydrophobic aerogels for oil-spill cleanup — synthesis and characterization. *J. Non-Cryst. Solids*, *292*, 127-137.

Ribeiro, T.H., Rubio, J., Smith, R.W. (2003). A dried hydrophobic aquaphyte as an oil filter for oil/water emulsions. *Spill Sci. Technol. B.*, *8*, 483-489.

Ruthven, D.M., (1984). *Principles of adsorption and adsorption process*. USA: John Wiley & Sons.

Richardson, J.F., Zaki, W.N. (1954). Sedimentation and fluidization: Part I. *Trans. Instn. Chem. Eng., 32*, 35-53.

Robeson, L.M., Axelrod, R., Manuel, T.A. (1992). *US Patent 5,120,598*.

Saxena, S.C., Vogel, G.J. (1977). The measurement of incipient fluidization velocities in a bed of coarse dolomite at temperature and pressure. *Trans ChemE., 55*, 184-189.

Shafir, S., Van Rijn, J., Rinkevich, B. (2007). Short and long term toxicity of crude oil and oil dispersants to two representative coral species. *Environ. Sci. Technol., 41*, 5571-5574.

Simpson, E.J., Abukhadra, R.K., Koros, W.J., Schechter, R.S. (1993). Sorption equilibrium isotherms for volatile organics in aqueous solution: comparison of head-space gas chromatography and on-line UV stirred cell results. *Ind. Eng. Chem. Res.*, *32*, 2269-2276.

Sing, K.S.W., Everett, D.H., Haul, R.A.W., Moscou, L., Pierotti, R.A., Rouquerol, J., Siemieniewska, T. (1985). Reporting physisorption data for gas/solid systems with special reference to the determination of surface area and porosity. *Pure & Appl. Chem., 57*, 603-619.

Sircar, S., Hufton, J.R. (2000). Why does the linear driving force model for adsorption kinetics work. *Adsorption, 6*, 137-147.

Slejeiko, L., (1981). *Adsorption technology: A step by step approach to process evaluation and application*, New York: Marcel Dekker.

Sontheimer, H., Crittenden, J.C., Summers, R.S., (1988). *Activated carbon for water treatment*. Karlsruhe: DVGC-Forschungsstelle.

Standeker, S., Novak, Z., Knez, Z. (2007). Adsorption of toxic organic compounds from water with hydrophobic silica aerogels. *J. Colloid Interf. Sci.*, *310*, 362-368.

Standeker, S., Novak, Z., Knez, Z. (2009). Removal of BTEX vapours from waste gas streams using silica aerogels of different hydrophobicity. *J. Hazard. Mater.*, *165*, 1114-1118.

Su, F., Lu, C., Hu, S. (2010). Adsorption of benzene, toluene, ethylbenzene and p-xylene by NaOCl-oxidized carbon nanotubes. *Colloids Surf., A*, *353*, 83-91.

Van Rossum, G., Kersten, S.R.A., Van Swaaij, W.P.M. (2007). Catalytic and noncatalytic gasification of pyrolysis oil. *Ind. Eng. Chem. Res., 46*, 3959-3967.

Viraraghavam, T., Moazed, H. (2003). Removal of oil from water by bentonite. *Fresen. Environ. Bull.*, *12*, 1092-1097.

Vogal J.V. (1966). *U.S. Patent No. 3, 294, 167*. New York: U.S.

Tata, P., Witherspoon, J., Lue-Hing, C., (2003). *VOC emissions from wastewater plants: characterization, control, and compliance*. London: Lewis Publishers.

Tannous, K., Hemati, M., Laguerie, C., Characte´ ristiques au minimum de fluidisation et expansion des couches fluidise´ es de particules de la cate´ gorie D de Geldart. *Powder Technology, 80*, 55-72.

Thonglimp, V., Hiquily, N., Laguerie, C., (1984). Vitesse minimale de fluidisation et expansion des couches fluidise´es par un gaz. *Powder Technology, 38*, 233-253.

Veeraraghavan, S., Fan, L.T., Mathews, A.P. (1989). Modeling adsorption in liquid-solid fluidized beds. *Chem. Eng. Sci., 44*, 2333-2345.

Walker, J.D., Colwell, R.R., Petrakis, L. (1975). Degradation of petroleum by an alga, Prototheca zopfii. *Appl. Microb., 30*, 79–81.

Washburn, E.W. (1921). The dynamics of capillary flow. *Phys. Rev.*, 17, 273-283.

Weber, W.J., van Vliet, B.M., (1980). *Fundamental concepts for application of activated carbon in water and wastewater, in: Activated carbon adsorption of organics from the aqueous phase.* Ann Arbor: Ann Arbor Science.

Wei, Q.F., Mather, R.R., Fotheringham, A.F. (2005). Oil removal from used sorbents using a biosurfactant. *Bioresource Technol., 96*, 331-334.

Wen, C.Y., Fan, L.T., (1975). *Models for flow systems and chemical reactors*. New York: Marcel Dekker.

Wibowo, N., Setyadhi, L., Wibowo, D., Setiawan, J., Ismadji, S. (2007). Adsorption of benzene and toluene from aqueous solutions onto activated carbon and its acid and heat treated forms: influence of surface chemistry on adsorption. *J. Hazard. Mater., 146*, 237-242.

Wright, P.R., Glasser, B.J. (2001). Modeling mass transfer and hydrodynamics in fluidized-bed adsorption of proteins. *AICHE J., 47*, 474-488.

Yang, R. T., (2003). *Adsorbents: Fundamentals and Applications*. Hoboken: Wiley-Interscience.

Yue, Z., Mangun, C.L., Economy, J., Kemme, P., Cropek, D., Maloney, S. (2001). Removal of Chemical Contaminants from Water to below USEPA MCL Using Fiber Glass Supported Activated Carbon Filters. *Environ. Sci. Technol., 35*, 2844-2848.

Yoshiyuki, H., Toru, I., Tomoki, G., Takakiyo, G., Toro, U., Kenji, R. (1994). *European Patent, 0,441,512, B1*.

Zhou, Y.B., Tang, X.Y., Hu, X.M., Fritschi, S., Lu, J. (2008). Emulsified oily wastewater treatment using a hybrid-modified resin and activated carbon system. *Sep. Purif. Technol., 63*, 400-406.

Zhu, C., Yu, Q., Dave, R.N., Pfeffer, R. (2005). Gas fluidization characteristics of nanoparticle agglomerates. *AIChE J., 51*, 426-439.

Zhu, H., Qiu, S., Jiang, W., Wu, D., Zhang, C. (2011). A evaluation of electrospun polyvinyl chloride/polystyrene fibers as sorbent materials for oil spill cleanup. *Environ. Sci. Technol.*, *45*, 4527-4531.

APPENDIX A

EXPERIMENTAL PROTOCOLS

A.1. Preparation Protocol in IFB and PB Experiments

1. Connect the vent at the top of the fluidization column to a vacuum.
2. Load the Nanogel particles into the column.
3. Fill water into the fluidization column from the bottom until the air is completely removed by a vent at a high point in the system.
4. Feed the water flow at the top of the column through a distributor made up of a packed bed of glass beads supported by a steel wire mesh to prevent channeling.
5. Keep the static pressure constant during the experiments.

A.2. IFB Hydrodynamics Measurements

1. Increase the water flow rate until the Nanogel particles are inversely fluidized.
2. Increase the water flow rate significantly above that value until the bed height approach the entire length of the column.
3. Measure bed height and pressure drop data through the length mark of the fluidization column and the display of the differential pressure transmitter at each flow rate by gradually decreasing the flow of water until the bed defluidizes.

A.3. Emulsified Oil Adsorption Measurements in IFB or PB

1. Prepare a high-concentration, stable oil-in-water emulsion by continuously stirring with a magnetic stirrer in a large plastic container.

2. Inject the oil-in-water emulsion into the piping system by the pump upstream of the static mixers and the column.
3. Adjust the pump's stoke displacement and frequency to obtain a desired concentration of oil when the emulsion was mixed into the flowing water.
4. Take samples of water of about 250 ml, upstream and downstream of the column, at regular time intervals until the expanded bed height reached the bottom of the column.
5. Analyze the oil concentrations of samples by the HACH DR/890 colorimeter.

A.4. Toluene Adsorption Measurements in IFB or PB

1. Prepare the toluene solution in the tank by mixing a certain amount of toluene into tap water and stirred by using the high speed mixer for several minutes until toluene was totally dissolved in the water.
2. Inject the toluene solution into the piping system upstream of column by the pump.
3. Adjust the flow rate with ball valves to obtain a desired flow rate of solution.
4. Take samples of solution of about 100 ml, upstream and downstream of the column, at regular intervals.
5. Analyzed the toluene concentration of samples by using a GC equipped with a flame ionization detector (SRI 8610C) until the concentrations of the downstream sample is equal to the concentrations of the upstream sample, i.e., breakthrough has occurred.

A.5. Batch Equilibrium Measurements for Oil-in-water Emulsion

1. Add oil, tap water and Tween 80 into a blender at a certain proportion.
2. Blend the mixture for 3 min at 'blend' speed.
3. Mix six representative weights of TLD 301 Nanogel, in the range of 20-400 mg, with 100 mL oil-in-water emulsions prepared in steps 1 and 2 in glass bottles.
4. Shake these bottles in an Innova 4080 incubator shaker (200 rpm) at room temperature for 3 h.
5. Withdraw the samples and analyze them by the HACH DR/890 colorimeter.

A.6. Batch Kinetics Measurements for Oil-in-water Emulsion

1. Follow steps 1 and 2 in *A.4*.
2. Mix 100 mg of TLD 301 Nanogel with 100 mL oil-in-water emulsions prepared in step 1 in a number of glass bottles.
3. Shake these bottles in an Innova 4080 incubator shaker (200 rpm) at room temperature for different time periods.
4. Analyze the concentration of each of the liquid samples by the HACH DR/890 colorimeter.

A.7. Batch Equilibrium Measurements for VOC Solution

1. Prepare 100 mL VOC solutions of different initial concentrations in sealed glass bottles to prevent VOC vapor from escaping.
2. Mix 100 mg TLD 301 Nanogel with VOC solutions in these sealed bottles.

3. Shake these bottles in an Innova 4080 incubator shaker (200 rpm) at room temperature for 3 h.
4. Withdraw the samples and analyze them by the GC.

A.8. Batch Kinetics Measurements for VOC Solution

1. Prepare 100 mL VOC solution of desired initial concentration in sealed glass bottles.
2. Mix 100 mg TLD 301 Nanogel with this VOC solution using a magnetic stirrer (Cimarec).
3. Measure the VOC concentration of the liquid sample by the GC at different time intervals.
4. Stop the experiment when the concentration approaches the equilibrium concentration.

APPENDIX B

MATLAB PROGRAMS

B.1. Linear Driving Force Model

Program 1

```
function dy=toluene(t,y)
global para
V=para(1);
m=para(2);
dp=para(3);
a=para(4);
kt=para(5);
K=para(6);
n=para(7);
dy=zeros(3,1);
dy(1)=-0.6*m*a*kt*(y(1)-y(2))/dp/V;
dy(2)=0.6*1000*a*kt*(y(1)-y(2))/dp/K/n/y(2)^(n-1);
dy(3)=0.6*1000*a*kt*(y(1)-y(2))/dp;
```

Program 2

```
clear all
global para
para=[0.1,0.1,125,6316,0.5e-3,223,1.15];
ts=[0,1,2,3,4,6,8,10,15,30,60,90,120,150,180];
y0=[0.339,1e-20,1e-20]';
options = odeset('RelTol',1e-8,'initialstep',0.00001);
```

```
[t,y] = ode23(@toluene,ts,y0,options);
treal=[0,1,2,3,4,6,8,10,15,30,60,90,120,150,180];
creal=[338.8,327.0,302.4,285.0,298.4,289.3,285.9,283.0,274.1,265.9,259.2,249.6,
245.1,249.9,251.8];
plot(t,1000*y(:,1),'k',t,1000*y(:,2),'k:',treal,creal,'Ko')
xlabel('t(min)'); ylabel('C(mg/L)');
A=y(:,1);
for i=1:1:13
B(i)=(creal(i)-A(i)*1000)^2;
end
B2=sum(B)
```

B.2. Model for Oil Adsorption in IFB

Program 1

```
function dy=breakthroughdisperse(t,y)
% Constant used in the calculation %
global para
H=para(1); % Bed Height Unit: m (TLD 301 110g 4% Tween 80)
vis=para(2); % Viscosity Unit: Ns/m2
c=para(3); % Inlet Concentration Unit: g/L (TLD 301 110g 4% Tween 80)
m=para(4); % Weight of Nanogels Unit: kg
u=para(5); % Flow superficial velocity Unit: m/s
k1=para(6); % Unit: s-1
```

```
a=para(7); % Cross sectional Area of Column Unit: m2
k2=para(8); % Freundlich Constnat K
n1=para(9); % Freundlich Constant 1/n
dp=para(10); % Particle Density Unit: g/ml
d=para(11); % Particle Size Unit: m (TLD 301)
N=para(12);
Re=d*u*1000/vis; % Re Number
D=vis*Re/1000/(0.2+0.011*Re^(0.48)); % Dax Unit: m2/s
e=1-m/dp/a/H/1000; % Liquid void fraction
h1=H/(N-1);
% procedure for PDEs %
dy=zeros(N-1,1);
dy(1)=D*(y(2)-2*y(1)+u*h1*c/(u*h1+D*e)+D*e*y(1)/(u*h1+D*e))/h1/h1-
u*(y(1)-u*h1*c/(u*h1+D*e)-D*e*y(1)/(u*h1+D*e))/h1/e-k1*(1-e)*(y(1)-(y(N-
1)/k2)^(1/n1))/e;
for i=2:1:N-3
dy(i)=D*(y(i+1)-2*y(i)+y(i-1))/h1/h1-u*(y(i)-y(i-1))/h1/e-k1*(1-e)*(y(i)-(y(N-
1)/k2)^(1/n1))/e;
Y(:,i)=[y(i)];
end
dy(N-2)=D*(y(N-3)-y(N-2))/h1/h1-u*(y(N-2)-y(N-3))/h1/e-k1*(1-e)*(y(N-2)-
(y(N-1)/k2)^(1/n1))/e;
dy(N-1)=k1*((u*h1*c/(u*h1+D*e)+D*e*y(1)/(u*h1+D*e)+y(N-2))/2/(N-
```

```
1)+(sum(Y)+y(1)+y(N-2))/(N-1)-(y(N-1)/k2)^(1/n1))/dp;
```

Program 2

```
Clear
global para
para=[0.4,1.005e-3,0.199,0.1,0.018,0.284,0.004558,223,1.15,0.125,9.5e-4,20];
% para [H1, vis, c, m, u, k1, a, k2, n1, dp, d,N]
% Time Span (s)
t0=0;tf=2400;
N=para(12);
% Initial Value
%%y0=zeros(1,2*N-1)';
y0=0.0000001*ones(N-1,1);
options = odeset('RelTol',1e-7);
[t1,y1] = ode23(@breakthroughdisperse,[t0 tf],y0,options);
% Experimental Data
treal=[0,3,6,9,12,15,20,25,30,35,40]; %(TLD 301 55g 4% Tween 80)
creal=[0,58,126,167,188,192,194,192,199,200,201]; %(TLD 301 55g 4% Tween
80)
plot(t1/60,y1(:,N-2)*1000,'k',treal,creal,'k*')
xlabel('t(min)');
ylabel('C(mg/L)');
```

B.3. Model for Toluene Adsorption in PB

Program 1

```
function dy=breakthroughdisperse(t,y)
% Constant used in the calculation %
global para
H=para(1); % Bed Height Unit: m (TLD 301 110g 4% Tween 80)
vis=para(2); % Viscosity Unit: Ns/m2
c=para(3); % Inlet Concentration Unit: g/L (TLD 301 110g 4% Tween 80)
m=para(4); % Weight of Nanogels Unit: kg
u=para(5); % Flow superficial velocity Unit: m/s
k1=para(6); % Unit: s-1
a=para(7); % Cross sectional Area of Column Unit: m2
k2=para(8); % Freundlich Constnat K
n1=para(9); % Freundlich Constant 1/n
dp=para(10); % Particle Density Unit: g/ml
d=para(11); % Particle Size Unit: m (TLD 301)
N=para(12);
Re=d*u*1000/vis; % Re Number
D=vis*Re/1000/(0.2+0.011*Re^(0.48)) % Dax Unit: m2/s
e=1-m/dp/a/H/1000; % Liquid void fraction
h1=H/(N-1);
 % procedure for PDEs %
dy=zeros(2*N-4,1);
```

```
dy(1)=D*(y(2)-2*y(1)+u*h1*c/(u*h1+D*e)+D*e*y(1)/(u*h1+D*e))/h1/h1-
u*(y(1)-u*h1*c/(u*h1+D*e)-D*e*y(1)/(u*h1+D*e))/h1/e-k1*(1-e)*(y(1)-(y(N-
1)/k2)^(1/n1))/e;
for i=2:1:N-3
dy(i)=D*(y(i+1)-2*y(i)+y(i-1))/h1/h1-u*(y(i)-y(i-1))/h1/e-k1*(1-e)*(y(i)-(y(i+N-
2)/k2)^(1/n1))/e;
end
dy(N-2)=D*(y(N-3)-y(N-2))/h1/h1-u*(y(N-2)-y(N-3))/h1/e-k1*(1-e)*(y(N-2)-
(y(2*N-4)/k2)^(1/n1))/e;
for i=N-1:1:2*N-4
    dy(i)=k1*(y(i-(N-2))-(y(i)/k2)^(1/n1))/dp;
end
```

Program 2

```
Clear
global para
para=[0.35,1.005e-3,0.187,0.1,0.0026,0.284,0.004558,23,1.15,0.125,9.5e-4,20];
% para [H1, vis, c, m, u, k1, a, k2, n1, dp, d,N]
% Time Span (s)
t0=0;tf=4800;
 N=para(12);
 % Initial Value
 y0=0.0000001*ones(2*N-4,1);
```

```
options = odeset('RelTol',1e-7);
[t,y] = ode23(@breakthroughdisperse,[t0 tf],y0,options);
 % k=342,1/n=1
global para
para=[0.35,1.005e-3,0.187,0.1,0.0026,0.123,0.004558,342,1,0.125,9.5e-4,20];
% para [H1, vis, c, m, u, k1, a, k2, n1, dp, d,N]
 % Time Span (s)
t0=0;tf=4800;
 N=para(12);
 % Initial Value
 y0=0.0000001*ones(2*N-4,1);
options = odeset('RelTol',1e-7);
[t1,y1] = ode23(@breakthroughdisperse,[t0 tf],y0,options);
 % Experimental Data
treal=[0,3,13,23,33,43,53,63,73];
creal=[0,0,0,44,112,153,171,185,194];
 plot(t/60,y(:,N-2)*1000,'k',t1/60,y1(:,N-2)*1000,'k--',t2/60,y2(:,N-2)*1000,'K-
.',treal,creal,'k*')
xlabel('t(min)');
ylabel('C(mg/L)');
```

APPENDIX C

MODEL FOR THE ADSORPTION OF ORGANICS IN A CONTINUOUS FLUIDIZED BED

At the steady state, a mass balance on the organic for the down-flowing liquid phase gives:

$$u_L \frac{dC}{dz} = -\frac{1}{2} C_s K'[(C - C_{fu}) + (C - C_{fd})] \tag{C.1}$$

with the boundary condition:

$$C(0) = C_0 \tag{C.1a}$$

where u_L is the down flowing liquid superficial velocity, C_s is the solid concentration determined by the initial amount of aerogels added to the bed and bed volume, C_{fu} and C_{fd} are the organic concentrations of the up-flowing and down-flowing Nanogels in equilibrium with the liquid concentration given by the adsorption equilibrium isotherm, e.g., Freundlich equation, K' is the rate constant from the LDF model, and C_0 is the inlet organic concentration.

A mass balance on the organic in the up-flowing and down-flowing solid phases gives:

$$-N \frac{dq_u}{dz} = \frac{1}{2} C_s K'(C - C_{fu}) \tag{C.2}$$

$$N \frac{dq_d}{dz} = \frac{1}{2} C_s K'(C - C_{fd}) \tag{C.3}$$

with the boundary conditions at the top and bottom:

$$q_u(L) = 0 \tag{C.2a}$$

$$q_d(0) = q_c \tag{C.3a}$$

where N is the down flowing liquid superficial velocity, and q_c represents a critical mass of adsorbed organic of Nanogels, at which the Nanogels sink to the bottom of the column and begin to leave.

Equations (C.1, C.2 and C.3) can be solved simultaneously to get the concentration profiles of Nanogel and organic in the column, which can be used to compare with the experimental data. These comparisons can provide the insight needed to improve and fine-tune the model. The modified model will be used to predict the effect of varying operating conditions on the performance of the continuously operating fluidized bed adsorber and can be used for scale up if improved adsorption capacity and efficiency are experimentally observed.